ISTANBUL TECHNICAL UNIVERSITY ★ GRADUATE SCHOOL OF SCIENCE ENGINEERING AND TECHNOLOGY

COMPUTATIONAL INVESTIGATION OF ORGANIC REACTIONS VIA MECHANISTIC APPROACHES

Ph.D. THESIS

Esra BOZ

Chemistry Department

Chemistry Programme

MAY 2018

ISTANBUL TECHNICAL UNIVERSITY ★ GRADUATE SCHOOL OF SCIENCE
ENGINEERING AND TECHNOLOGY

COMPUTATIONAL INVESTIGATION OF ORGANIC REACTIONS VIA MECHANISTIC APPROACHES

Ph.D. THESIS

Esra BOZ
(509112006)

Chemistry Department

Chemistry Programme

Thesis Advisor: Prof. Dr. Nurcan TÜZÜN

MAY 2018

İSTANBUL TEKNİK ÜNİVERSİTESİ ★ FEN BİLİMLERİ ENSTİTÜSÜ

ORGANİK TEPKİMELERİN MEKANİSTİK YAKLAŞIMLAR KULLANILARAK HESAPSAL İNCELENMESİ

DOKTORA TEZİ

Esra BOZ
(509112006)

Kimya Anabilim Dalı

Kimya Programı

Tez Danışmanı: Prof. Dr. Nurcan TÜZÜN

MAYIS 2018

Esra BOZ, a Ph.D. student of İTU Graduate School of Science Engineering and Technology student ID 509112006, successfully defended the thesis entitled "COMPUTATIONAL INVESTIGATION OF ORGANIC REACTIONS VIA MECHANISTIC APPROACHES", which she prepared after fulfilling the requirements specified in the associated legislations, before the jury whose signatures are below.

Thesis Advisor : **Prof. Dr. Nurcan TÜZÜN** ....
Istanbul Technical University

Jury Members : **Prof. Dr. Mine YURTSEVER** ....
Istanbul Technical University

Prof. Dr. Ömer ZAİM ....
Trakya University

Assoc. Prof. Dr. Barış YÜCEL ....
Istanbul Technical University

Prof. Dr. Alimet ÖZEN ....
Piri Reis University

Date of Submission : 7 May 2018
Date of Defense : 21 May 2018

FOREWORD

First, I would like to thank my supervisor Prof. Dr. Nurcan Tüzün for her scientific guidance, helps, and patience throughout my Ph.D. thesis. I am grateful for her confidence in me and my research.

I owe my best thanks to Dr. Matthias Stein for hosting me in his group at Max Planck Institute for Dynamics of Complex Technical Systems during the last two years of my Ph.D. course.

I would like to present my acknowledgements to Istanbul Technical University Research Fund BAP (Project numbers: 38209 and 39944) and the National Center for High Performance Computing of Turkey (UHEM) under Grant number 10732009 and 5004722017 for their financial support and providing the computer resources. I would also like to thank The Scientific and Technological Research Council of Turkey (TUBITAK) for granting me the 2214-A Research Grant and providing financial support during the course of my Ph.D. thesis.

I wish to express my special thanks to Dr. Feza Toker, for his precious mind, support and help.

May 2018

Esra BOZ
(Chemist)

TABLE OF CONTENTS

Page

FOREWORD .... **vii**
TABLE OF CONTENTS .... **ix**
ABBREVIATIONS .... **xi**
SYMBOLS .... **xiii**
LIST OF TABLES .... **xv**
LIST OF FIGURES .... **xvii**
SUMMARY .... **xix**
ÖZET .... **xxiii**
1. INTRODUCTION **1**
2. Ag-CATALYZED AZIDE ALKYNE CYCLOADDITION: A DFT APPROACH **3**
  2.1 Introduction 3
  2.2 Methods 5
  2.3 Results and Discussion 6
    2.3.1 Mononuclear mechanism 8
    2.3.2 Dinuclear mechanism 10
    2.3.3 Dinuclear mechanism with PH_3 15
  2.4 Conclusion 20
3. SYNTHESIS, REACTIONS AND DFT STUDY OF TROPOLONE DERIVATIVES **23**
  3.1 Introduction 23
  3.2 Methods 25
  3.3 Results and Discussion 25
  3.4 Conclusion 32
4. REGIOSELECTIVITY PATTERNS IN RADICALIC CYCLIZATION OF DIOSPHENOL DERIVATIVES WITH DIFFERENT RING SIZE **33**
  4.1 Introduction 33
  4.2 Computational Methods 34
  4.3 Results and Discussion 35
    4.3.1 Experimental findings 35
    4.3.2 Computational results 37
  4.4 Conclusions 42
5. CONTROL OF THERMODYNAMICS AND MICROKINETICS OF THE REDUCTIVE AMINATION REACTION BY ASSISTANCE OF SOLVENT AND CO-CATALYST **45**
  5.1 Introduction 45
  5.2 Computational Methods 48
  5.3 Results and Discussion 49
    5.3.1 Reaction thermodynamics 49
    5.3.2 Reaction mechanism 50
      5.3.2.1 The uncatalyzed reaction in neutral media 51
      5.3.2.2 Explicit water-coordination 55

5.3.2.3 The role of an acid as a co-catalyst 58
5.4 Conclusion.. 61
6. CONCLUSIONS AND RECOMMENDATIONS 65
REFERENCES 69
CURRICULUM VITAE 83

ABBREVIATIONS

AAC : Azide-alkyne cycloaddition
AgAAC : Ag(I)-catalyzed azide-alkyne cycloaddition
APT : Atomic polar tensors
B3LYP : Becke-Three Parameter Lee, Yang, Parr Density Functional
BPW91 : Becke and the PW91 GGA correlation functional of Perdew and Wang
CuAAC : Cu(I)-catalyzed azide-alkyne cycloaddition
DFT : Density Functional Theory
DMF : N,N-dimethylformamide
ECP : Effective Core Potential
HIV : Human Immunodeficiency Virus
HMBC : Heteronuclear Multiple Bond Correlation
IRC : Intrinsic Reaction Coordinate
M05 : Minnesota functionals, in 2005
M06L : Minnesota functionals, Local functional in 2006
MP : Møller–Plesset perturbation
MP2 : the second order Møller-Plesset perturbation theory
MWB28 : the Wood-Boring quasirelativistic Stuttgart large-core ECP
NBO : Natural Bond Orbital
PCP-SAFT : Perturbed Chain Polar Statistical Associating Fluid Theory
TBTA : Tris(benzyltriazolylmethyl)amine
THF : Tetrahydrofuran
TS : Transition State
SMD : Solvation model based on density
vdW : Van der Waals
ωB97XD : Functional by Head-Gordon and coworkers, which includes version of Grimme's D2 dispersion

SYMBOLS

Å : Angstrom
°C : Celcius
K : Kelvin
K_f : Thermodynamic equilibrium constant
ΔG : Relative Gibbs free energies

LIST OF TABLES

Page

Table 4.1 : Activation barriers calculated at UM05/6-311++G(d,p) level in benzene with PCM for the cyclization of 1 leading to different products. ($\Delta G^{\ddagger}$: Free energy of activation) **38**
Table 4.2 : Activation barriers calculated at UM05/6-311++G(d,p) level in toluene with PCM for the cyclization of 6 leading to different products. ($\Delta G^{\ddagger}$: Free energy of activation) **39**
Table 5.1 : The thermodynamics and solvent effects of the reductive amination reaction of various aldehydes with diethylamine ($(C_2H_5)_2NH$). ($\Delta G°r$, kcal/mol) **50**
Table 5.2 : Relative Gibbs free energies of the transition state and intermediate structures for reductive amination reaction in neutral media, in neutral media with explicit water assistance and in acidic media, respectively. **53**

LIST OF FIGURES

Page

Figure 2.1 : Ag (I) catalyzed AAC reaction between phenylacetylene and benzyl azide [32, 33].. **4**
Figure 2.2 : Proposed catalytic cycle for AgAAC reaction [33] (X: -Ph, $-C(CH_3)_3$, $-C_6H_{11}$, phosphadamantane derivative; Y: $-OCH_3$, $-CH_2OH$, $-COOCH_3$, $-CON(C_3H_7)_2$, $-CH_2N(CH_3)_2$) **5**
Figure 2.3 : Energy profile for the mononuclear Ag catalyzed azide-alkyne cycloaddition reaction path for model (M), real (R) and real ligand (RL) sets. Energies are not to scale. **8**
Figure 2.4 : 3D geometries of the structures involved in monometallic AgAAC reaction path for model (M) and real (R) sets. Selected bond lengths (in Å) and APT charges are shown on figures. **9**
Figure 2.5 : 3D geometry, selected bond lengths (in Å) and APT charges of the π type coordination of the silver (I) acetylide with lamellar structure. **11**
Figure 2.6 : 3D geometry, selected bond lengths (in Å) and APT charges of the Ag_2_A_M structure.. **12**
Figure 2.7 : 3D geometries, selected bond lengths (in Å) and APT charges of the type 1, 2, 3 transition state structures (Ag_2_TS_{AC}_M). (Energies are relative free energies with respect to the sum of the free energies of initial silver acetylide and azide structures).. **13**
Figure 2.8 : 3D geometries selected bond lengths (in Å) and APT charges of C, TS_{CD} and D structures for the Ag_2_M_1. .... **14**
Figure 2.9 : Energy profile for the binuclear Ag catalyzed azide-alkyne cycloaddition reaction path for model (M) set via Ag_2_TS_{AC}_M_1, Ag_2_TS_{AC}_M_2 and Ag_2_TS_{AD}_M_3 transition state structures. Energies are not to scale. **14**
Figure 2.10 : 3D geometries, selected bond lengths (in Å), and APT charges of structures for the Ag_2_R set.. **16**
Figure 2.11 : 3D geometries, selected bond lengths (in Å), and APT charges of A, TS_{AD} and D structures for the Ag_2_RL set. **17**
Figure 2.12 : Energy profile for the binuclear Ag catalyzed azide-alkyne cycloaddition reaction path for real (R) and real ligand (RL) sets. Energies are not to scale. **18**
Figure 2.13 : 3D geometries, selected bond lengths (in Å), and APT charges of A, TS_{AD} and D structures for the Ag_1_RL set. **19**
Figure 3.1 : Derivatives of tropolone.. **24**
Figure 3.2 : Synthesis of diosphenol thiocarbamates with $ClC(S)NMe_2$ and reactions of thiocarbamates with halides. **24**
Figure 3.3 : Synthesis of tropolone thiocarbamate with $ClC(S)NMe_2$. **26**
Figure 3.4 : Halide treatment and Newman-Kwart reaction of 10.......................... **26**
Figure 3.5 : Hydrolysis of 11. .... **26**
Figure 3.6 : A proposed mechanism for the formation of 11 from 10...................... **27**
Figure 3.7 : A proposed mechanism for the formation of 21 from 17...................... **27**

Figure 3.8 : 3D geometries, selected bond lengths (in Å) and relative free energies of E and Z isomers with minimum energy for 16 and 20. .... **28**
Figure 3.9 : APT charges on the selected atoms of 16_E and 20_E. **29**
Figure 3.10 : 3D geometries, free energies of activation and selected bond lengths (in Å) of transition states of E isomers with minimum energy for 16 and 20. .... **30**
Figure 3.11 : Reaction pathways of 16_E for two possible elimination products (Energies are not to scale)... **31**
Figure 3.12 : Reaction pathways of 20_E for two possible elimination products (Energies are not to scale)... **31**
Figure 4.1 : Synthesis of oxabicycloalkanones via radicalic cyclization of diosphenol-ω-haloalkyl ethers **34**
Figure 4.2 : Synthesis of 2-(3-iodopropoxy) cyclohepta-2,4,6-trienone from tropolone 5 in the presence of 1,3-diiodopropane and K_2CO_3 as base in boiling acetone. **35**
Figure 4.3 : Proposed mechanism for the synthesis of 2-(3- hydroxy propyl) cyclohepta-2,4,6-trienone. **36**
Figure 4.4 : Formation of 11 via H-abstraction... **37**
Figure 4.5 : TS's and intermediates leading to possible products after the radicalic initiation step... **38**
Figure 4.6 : Critical bond lengths (in Å, black) and APT charges (blue) on the TS structures and intermediates... **40**
Figure 4.7 : Critical bond lengths (in Å, black) and APT charges (blue) on the TS structures and intermediates... **41**
Figure 5.1 : Production of long chain diethylamines from aldehydes via reductive amination. **45**
Figure 5.2 : Proposed mechanism for the reductive amination of aldehydes. **46**
Figure 5.3 : Reaction mechanism including transition state and intermediate structures (top) and the energy profile for reductive amination reaction in neutral media (bottom). ($R_1 = R_2 = -CH_2CH_3$) **52**
Figure 5.4 : Details of the formation of the imine 5a and enamine 5b intermediates after proton abstraction to release water via TS_2a (C_α position) and via TS_2b (C_β position). **54**
Figure 5.5 : Reaction mechanism including transition states and intermediates and the energy profile for reductive amination reaction with explicit water assistance. ($R_1 = R_2 = -CH_2CH_3$) **56**
Figure 5.6 : The effect of the water assistance on pre-complex formation. (Distances are given in Å, black; NBO charges are presented in blue.).................. **57**
Figure 5.7 : Formation of the enol structure (3) from the aldehyde (1) in acidic conditions via protonation of the carbonyl oxygen and keto-enol tautomerization. **59**
Figure 5.8 : Reaction mechanism including identified transition state and intermediate structures and the energy profile for reductive amination reaction in the presence of an acid as a co-catalyst. ($R_1 = R_2 = -CH_2CH_3$) **60**
Figure 5.9 : Details of the role of the co-catalyst in the amine addition step. The first transition states (TS_1 and TS_7) from different precursors (1 and 3) via neutral and co-catalyst routes. **62**

COMPUTATIONAL INVESTIGATION OF ORGANIC REACTIONS VIA MECHANISTIC APPROACHES

SUMMARY

The importance of the theoretical approaches and computational tools has arised significantly in the past decades. The increase in performance of scientific computation has enabled fast and accurate calculations by parallel computing. Moreover, the recent developments in the Density Functionals Theory, such as new realease of advanced hybrid functionals facilitated fast and satisfactory results to explain the complex reaction network of various systems.

The main concept and purpose of this Ph.D. thesis is understanding the mechanisms of different classes of organic reactions. For this purpose, for each specific reaction system, all the possible transition states and intermediate structures through the reaction coordinate are evaluated and the detailed mechanism is investigated. Next step is focusing on the several possible pathways of the process which lead to various products and analyze them by means of thermodynamics and kinetics. Herein, computational chemistry methods have been utilized which are powerful tools to explain the outcome of the experiments. Understanding the mechanism in detail will enable synthesizing custom made products and is crucial for both the development of the currently employed procedures.

In the scope of this thesis, several computational modeling approaches have been utilized in order to investigate the reaction mechanisms of several systems. The thesis contains four chapters. First one is an organometallic cycloaddition reaction, following two are different reactions of tropolone and diosphenol derivatives and the last one is a co-catalyst assisted reductive amination reaction.

Triazoles are the building blocks of various biologically important compounds. They are utilized in many biological applications, including treatment of tumors, HIV, allergy, fungal infection and microbial diseases, since they can mimic peptide bonds. For the first time, 1,2,3-triazoles were assembled synthetically via Huisgen 1,3-dipolar cycloaddition of azides and alkynes (AAC). However, synthesis with this procedure is not regioselective and the reaction rate is very low even at high temperatures. In 2001, Sharpless et al. reported the first study on Cu catalyzed Click chemisty and since then, this methodology has found widespread usage, varying from functional to biological materials. Triazoles can be synthesized regioselectively with a very high rate in bening reaction conditions, in different solvents, both protic and aprotic, via Click procedure. After the successful application of the Cu catalyst, several transition metals which have been effectively used in alkyne cyclization reactions were tested. In 2005, ruthenium metal, whose catalytic activity on alkynes has been formerly known, was found as a catalyst for AAC that produces 1,5-disubstituted triazoles with internal alkynes. Ag and Au metals have also been tested as good candidates since they are congeners of the efficient Cu catalyst. In 2011,

McNulty et al. reported the first Ag (I) catalyzed reaction at room temperature in the absence of Cu metal. This reaction is promising in the sense that it is the first successful application of Ag catalyst alone in AAC reaction and has the advantage of being non toxic, which is especially crucial in biological applications.

The first successful and promising Ag catalyzed azide alkyne cycloaddition has been investigated by quantum mechanical calculations as a part of this thesis. The feasibility of the experimentally proposed reaction mechanism was investigated by modelling the profound intermediates and the transition state structures connecting them. Then, the number of metal atoms involved in the reaction process was examined comparatively, which is one of the main questions considered in mechanistic studies of Click reactions. Elucidating the reaction mechanism will enable more control over the synthesis and help to obtain tailor made products in good yields without involving toxic copper.

Tropolone is classified as a diosphenol, whose derivatives are known to act as medicaments. Stipitatic acid, puberulonic acid, colchicine, and hinokitol are some examples of tropolone derivatives, which have been isolated from natural products and have antimitotic, antiviral, antibacterial, anticancer effects. Tropolone and its derivatives are also used in some reactions as a starting material for synthetic purposes. Therefore, finding new and easy synthetic methods for obtaining tropolone derivatives is a valuable task in synthetic organic chemistry. Thus, quantum mechanical calculations are substantial in order to provide insights into the synthetic pathway and the nature of the regioselectivity in comparison to its analogous.

Second chapter deals with experimentally obtained regioselectivity of a tropolone system which shows structural similarity to diosphenol with different ring sizes. DFT calculations were performed on the key elimination step of the mechanism in order to elucidate the factors that led to different regioselectivity in the five-membered diosphenols and seven-membered tropolone. For this purpose, the key steps were modeled for both reagents by using computational tools to account on the proposed reaction mechanism and to investigate the structural and electronic effects that caused the difference in these two cases. The experimentally observed regioselectivity was correlated to the calculated activation barriers on five and seven-membered systems in the elimination step such that in both cases, experimentally observed product was favored over the alternative one. Thus, quantum mechanical calculations have provided insights into the synthetic pathway and regioselectivity of the reaction, in comparison to the analogous five-membered system.

Third chapter focuses on the radicalic reactions of 6- and 7-membered diosphenol derivatives with a significant difference in reactivity, ring size, aromaticity and stability. While the former is producing a mixture of products, the latter is resulting with a single product, regioselectively. DFT calculations were performed following the experimental studies in order to describe the outcomes correctly. Therefore, all possible reaction pathways were investigated for both structures to shed light on different selectivity routes governed by several factors. The driving factors for the observed regioselectivity was discussed in terms of the charge distribution at the reactive atoms, entropy factors, variation of dihedral torsion angle between the radicalic center and functionalized double bond and aromatization of the ring.

Amines are among the most important and frequently used chemical compounds due to their biologically active features and wide applications in industry. Reductive amination reactions are efficient and facile routes to synthesize long chain amines by using a diversity of aldehydes and ketones, and a variety of amines. The general route for the reductive amination is well documented. The exact mechanism, however, is dependent on the pH of the reaction medium and thus, the protonation state of the intermediates and the role of a coordinating solvent. The parameters affecting reaction performance and the selectivity such as type of the substrate and reaction conditions are still not fully understood. Fourth chapter presents a computational work on the mechanism of reductive amination including neutral and co-catalyst assisted (as explicit water and acid) reaction conditions. The reaction mechanism and the energy profile were characterized by MP2 calculations and an implicit SMD approach to account for polarity effects of the solvent. With explicit water assistance, the addition step proceeded in a stepwise fashion rather than concerted and the activation barrier was lowered. In the co-catalyst assisted system, the first part of the reaction (nucleophile addition) is kinetically disfavored compared to the neutral one and second half of the reaction is thermodynamically driven by the presence of an acid as a co-catalyst. Consequently, altering the reaction parameters does not only influence the reaction kinetics, but also the thermodynamic profile of the pathways in all cases. Further understanding on the reaction dynamics is essential to develop a microkinetic model of the reaction, to control and steer the process in order to rationally design reaction routes.

Optimizing the reaction conditions requires realising each mechanism in detail, through the process. In this study, we aim to investigate the feasibility of the experimentally proposed reaction mechanism by modelling the profound intermediates and the transition state structures connecting them. The overall interpretation of the results of this thesis will serve to a better understanding of the reaction thermodynamics, as well as kinetics of the processes. Elucidating the reaction mechanism will enable more control over the synthesis, help to obtain tailor made products in good yields and develop new alternatives for chemistry and beyond.

ORGANİK TEPKİMELERİN MEKANİSTİK YAKLAŞIMLAR KULLANILARAK HESAPSAL İNCELENMESİ

ÖZET

Son yıllarda, özellikle kimyasal tepkimelerin anlaşılması ve proseslerin yorumlanması konusunda teorik yaklaşımların ve hesaplamalı kimya yöntemlerinin önemi artmıştır. Bunun sebeplerinden biri, bilimsel hesaplama yöntemlerindeki performans artışıdır. Bu performans artışı bilgisayar teknolojilerinde sağlanan gelişmeyle birlikte hızlı ve kesin sonuçlar sağlayan paralel hesaplamaların yapılabilmesinden kaynaklanmaktadır. Ayrıca, Yoğunluk Fonksiyoneli Teorisi (YFT) alanında yapılan çalışmalar ve geliştirilen yeni fonksiyoneller sayesinde, kompleks reaksiyon sistemlerinin hızlı ve doğru bir biçimde yorumlanması mümkün olmuştur.

Bu doktora tezinin genel çerçevesi ve amacı, çeşitli organik reaksiyonların mekanizmalarını hesapsal kimya yöntemleri kullanarak incelemektir. Bu amaçla ilk olarak, her sisteme ait olası geçiş konumları ve ara ürünler modellenmiş; elde edilen veriler termodinamik ve kinetik olarak incelenmiştir. Söz konusu reaksiyonların deneysel çıktılarını ve ürün dağılımlarını açıklamak için olası yolların aktivasyon bariyerleri ve tepkime enerjileri karşılaştırılmıştır. Çözücü polaritesinin tepkime üzerine ve yük dağılımına etkisi çeşitli hesapsal kimya metotları kullanılarak incelenmiştir.

Tez dört ana bölümden oluşmaktadır. İlk bölümde organometal katalizörlü bir siklokatılma tepkimesi incelenmiştir. İkinci ve üçüncü bölümler tropolon türevlerinin halkalaşma tepkimelerinden oluşmaktadır. Son bölümde ise indirgen aminleştirme tepkimelerine ko-katalizörün etkisi incelenmiştir. Her bölümde, mevcut sistemin özelliklerini açıklayabilecek uygun hesapsal modelleme yaklaşımları kullanılmıştır.

Triazoller, biyolojik önem taşıyan birçok bileşiğin yapıtaşıdır. Peptit bağlarını taklit edebilme özellikleri sayesinde, tümör tedavisi, HIV, alerji, mantar enfeksiyonları ve mikrobiyal hastalıklar gibi çeşitli biyolojik uygulama alanları bulunmaktadır. 1,2,3-triazoller ilk olarak, Huisgen 1,3-dipolar azit ve alkin siklokatılma reaksiyonları ile sentezlenmiştir. Ancak bu prosedür, yüksek sıcaklıklarda bile düşük verimle ve ürün seçiciliği olmadan gerçekleşmektedir. 2001 yılında, Sharpless et al. tarafından Cu katalizörlü klik reaksiyonu ortaya konulmuştur ve bu metot çeşitli materyallerin sentezinde geniş uygulama alanı bulmuştur. Triazoller, klik metotu kullanılarak çeşitli solventler içinde yüksek verimli ve regioseçici olarak sentezlenebilmektedir. Cu metalinin başarılı uygulamalarını takiben çeşitli geçiş metallerinin bu metottaki etkinliği test edilmiştir. Alkinler üzerindeki katalitik aktivitesi daha önce bilinen Ru metali 2005 yılında AAC reaksiyonlarında başarı sağlanmış ve iç alkinler kullanılarak 1,5-disübstitüe triazoller elde edilmiştir. Daha sonra Cu benzeri olan Au ve Ag metallerinin potansiyel aktiviteleri üzerine deneyler yapılmıştır. 2011 yılında ilk defa McNulty et al. tarafından oda sıcaklığında ve Cu metali kullanılmadan Ag (I) katalizörlü reaksiyon başarıyla gerçekleştirilmiştir. Bu reaksiyon, Ag katalizörlü klik

tepkimelerinin başarılı ilk örneği olması ve gümüşün toksik özellik göstermemesi sayesinde biyolojik uygulamalarda kullanılabilirliği nedeniyle büyük önem taşımaktadır.

Birinci bölümde, Ag katalizörlü azit alkin siklokatılma reaksiyonu hesapsal yöntemler kullanılarak incelenmiştir. Bu reaksiyon, Ag metalinin klik reaksiyonlarındaki ilk başarılı örneğidir. Bu sebeple, deneyciler tarafından önerilmiş olan reaksiyon mekanizmasının detaylı olarak incelenmesi, sentez yönteminin ve reaksiyon veriminin geliştirilmesine katkı sağlayacaktır. Klik reaksiyonlarındaki temel sorulardan biri, reaksiyonda aktif olarak rol alan metal atomlarının sayısıdır. Mekanistik çalışmalar sırasında ayrıca, etkin metal sayısını tespit etmek için, farklı sayıda metal içeren sistemler karşılaştırmalı olarak incelenmiştir.

Tropolon ve diosfenol türevleri ilaç özelliği gösteren ve farklı ilaç sentezlerinde kullanılan bileşiklerdir. Stipitatik asit, puberulonik asit, kolşisin ve hinokitol bazı tropolon türevleridir. Bunlar çeşitli doğal bileşiklerden ekstrakte edilebilmekte ve antiviral, antibakteriyal ve antikanser özellik göstermektedir. Tropolon ve türevleri, birçok sentez reaksiyonunda başlangıç bileşiği olarak kullanılmaktadır. Bu sebeple tropolon türevlerinin eldesi, sentetik organik kimyanın önemli konularından biridir. Bu sebeple, bu reaksiyonların kuantum mekaniksel hesaplarla incelenmesi, mekanizmalarının aydınlatılması ve analogları ile karşılaştırılması önem taşımaktadır.

İkinci bölümde, tropolon türevlerinin reaksiyonlarında görülen yerseçicilik ile halka büyüklüğü arasındaki ilişki ele alınmıştır. Bu amaçla, yerseçilikte belirleyici olan ayrılma basamağı (eliminasyon), 5 ve 7 üyeli halkalar için YFT hesaplarıyla incelenmiştir. Farklı büyüklükteki halkalarda etkin olan yapısal ve elektronik özellikler karşılaştırılmıştır. Her iki sistemde görülen aktivasyon enerjisi farkına göre seçicilik açıklanmıştır.

Üçüncü bölümde, 6- ve 7-üyeli diosfenol türevlerinin reaktivite, aromatiklik ve stabilite açısından gösterdikleri belirgin farkların açıklanması hedeflenmiştir. Aynı şartlarda gerçekleştirilen 6 üyeli bileşiğin radikalik reaksiyonunda ürün karışımı elde edilirken, 7 üyeliye ait reaksiyon regioseçici olarak tek bir ürün oluşturmaktadır. Deneysel çalışmaların sonucunu açıklamak ve söz konusu ürün dağılımını inclemek için YFT hesapları yapılmıştır. İki yapı için seçicilik farkını oluşturan çeşitli faktörler tespit edilmiştir. Bu aşamayı kontrol eden faktörler, reaktif atomlar arasındaki yük dağılımı, entropi katkıları, radikalik merkez ve fonksiyonel çift bağ arasındaki dihedral açısı ve halkanın aromatikliği gibi etkenlerdir.

Aminler geniş çaptaki endüstriyel kullanımları ve biyolojik aktiviteleri sebebiyle, en önemli ve sık kullanılan kimyasal bileşiklerden biridir. İndirgen aminleştirme reaksiyonları, çeşitli aldehit ve ketonların basit aminlerle reaksiyonu sonucunda uzun zincirli aminlerin sentezlenmesi için kullanılan en etkin ve kolay yöntemlerden biridir. İndirgen aminleşme reaksiyonlarının ana basamakları literatürde geniş yer bulmaktadır. Ancak reaksiyon mekanizması, ortamın pH değerine, ara ürünlerin protonasyon seviyesine ve ara yapılara koordine olan solvent moleküllerine bağlı olarak değişebilmektedir. Bu parametrelerin reaksiyon verimini ve seçiciliğini etkilemekte olduğu bilinmektedir, ancak etki yolları tamamen anlaşılamamıştır.

Dördüncü bölümde indirgen aminleşme reaksiyonlarının mekanizması nötral ve ko-katalizör eşliğindeki koşullarda hesapsal olarak incelenmiştir. Reaksiyonun mekanizması ve enerji profili MP2 yöntemi ile hesaplanmış, çözücünün sisteme etkisi SMD yaklaşımı ile karakterize edilmiştir. Sonuç olarak reaksiyon parametrelerinin değiştirilmesiyle, reaksiyonların hem termodinamik hem de kinetik profillerinde değişimler görülmüştür. Reaksiyon dinamiklerinin daha iyi anlaşılması, mikrokinetik modellerin oluşturulmasını ve rasyonel reaksiyon tasarımlarının yapılmasını sağlayacaktır.

Bu tezden elde edilen sonuçlar, söz konusu reaksiyonların termodinamik ve kinetik özelliklerinin daha iyi anlaşılması açısından önem teşkil etmektedir. Üzerinde çalışılan reaksiyonun dinamikleri, olası kararlı ara ürün oluşumu, çözücünün tepkime hızına ve seçiciliğine etkisi gibi noktaların aydınlatılması, reaksiyon koşullarının optimize edilmesi ve hedef odaklı ürün sentezi için kritik önem taşımaktadır. Yapılan hesapsal çalışmalar, mevcut sentez şartlarına alternatif bakış açıları ve yeni teknikler sağlamayı hedeflemektedir.

1. INTRODUCTION

The main concept and purpose of this thesis is understanding the mechanisms of different classes of organic reactions with the help of computational chemistry tools. Generally, the flow of a computational study consists of several steps. First, all the possible transition states and intermediate structures through the reaction coordinate are evaluated and the detailed mechanism is investigated by using a suitable computational methodology, such as Density Functional Theory or ab initio calculations. Next step is focusing on the several possible pathways of the process which may lead to various products and analyze them by means of thermodynamics and kinetics. By this way, electronic or structural effects that lead to the observed products are explained or in some cases, anticipated products are identified. Thus, computational chemistry tools have been utilized as powerful agents to explain the outcome of the experiments.

The thesis contains four chapters and each of them deals with a specific reaction. First chapter targets an organometallic cycloaddition reaction, following two are different examples of cyclization reactions and the last one is a co-catalyst assisted reductive amination reaction. In the scope of each chapter, several computational modelling approaches have been utilized in order to investigate the reaction mechanisms of each system.

In the first chapter, this first successful and promising Ag catalyzed azide alkyne cycloaddition has been investigated by quantum mechanical calculations. The feasibility of the experimentally proposed reaction mechanism was investigated by modelling the profound intermediates and the transition state structures connecting them. Then, the number of metal atoms involved in the reaction process was examined comparatively, which is one of the main questions considered in mechanistic studies of Click reactions. Elucidating the reaction mechanism will enable more control over the synthesis and help to obtain tailor made products in good yields without interfering of toxic copper.

Second chapter deals with experimentally obtained regioselectivity of a tropolone system with different ring size. DFT calculations were performed on the key elimination step of the mechanism in order to elucidate the factors that led to different regioselectivity in the five-membered diosphenols and seven-membered tropolone. The experimentally observed regioselectivity was correlated to the calculated activation barriers on five and seven-membered systems in the elimination step such that in both cases, experimentally observed product was favored over the alternative one. Thus, quantum mechanical calculations have provided insights into the synthetic pathway and regioselectivity of the reaction in this study, in comparison to the analogous five-membered system.

Third chapter focuses on the radicalic reactions of 6- and 7-membered diosphenol derivatives with a significant difference in reactivity, ring size, aromaticity and stability. While the former is producing a mixture of products, the latter is resulting with a single product, regioselectively. DFT calculations were performed following the experimental studies in order to describe the outcomes correctly. Therefore, all possible reaction pathways were investigated for both structures to shed light on different selectivity routes governed by several factors. The driving factors for the observed regioselectivity was discussed in terms of the charge distribution at the reactive atoms, entropy factors, variation of dihedral torsion angle between the radicalic center and functionalized double bond and aromatization of the ring.

Fourth chapter presents a computational work on the mechanism of reductive amination including neutral and co-catalyst assisted (as explicit water and acid) reaction conditions. The reaction mechanism and the energy profile were characterized by MP2 calculations with an implicit solvent approach to account for polarity effects of the solvent. Altering the reaction parameters (pH of the media, explicit water assistance) does not only influence the reaction kinetics, but also the thermodynamic profile of the pathways in all cases. Consequently, further understanding on the reaction dynamics is essential to develop a microkinetic model of the reaction, to control and steer the process in order to rationally design reaction routes.

2. Ag-CATALYZED AZIDE ALKYNE CYCLOADDITION: A DFT APPROACH [1]

2.1 Introduction

Triazoles are 5-membered heterocycles, which are the building blocks of many biologically important compounds. They are utilized in many biological applications, including treatment of tumors [1, 2], HIV [3], allergy [4], fungal infection [5, 6] and microbial [7-11] diseases, since they can mimic peptide bonds [12]. For the first time, 1,2,3-triazoles were assembled synthetically via Huisgen 1,3-dipolar cycloaddition of azides and alkynes (AAC) [13, 14]. However, synthesis with this procedure is not regioselective and the reaction rate is very low even at high temperatures. In 2001, Sharpless et al. reported the first study on Cu catalyzed click chemisty and since then, this methodology has found widespread usage, varying from functional to biological materials [15, 16]. Triazoles can be synthesized regioselectively with a very high rate in bening reaction conditions, in different solvents, both protic and aprotic, via click procedure [12, 17-22]. After the successful application of the Cu catalyst, the scientists have searched for different transition metal analogues. Several transition metals which have been effectively used in alkyne cyclization reactions were tested [12, 23-27]. In 2005, ruthenium metal, whose catalytic activity on alkynes has been formerly known, was found as a catalyst for AAC that produces 1,5-disubstituted triazoles with internal alkynes [25-27]. Ag and Au metals have also been tested as good candidates since they are congeners of the efficient Cu catalyst. In a recent study, Veige et al. reported an inorganic version of click reaction with Au metal (Au-iClick) [28, 29]. In the literature, there are examples of Ag acetylides reacting with azides via assistance of Cu [30]. It has been reported by Silvestri et al. that Au (I) and Ag (I) acetylides are available with Cu (I) salts via a π complexation. However, in their work, no triazole product could be obtained with silver acetlylides in the absence of Cu or with only silver in its salt form [30]. In the work of Connell *et*

---

[1] This chapter is based on the paper "Boz, E and Tüzün, N. Ş. (2016). Ag-catalyzed azide alkyne cycloaddition: a DFT approach. Dalton Transactions, 45, 5752-5764. doi: 10.1039/c5dt04902d.

al. on Ag catalyzed azide-alkyne cycloaddition, the catalytic activity of binuclear $\{Ag_2(TBTA)_2\}(BF_4)_2$ complex was reported to arise from trace copper impurity coming from the ligand preparation step [31]. In 2011, McNulty *et al.* reported the first Ag (I) catalyzed reaction at room temperature in the absence of Cu metal (Figure 2.1) [32, 33].

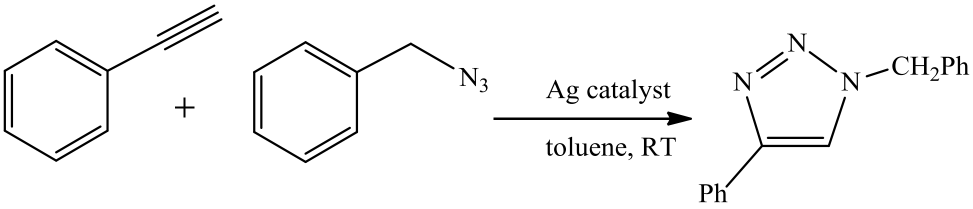

Figure 2.1 : Ag (I) catalyzed AAC reaction between phenylacetylene and benzyl azide [32, 33].

In their work, instead of silver salts, silver complexes that have lower toxicity were used. $\{Ag^+(L_2)(X^-)\}$ type complexes were studied using different types of hemilabile and bidentate P,O- and P,N-type ligands. Finally, they synthesized a stable crystalline complex using silver acetate and diisopropylamide ligand. Reaction conditions were optimised by investigating the effect of various silver (I) salts (AgOAc, Ag_2O, $AgNO_3$, AgOTf), several additives (benzoic acid and caprylic acid), ligands and the catalyst loading. As a result, 1,4-triazole product was obtained regioselectively in 98% yield from the reaction of phenylacetylene and benzyl azide in the optimum conditions. Later, Yanez et al. reported the successful alkyne-azide cycloaddition catalyzed by silver chloride and a silver N-heterocyclic carbene complex [34]. In their work, Ag_2O, $AgNO_3$ and Ag_2SO_4 have not promoted AgAAC reaction [34]. In the literature, a mechanism has been proposed for the AgAAC reaction (Figure 2.2) initiated with silver (I) acetylide structure, however, the key catalytic intermediates have not been identified or isolated in experiments [33]. In this study, the mechanism of AgAAC reaction will be studied by quantum mechanical calculations as a part of our ongoing interest in metal catalyzed azide-alkyne cycloaddition reactions [35]. This reaction is promising in the sense that it is the first successful application of Ag catalyst alone in AAC reaction.

Optimizing the reaction conditions, especially in terms of catalyst, requires understanding the mechanism in detail. In this study, we aim to investigate the feasibility of the experimentally proposed reaction mechanism by modelling the profound intermediates and the transition state structures connecting them.

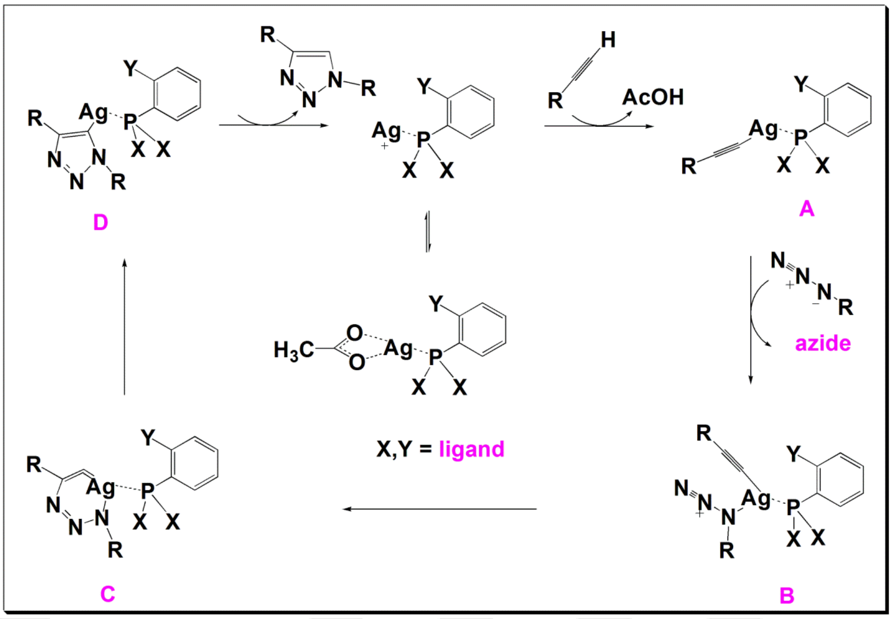

Figure 2.2 : Proposed catalytic cycle for AgAAC reaction [33] (X: -Ph, -$C(CH_3)_3$, -C_6H_{11}, phosphadamantane derivative; Y: -OCH_3, -CH_2OH, -$COOCH_3$, -$CON(C_3H_7)_2$, -$CH_2N(CH_3)_2$).

Elucidating the reaction mechanism will enable more control over the synthesis, help to obtain tailor made products in good yields and develop new alternatives for click chemistry and beyond.

2.2 Methods

In this study, a model system (M) has been studied with methyl substituted azide and alkyne compounds. Then, an experimentally studied reactant set, consisting of phenylacetylene and benzyl azide was investigated (Table inserted in Figure 2.3). This set has been referred to as real system (R) in the manuscript. In order to reduce structural influence stemming from the steric and electronic effects of substituted phosphane ligands reported in the experimental work, PH_3 has been considered as ligand in the catalyst for M and R systems. PH_3 ligand on the real system (R) has been modified to PPh_3 in order to generate a real ligand set (RL) to imitate the experimentally studied set [33]. Monometallic and bimetallic compounds are specified as Ag_1 and Ag_2, respectively. Structure A is named after the silver (I) acetylide ligand complex of the related system (Figure 2.2). Van der Waals (vdW) complex between silver (I)-acetylide-ligand and azide is labeled as B (Figure 2.2). Six membered metallacycle is stated as structure C and the triazole ring coordinated to silver is denoted as D (Figure 2.2). Three different transition states are defined as

TS_{AC}, TS_{CD}, and TS_{AD} where subscripts are labeled by the intermediates on both sides. Ag-Ag interactions are emphasized in 3D structures which have been specified as a strong affinity in the literature with a short distance of 2.88 Å, whereas in 2D pathways this relationship is ignored for clarity [36-38]. For bimetallic complexes, the numbering in Figure 2.6 will be used.

A preliminary benchmark calculation has been performed on a set of functionals (B3LYP, BPW91, M06L, ωB97XD) which have been used very frequently or reported to perform well especially with transition metals. For this purpose, the X-ray structures of Ag-catalyst complexes reported in the work of McNulty et al. have been used for comparative purposes. Among them ωB97XD [39] functional with MWB28 effective core potential and 6-31+G* basis set combination has been found not only to perform well on the system of concern, but also has a reasonable computational cost. All geometries were fully optimized with ωB97XD [39] functional and 6-31+G(d) basis set for all main group elements and MWB28 effective core potential for silver atom using Gaussian 09 software [40]. Frequency calculations were used to verify all stationary points with zero imaginary frequency and transition states having a single imaginary frequency.

Intrinsic reaction coordinate (IRC) calculations were performed on the transition state structures in order to confirm expected reactant and product on both sides [41, 42]. All energies referred in text are relative free energies calculated at 298 K in the gas phase. Atomic charges derived from atomic polar tensors (APT) are calculated at the same level of theory.

2.3 Results and Discussion

A reaction mechanism for Ag catalyzed AAC reaction has been suggested by McNulty et al., based on the generally accepted pathway for CuAAC (Figure 2.2) [33]. In the AgAAC experiment, transformation of a deuterated alkyne ended up a triazole with 55% loss of deuterium which is consistent with the silver (I) acetylide formation [33]. In the case of CuAAC, several experiments showed that CuAAC reactions do not reveal a product in the case of internal alkynes [15, 16, 43]. Based on this fact, Cu acetylide was proposed as the starting structure of the catalytic cycle and this suggestion has been supported by several computational and experimental studies [25, 44-49]. Thus, the pathway for AgAAC reaction was proposed to start with the formation of Ag-acetylide structures. Ag (I) complexes have been utilized as stoichiometric oxidant or catalyst in many oxidation reactions [50]. Stable and easily prepared solids of Ag acetylides have been reported in the literature [30]. They are reported to be polymeric species with limited solubility [51]. In this study, possible coordinations and configurations of silver (I) complexes have been investigated since the reaction is proposed to start with Ag-acetylides whose structures have not been determined experimentally and have a key importance in the reaction mechanism.

In a previous study, Ag-acetylide dissolving in pyridine was attributed to the Ag-N(pyridine) coordinate bond formation breaking up aggregates [30]. Likewise, in the AgAAC case, whether concerted or stepwise, there is a close Ag-N distance (between 2.16 - 2.38 Å) in the pathway of all covered cycloaddition reactions herein, which may help in preventing aggregation. This has been observed in the case of CuAAC where azide and ligands prevent formation of oligomeric copper aggregates [12, 44, 45].

Mono and dinuclear Ag-acetylides have been suggested in AgAAC as in the congener Cu case [33]. In CuAAC, there has been a debate on the number of copper atoms involved in the reaction and a consensus has been reached by theoretical calculations and experiments that more than one copper atom is actively involved in the reaction [12, 46, 47]. Accordingly, in this study, mono Ag and bis-Ag-acetylide structures with differing number of alkynes and ligands were modelled based on the experimental proposal and the well-known facts about the Cu catalyzed analog.

In the proposed mechanism, alkyne is coordinated to the silver in σ fashion via deprotonation of alkyne and yields a silver (I) acetylide. After azide coordination to the metal center and the cycloaddition steps, triazole compound is generated (Figure 2.2).

In modelling the proposed mechanism, ωB97XD functional and 6-31+G(d) basis set for all main group elements and MWB28 effective core potential for silver atom has been utilized for the three investigated systems (Please refer to the first paragraph of methodology for details of nomenclature and M, R and RL abbreviations used in the work).

2.3.1 Mononuclear mechanism

First, the monometallic mechanism that has been suggested in the literature was investigated, starting from Ag-acetylide with PH_3 ligand, Ag_1_A_M (Figure 2.4) [33]. At the initial step, azide group is coordinated to the silver metal while terminal nitrogen atom attacks to the more electropositive carbon (-0.23 vs -0.52) on the alkyne. In quantum mechanical calculations, existence of a van der Waals (vdW) complex before oxidative coupling step of metal-acetylide and azide has been questioned in various studies on both Ru and Cu catalyzed reactions and its possible presence on the reaction path was found to depend on the metal, ligands and the methodology [35, 47, 52]. In a recent experimental report, Cu-azide complexes in a CuAAC reaction could be identified for the first time in solution [20], presence of this complex is found to be depended on the methodology. With mono Ag, full convergence of such a complex could not be achieved at the level of theory in this study. In a concerted fashion, the coupling of methyl azide and propyne forms the triazole compound (Ag_1_D_M) via Ag_1_TS_{AD}_M with an activation barrier of 27.6 kcal/mol while the related structures of the stepwise mechanism could not be found (Figure 2.3).

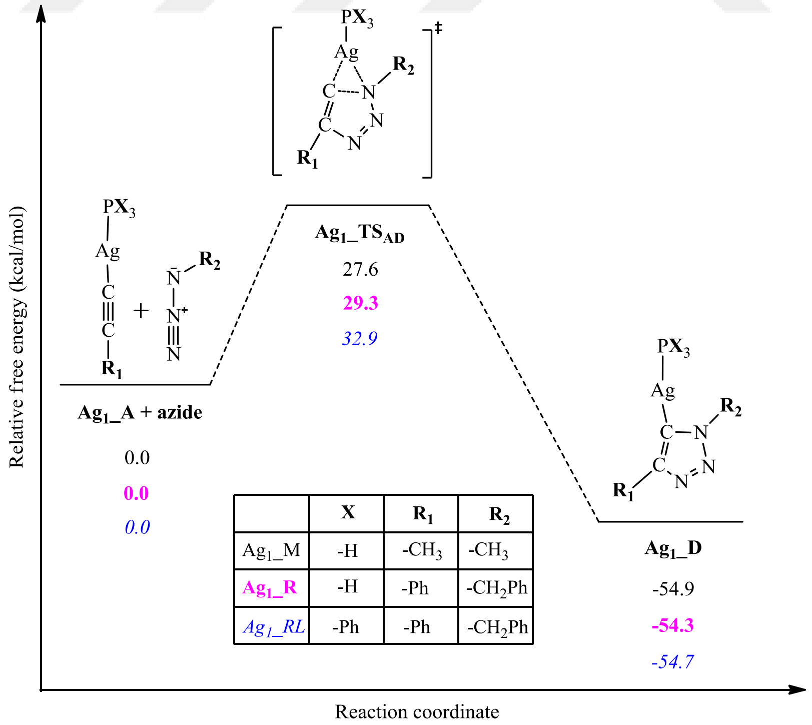

	X	R_1	R_2
Ag_1_M	-H	$-CH_3$	$-CH_3$
Ag_1_R	-H	-Ph	$-CH_2Ph$
Ag_1_RL	-Ph	-Ph	$-CH_2Ph$

Figure 2.3 : Energy profile for the mononuclear Ag catalyzed azide-alkyne cycloaddition reaction path for model (M), real (R) and real ligand (RL) sets. Energies are not to scale.

In analogous Cu and Ru pathways, mostly stepwise addition was reported to take place [27, 35]. In a study on CuAAC, the activation barrier of concerted monometallic mechanism has been found to be almost similar to the uncatalyzed process [53]. This could not explain the catalytic rate increase by the copper metal and led to a conclusion of stepwise mechanism for the reaction. In a latest topological study on CuAAC reaction, this concerted addition was reported to be favored depending on both ligands and the functionals used in the calculations [52]. Likewise, a concerted reaction pathway was found for mono Ag acetylide. In this system, a 6-membered metallacycle is unlikely to form, mainly due to the olefinic carbons. Terminal carbon in the alkyne should undergo hybridization to allow an sp^2-like structure to form a 6-membered ring.

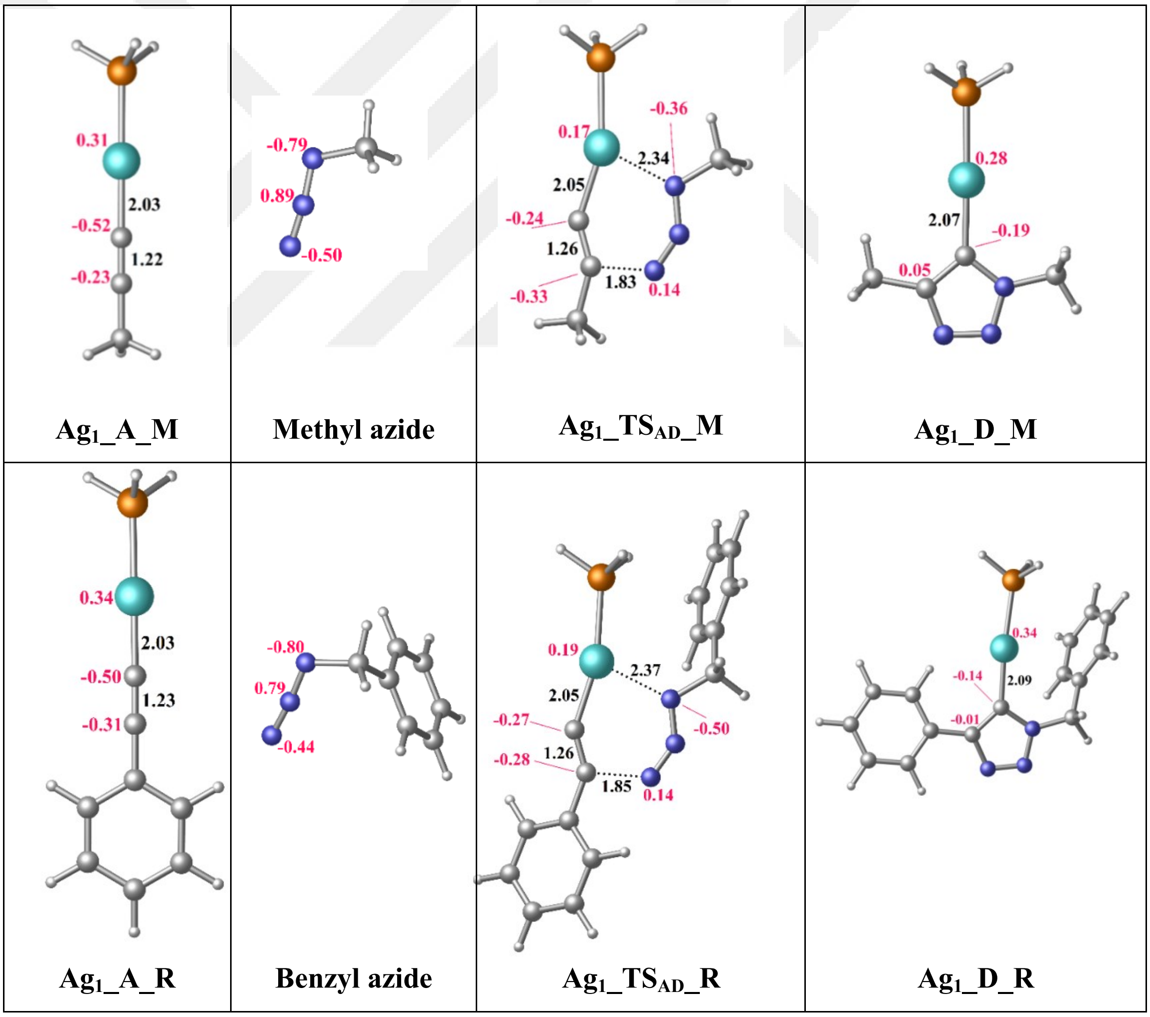
0.31
2.03
-0.52
1.22
-0.23
-0.79
0.89
-0.50
-0.36
0.17
2.34
2.05
-0.24
1.26
1.83
0.14
-0.33
0.28
2.07
-0.19
0.05
0.34
2.03
-0.50
1.23
-0.31
-0.80
0.79
-0.44
0.19
2.37
2.05
-0.27
-0.50
-0.28
1.26
1.85
0.14
0.34
-0.14
2.09
-0.01

Ag$_1$_A_M | Methyl azide | Ag$_1$_TS$_{AD}$_M | Ag$_1$_D_M

Ag$_1$_A_R | Benzyl azide | Ag$_1$_TS$_{AD}$_R | Ag$_1$_D_R

Figure 2.4 : 3D geometries of the structures involved in monometallic AgAAC reaction path for model (M) and real (R) sets. Selected bond lengths (in Å) and APT charges are shown on figures.

However, without any external assistance for coordination, this metallacycle is highly unfavorable in this case. The Ag-triazolide formation is exergonic by a relative free energy of -54.9 kcal/mol (Figure 2.3). The Ag metal can further detach by protonation of the heterocyclic ring and the catalytic turnover takes place. Then, monometallic mechanism has been explored by using the experimentally studied substrates which are phenylacetylene and benzyl azide (Real system). This reaction has the same concerted features as in the model mechanism. The activation barrier is 29.3 kcal/mol which is even higher than the model reaction.

Substituents on azide and alkyne have not caused dramatic changes in structures, charges and the pathway. The p-orbital in the olefinic carbon bonded to phenyl group is participating in the delocalization while the other p-orbital is interacting with the azide during cyclization. Thus, this carbon is slightly more negative as compared to its CH_3 (Ag_1_A_M) substituted analogue (-0.31 *vs.* -0.23).

2.3.2 Dinuclear mechanism

In the experimental study, no reaction was observed when started with silver phenyl acetylide and benzyl azide without catalyst [33]. This result showed that the catalyst has a role in both acetylide and product formation which invoked the idea of the presence of a bimetallic complex.

Different dinuclear Ag-acetylide structures containing one or two alkynes with one or two ligands have been considered as starting Ag-acetylide structures. These are as follows:

I. $[L\text{-}Ag\text{-}C{\equiv}C\text{-}R]_2$ type of (R = alkyl and L = ligand) dimeric silver (I) acetylide (Figure 2.5) structure where two $Ag\text{-}C{\equiv}C\text{-}R$ are linked to each other via π-coordination: Two different configurations of Ag-acetylide structure as active starting species have been modelled in this study. However, starting with these structures, a plausible mechanism could not be obtained. The basis set and the functional was changed, however, transition states for the reaction could not be obtained.

II. Cationic Ag acetylide structures containing two silver atoms with two ligands and one alkyne group were also tried, however, transition states could not be located for some of the steps.

III. For obtaining the electroneutrality (as in the work of Straub et al. on CuAAC) [22] Ag-acetylide structure with two Ag, two alkynes, and one ligand has been chosen (Ag_2_A_M structure in Figure 2.6). This model is based on CuAAC studies as well, especially on Fokin/Ahlquist model [21].

In case I, the structure in Figure 2.5 which involves $\mu_2-\eta^1-\eta^2$ type of bonding modes of Ag has been found as the most stable structure among the possible conformers and configurations. In this structure, the lamellar orientation of Ag-acetylides is maintained by π complexation of the Ag atoms with the olefins. An alternative structure with parallel phenyl groups headed towards the same direction is less stable by 13.6 kcal/mol. However, starting with the lamellar structure, neither transition state for azide addition nor the expected azide-Ag-acetylide complex could be located.

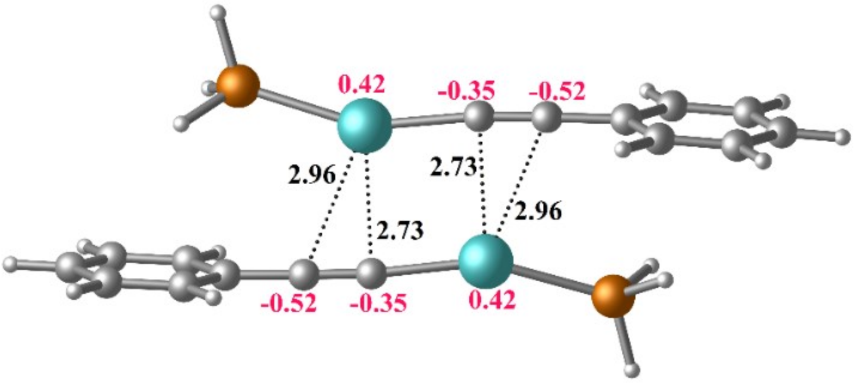

Figure 2.5 : 3D geometry, selected bond lengths (in Å) and APT charges of the π type coordination of the silver (I) acetylide with lamellar structure.

Azide addition to this Ag-acetylide structure was disfavored due to the stability of the $\mu_2-\eta^1-\eta^2$ complex. When the azide approaches, it is expected to hinge from the metal site first as in copper analogs. If the azide forms a complex, the strong π-coordination between the alkyne and the metal will be disturbed and weakened. In that case, Ag cannot compensate its loss with coordinating to other atoms in the system. Additionally, azide complexation will force the Ag atom to undergo pyramidilization which will disturb the well-established π-complex structure. This could lead to fragmentation as well.

The other alternative acetylide structure for the dinuclear case was μ_2-η^1-η^1 bonding mode (Case III) (Figure 2.6). Among the possible configurations, Ag_2_A_M was found as the most stable structure.

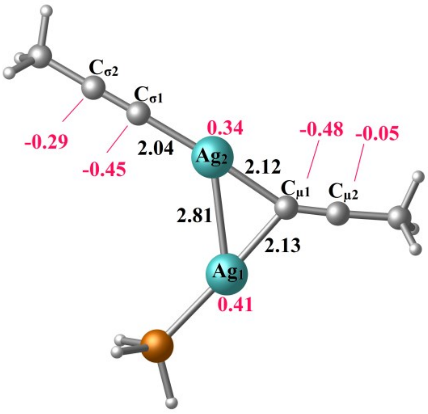

Figure 2.6 : 3D geometry, selected bond lengths (in Å) and APT charges of the Ag_2_A_M structure.

In this structure, the Ag-Ag distance is calculated as 2.81 Å. In the multinuclear silver (I) centered structures, argentophilicity, which can cause various unusual structural characteristics, is observed [54]. The theoretical studies by Pyykkö et al. have shown that the distance and the strength of metallophilic interactions depended strongly on the nature of the ligands [55-59]. Concerning the ligands considered in the AgAAC study herein, several computational studies have been carried on the dimer form of a silver-phosphine structure [H_3PAgCl], and Ag–Ag distances have been determined between 2.87–2.92 Å in the literature [54]. In our calculations, the Ag-Ag distances in the following silver-acetylide structures have been found as 2.81, 2.82 and 2.86 Å in M, R and RL systems, respectively. These distances are not only significantly shorter than that of the van der Waals radii for silver (3.44 Å) [60], but also shorter from the reported Ag-Ag separation of 2.88 Å in the metallic state [37] and the shortest interatomic distance in the ccp crystals of silver metal (2.89 Å) [36]. The calculated Ag–Ag distances become even shorter in the following intermediate structures of the pathway, fairly referring to a strong metallic interaction throughout the mechanism [37]. In a silver catalyzed reaction, the reactivity of Ag catalyst was attributed to electronic interactions between the two silvers and the unique coordination feature of the disilver (I) core [61]. In this study, unreactive nature of the silver (I) acetylide with lamellar structure (in Figure 2.5) could be attributed to the weak coordination between silver atoms with a distance of 3.32 Å.

The pathway of the AgAAC reaction is analyzed starting from the **A** structure. For the analysis, generally proposed mechanism was followed [33]. The reaction is proposed to start by azide addition. There are two different silver atoms in the Ag_2_A_M structure for azide coordination. In this step, three different transition states were investigated which involve coordination of azide to both Ag$_1$ and Ag$_2$: 1) Coordination to Ag$_1$ and attacking C$_\mu$ alkyne (via Ag$_2$_TS$_{AC}$_M_1), 2) coordination to Ag$_2$ and attacking C$_\mu$ alkyne (via Ag$_2$_TS$_{AC}$_M_2), 3) coordination to Ag$_2$ and attacking C$_\sigma$ alkyne (via Ag$_2$_TS$_{AD}$_M_3) (Figure 2.7). Unlike the first two cases, the last transition state led directly to 5-membered triazole structure. Relative free energies of these three transition states are 22.8, 27.9 and 26.1 kcal/mol, respectively. Transition states show that coordination to the more positively charged silver atom (Ag$_1$ vs Ag$_2$, Figure 2.6) is favored.

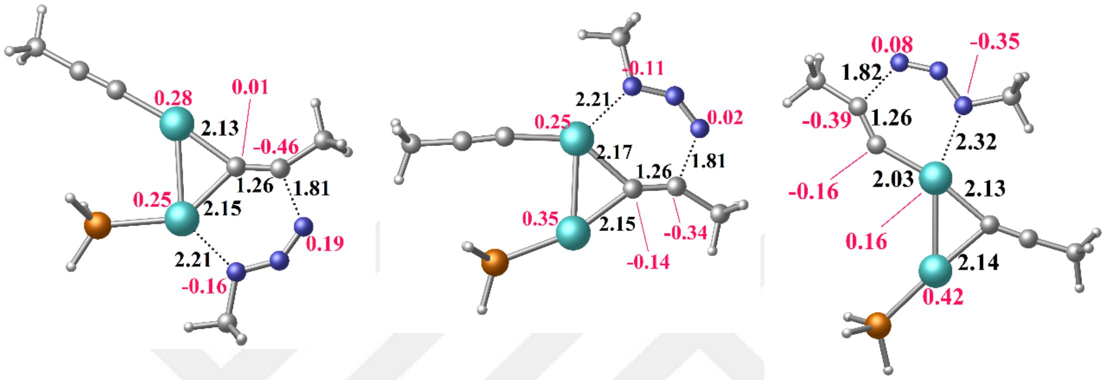

Ag$_2$_TS$_{AC}$_M_1 (22.8 kcal/mol)

Ag$_2$_TS$_{AC}$_M_2 (27.9 kcal/mol)

Ag$_2$_TS$_{AD}$_M_3 (26.1 kcal/mol)

Figure 2.7 : 3D geometries, selected bond lengths (in Å) and APT charges of the type 1, 2, 3 transition state structures (Ag$_2$_TS$_{AC}$_M). (Energies are relative free energies with respect to the sum of the free energies of initial silver acetylide and azide structures).

In Ag$_2$_TS$_{AC}$_M_1 and Ag$_2$_TS$_{AC}$_M_2 cases, critical bond lengths of the transition states are almost similar. In Ag$_2$_TS$_{AC}$_M_1, similar charge distribution of the silver atoms (0.25 and 0.28) provide stability to the structure. However, in Ag$_2$_TS$_{AD}$_M_3, there is a significant charge separation on silvers (0.42 and 0.16). In Ag$_2$_TS$_{AD}$_M_3, steric interactions between methyl group on the azide and C$_\mu$ alkyne cause a weaker coordination between Ag$_2$ and azide (2.32 Å) which led to a stronger interaction between Ag$_2$ and C$_\sigma$ alkyne (2.03 Å) as compared to other transition state structures. Ag$_2$_TS$_{AD}$_M_3 has slightly modified from the initial silver acetylide (A) complex, thus, Ag$_2$_TS$_{AD}$_M_3 is an early transition state and it is even earlier than Ag$_2$_TS$_{AC}$_M_2, leading to a lower barrier.

Following Ag$_2$_TS$_{AC}$_M_1 (Figure 2.9) a 6-membered metallacycle (C) has been formed. Then, the metallacycle Ag$_2$_C_M (Figure 2.8) has been exothermically converted to 1,4-disubstituted triazole ring (Ag_2_D_M) via a second transition state (Ag_2_TS_{CD}_M), which is directly coordinated to both silver metals. The highest point on the reaction path corresponds to TS_{AC}, where azide addition takes place.

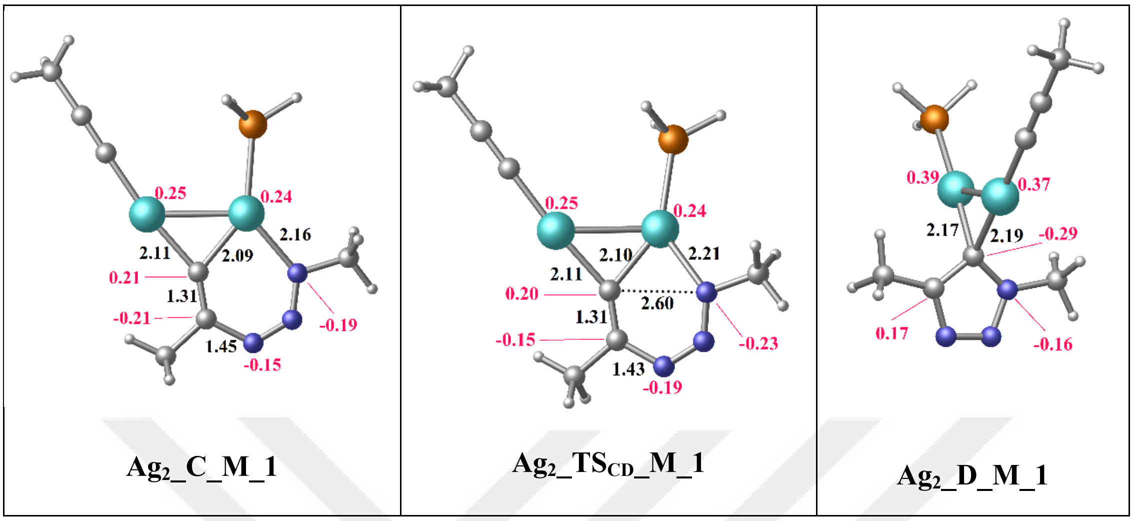
0.25
0.24
2.16
2.11
2.09
0.21
1.31
-0.21
-0.19
1.45
-0.15
0.25
0.24
2.10
2.21
2.11
0.20
2.60
1.31
-0.15
-0.23
1.43
-0.19
0.39
0.37
2.17
2.19
-0.29
0.17
-0.16

Ag_2_C_M_1 **Ag_2_TS_{CD}_M_1** **Ag_2_D_M_1**

Figure 2.8 : 3D geometries selected bond lengths (in Å) and APT charges of C, TS_{CD} and D structures for the Ag_2_M_1.

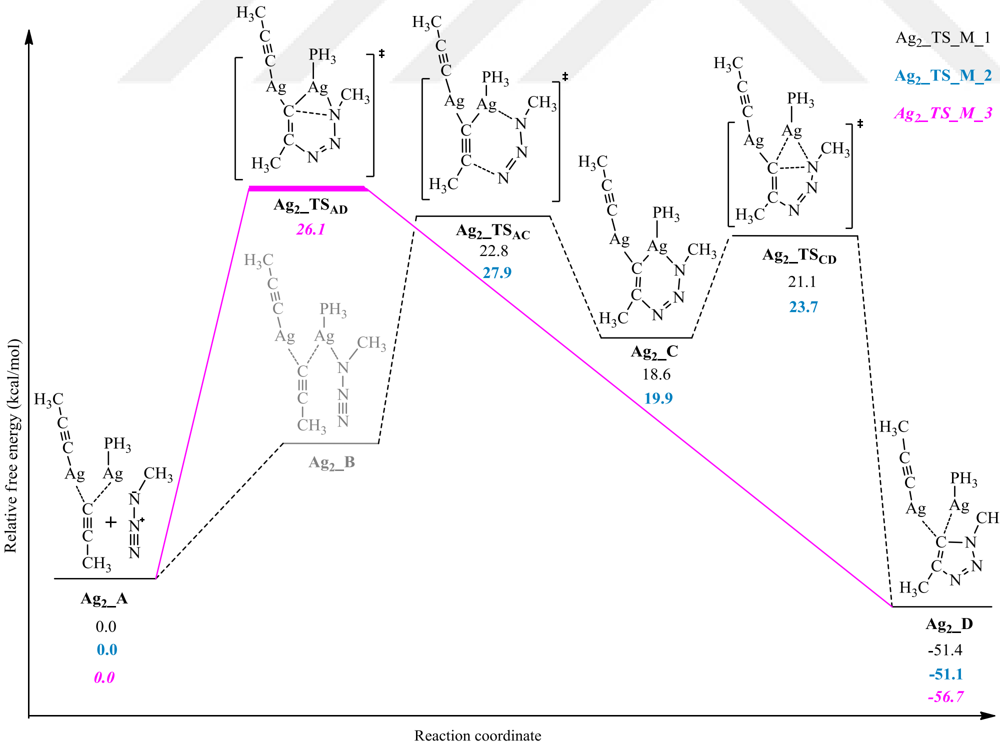
Ag₂_TS_M_1
Ag₂_TS_M_2
Ag₂_TS_M_3
Relative free energy (kcal/mol)
Reaction coordinate
Ag₂_A
0.0
0.0
0.0
Ag₂_B
Ag₂_TS_AD
26.1
Ag₂_TS_AC
22.8
27.9
Ag₂_C
18.6
19.9
Ag₂_TS_CD
21.1
23.7
Ag₂_D
-51.4
-51.1
-56.7
H₃C
PH₃
Ag
CH₃
N
C
‡

Figure 2.9 : Energy profile for the binuclear Ag catalyzed azide-alkyne cycloaddition reaction path for model (M) set via Ag_2_TS_{AC}_M_1, Ag_2_TS_{AC}_M_2 and Ag_2_TS_{AD}_M_3 transition state structures. Energies are not to scale.

Cyclization to 5-membered ring via Ag_2_TS_{CD}_M (Figure 2.8) is very close in energy to that of Ag_2_TS_{AC}_M (21.1 vs 22.8 kcal/mol) as in copper analogues (Figure 2.9) [35, 47, 52]. Triazole formation will take place via protonation of structure Ag_2_D_M. The alternative reaction path (Figure 2.9) via transition state Ag_2_TS_{AC}_M_2 (Figure 2.7) will follow the same intermediates and transition states, where they are 2-5 kcal/mol higher in energy. However, the reaction via Ag_2_TS_{AD}_M_3 has resulted with a concerted fashion, contrary to the other two cases. Thus, the model reaction is expected to proceed stepwise via addition to Ag_1 and $C_{\mu 2}$.

2.3.3 Dinuclear mechanism with PH_3

Then, a system with the experimentally studied reactants has been explored. For this purpose, addition reaction of benzyl azide and phenylacetylene has been modelled first by a model ligand, PH_3 (named R) then with the triphenylphosphine ligand (PPh_3) (named RL), as reported in the experiment [33]. In the real system (R), coordination mode of the Ag_2_TS_{AC}_M_1 (Figure 2.7) transition structure, which had the lowest barrier compared to Ag_2_TS_{AC}_M_2 and Ag_2_TS_{AC}_M_3, was used. Presence of benzyl and phenyl groups have not changed the geometry of the Ag-acetylide (Ag_2_A_R) complex, however the charges of the Ag atoms have become more positive with respect to Ag_2_A_M due to electron withdrawing effect of the phenyl groups (Figure 2.10). A van der Waals complex could not be located for this set. The transition state, Ag_2_TS_{AC}_R, has revealed a 6-membered intermediate which required a barrier of only 1.0 kcal/mol to form the 5- membered triazolide ring via reductive elimination (Ag_2_TS_{CD}_R). However, structures from IRC calculations have convergence problems, possibly because of the flat potential energy surface at that point of the reaction coordinate.

An analogous situation has also been reported for the case of CuAAC, by Calvo-Losada et al. that the nature of the mechanism, concerted vs stepwise could change depending on the ligand and solvent and it has been concluded that the "stability of the 6-membered metallacyclic intermediate" played the vital role [52]. Then, bimetallic real system has been investigated with the experimentally studied triphenylphosphine ligand (named RL).

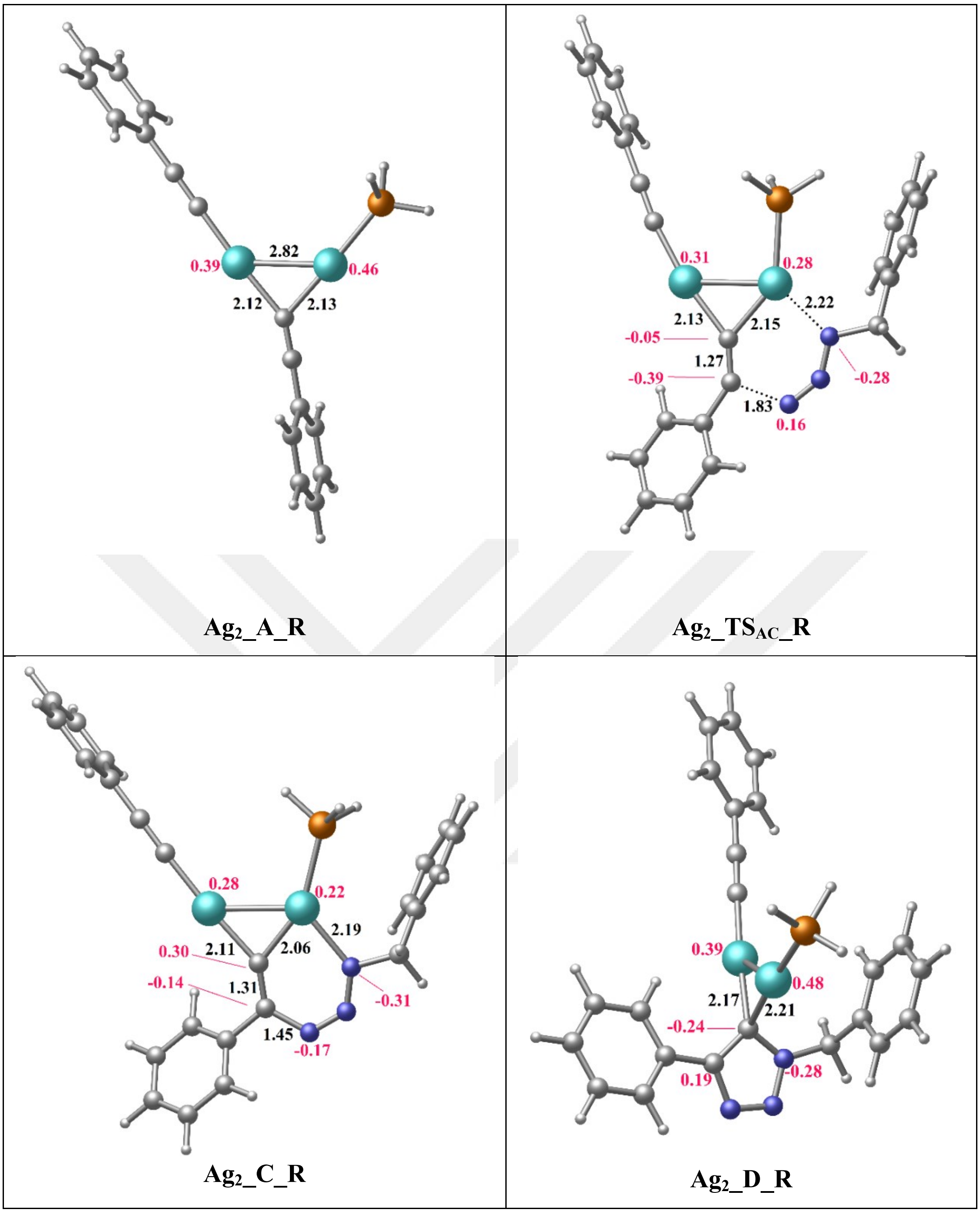
2.82
0.39
0.46
2.12
2.13
0.31
0.28
2.22
2.13
2.15
-0.05
1.27
-0.28
-0.39
1.83
0.16
0.28
0.22
2.19
0.30
2.11
2.06
-0.14
1.31
-0.31
1.45
-0.17
0.39
0.48
2.17
2.21
-0.24
0.19
-0.28

Ag$_2$_A_R

Ag$_2$_TS$_{AC}$_R

Ag$_2$_C_R

Ag$_2$_D_R

Figure 2.10 : 3D geometries, selected bond lengths (in Å), and APT charges of structures for the Ag$_2$_R set.

The coordination mode of the silver acetylide structure of the RL set (μ_2-η^1-η^2) (Ag$_2$_A_RL in Figure 2.11) is different from the analogues structures (μ_2-η^1-η^1, Ag$_2$_A_M in Figure 2.6 and Ag$_2$_A_R in Figure 2.10). However, whether started with μ_2-η^1-η^2 or μ_2-η^1-η^1 type, approaching azide transforms the coordination mode to μ_2-η^1-η^1 in the transition state and in the following structures. In this system, no 6-

membered metallacycle or transition state (TS_{AC}) for the oxidative addition could be obtained.

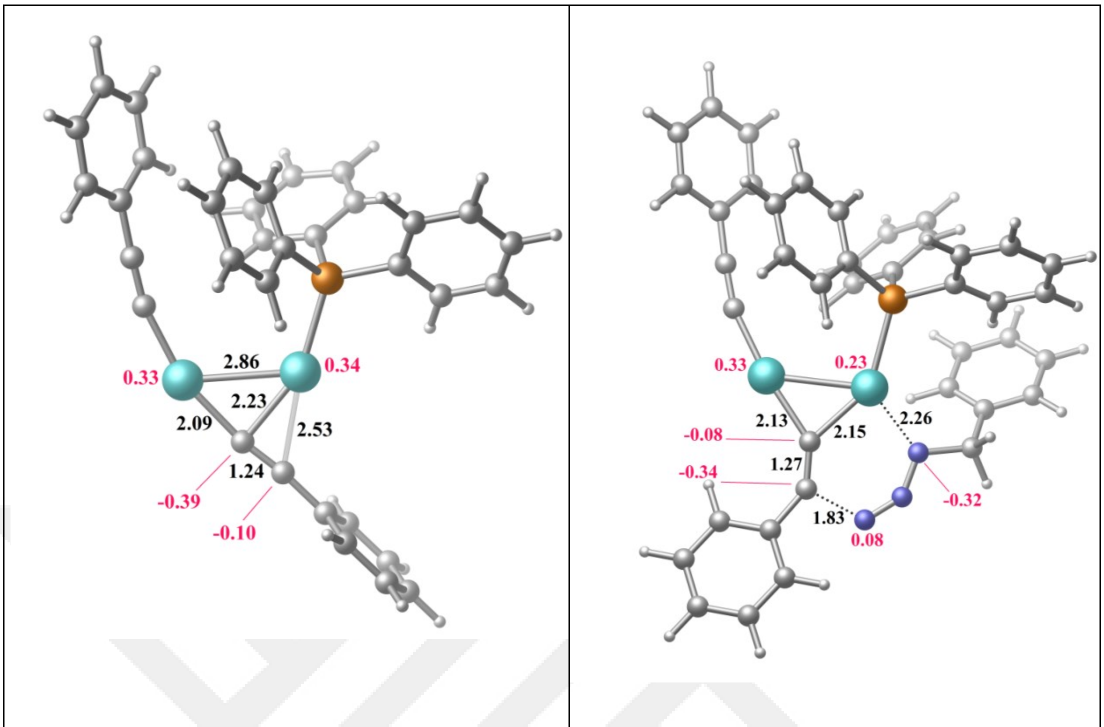
0.33
2.86
0.34
2.23
2.09
2.53
1.24
-0.39
-0.10
0.33
0.23
2.13
2.15
2.26
-0.08
1.27
-0.34
-0.32
1.83
0.08

Ag_2_A_RL

Ag_2_TS_{AD}_RL

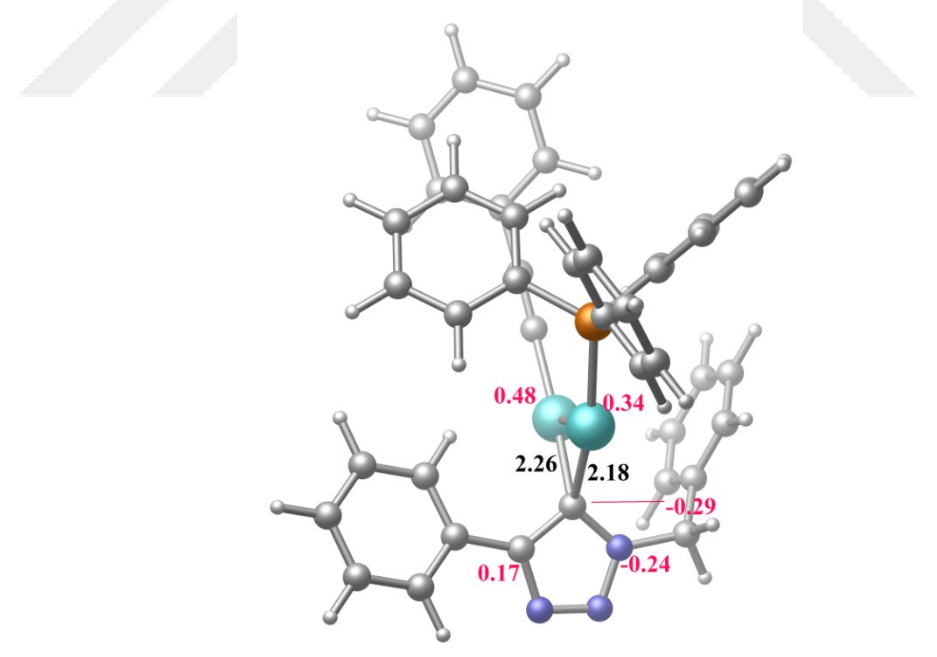
0.48
0.34
2.26
2.18
-0.29
0.17
-0.24

Ag_2_D_RL

Figure 2.11 : 3D geometries, selected bond lengths (in Å), and APT charges of A, TS_{AD} and D structures for the Ag_2_RL set.

Triazole could be directly obtained from the Ag-acetylide structure (Figure 2.12) in a concerted fashion. The main difference between Ag_2_R (PH_3 ligand) and Ag_2_RL

(PPh$_3$ ligand) systems (Figure 2.11) is steric effects stemmed by the phenyl groups on the phosphor atom.

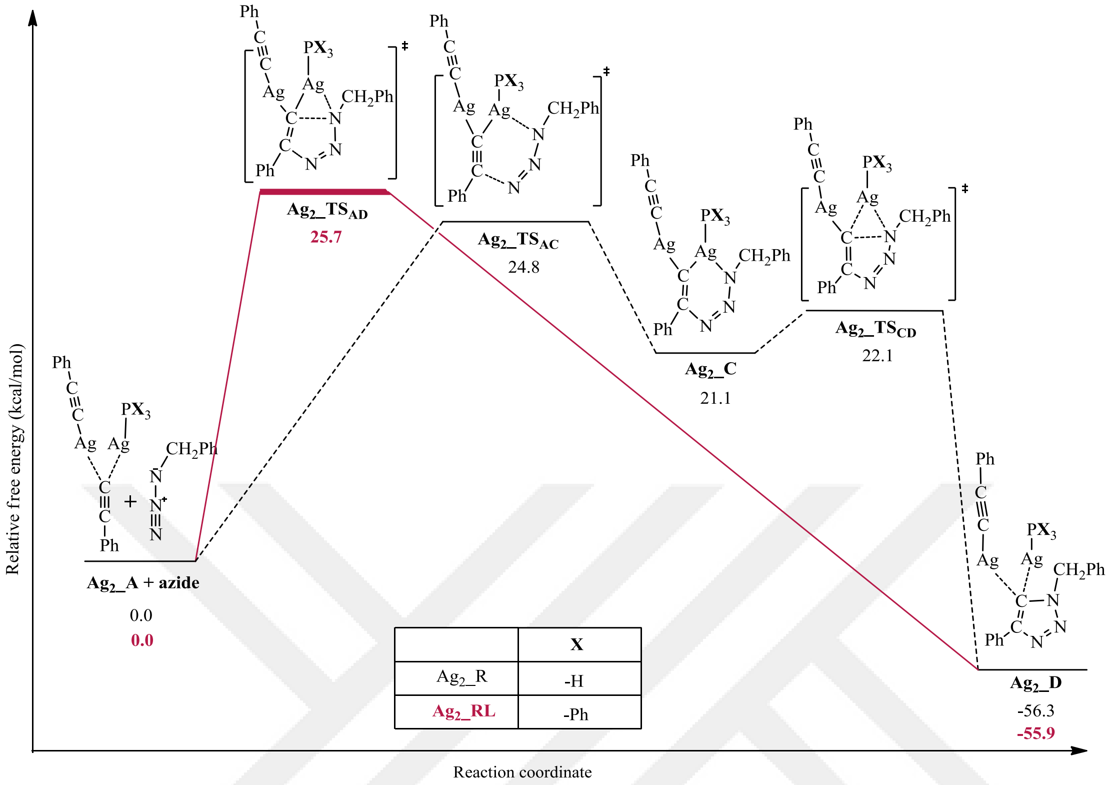

Figure 2.12 : Energy profile for the binuclear Ag catalyzed azide-alkyne cycloaddition reaction path for real (R) and real ligand (RL) sets. Energies are not to scale.

In the 6-membered metallacyclic structure C, the 3-membered ring formed by Ag atoms is coplanar with the 6-membered metallacycle, as in Ag$_2$_C_M. In the 5-membered ring, planarity of the two rings is perturbed and the rings are in perpendicular orientation with respect to each other. In transition state (Ag$_2$_TS$_{AD}$_RL), this planarity is disturbed by the Ag$_1$ atom which is almost 11.5° out of the plane of N-C-C which was 4.0° in Ag$_2$_TS$_{AC}$_R and 0.5° in the model case. The planarity imposed in the 6-membered metallacyclic structure causes unfavorable steric interactions due to the bulky substituents in the RL case (Figure 2.11). Thus, it is presumably highly unstable and cannot be located as a stationary point on the potential energy surface and forces the reaction to concerted fashion. The barrier for the reaction is 25.7 kcal/mol, which is a slightly higher value than that of model systems in this study. The question referring to the monometallic and bimetallic nature of the reaction was reverted for the RL system. A concerted mechanism with a barrier of 32.9 kcal/mol (Figure 2.3) could be obtained for the monometallic reaction for RL (Figure 2.13) system. This high barrier is almost competitive to the uncatalyzed case and incompatible with the nature of the catalysis.

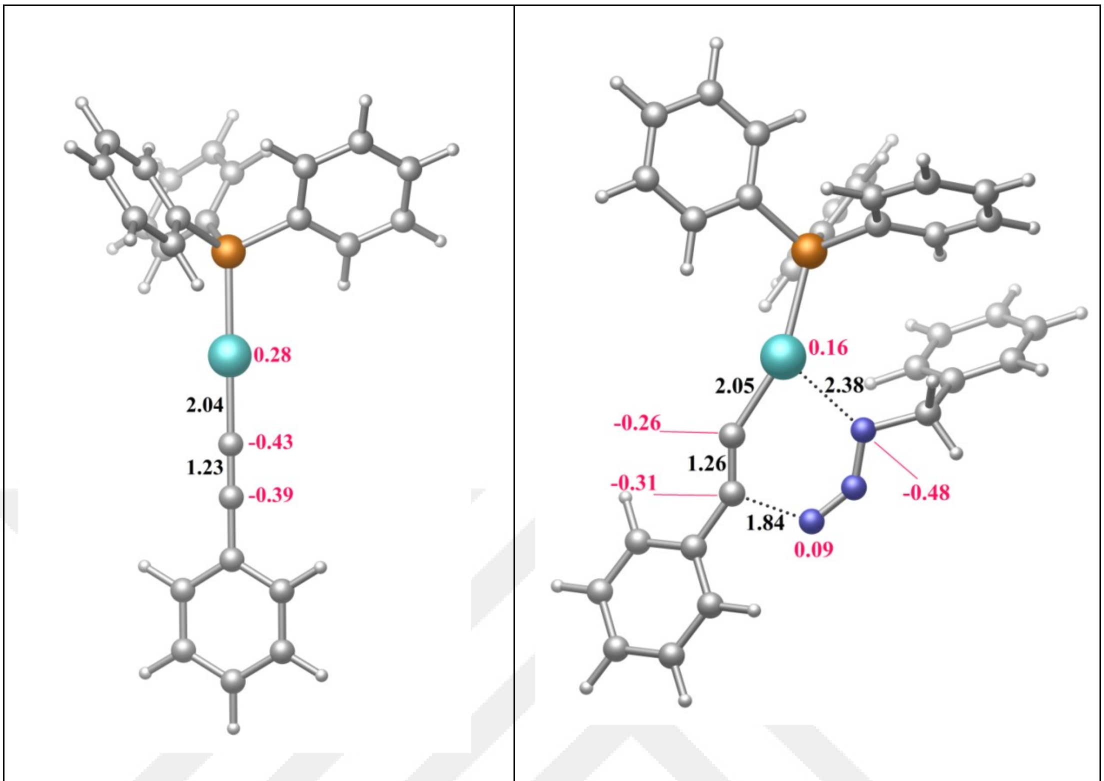
0.28
2.04
-0.43
1.23
-0.39
0.16
2.05
2.38
-0.26
1.26
-0.31
1.84
0.09
-0.48

Ag$_1$_A_RL **Ag$_1$_TS$_{AD}$_RL**

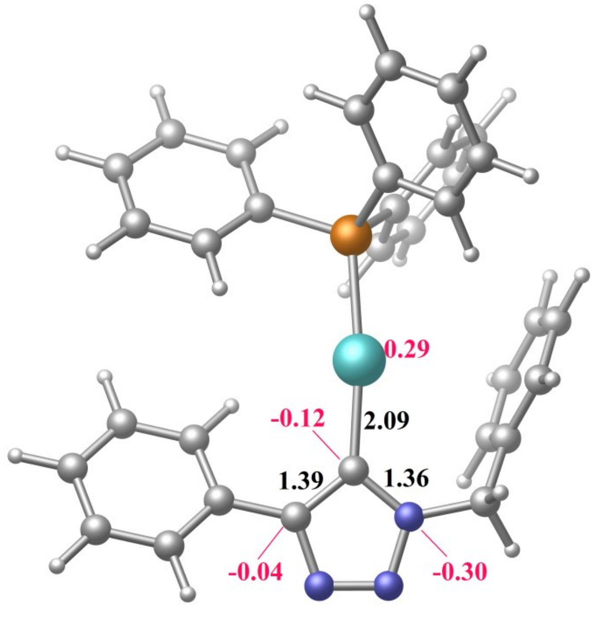
0.29
-0.12
2.09
1.39
1.36
-0.04
-0.30

Ag$_1$_D_RL

Figure 2.13 : 3D geometries, selected bond lengths (in Å), and APT charges of A, TS$_{AD}$ and D structures for the Ag$_1$_RL set.

The comparative stability of dinuclear vs mononuclear Ag-acetylides was also questioned. Formation of a dinuclear complex from mononuclear is exergonic [2 x (Ag_1_A_M) vs Ag_2_A_M + PH_3] by 9.4 kcal/mol which may contribute to dinuclear reference. Thus, a bimetallic path is more likely to occur according to calculations herein.

2.4 Conclusion

In this study, the mechanism for AgAAC reaction has been modelled for the first time with quantum mechanical calculations by considering the experimental proposal and the general CuAAC pathway. The calculations herein show that once the proposed silver acetylide structures form, their cycloaddition with azide following the proposed path is a facile reaction in terms of energetics.

The number of metal atoms involved in a click reaction is one of the main questions considered in mechanistic studies. In AgAAC reaction, comparison of mononuclear and binuclear paths shows that the barrier for binuclear cases are lower than that of mononuclear by 4.8, 4.5 and 7.2 kcal/mol in M, R and RL systems. Although not high, the effect of the barrier differences is reflected in the relative rates of mono and dinuclear cases. Assuming the pre-exponential factors to be equal, the dinuclear case is almost 600-30000 times faster than the mononuclear for M, R and RL systems at the reaction temperature, 80°C. This result is similar to a recent report on CuAAC where dinuclear complex was stated to be kinetically favored among the active mono- and bis-copper species [17]. As in copper case, a second silver atom is needed for assisting the terminal alkyne carbon to undergo hybridization from sp to sp^2. Furthermore, in a recent experimental study on silver (I) catalyzed carborane synthesis, presence of a bimetallic intermediate has been proved by mass spectrum analysis [62]. In the bimetallic paths, the Ag-Ag distances in several structures show that the argentophilic interactions are significant in the modeled silver complexes in this study.

All these results emphasize the critical role of a second metal atom in the reaction which can be concluded as the superiority of dinuclear mechanism to mononuclear case. The key intermediates and the number of Ag metals actively involved in AgAAC reaction presents a strong correlation with the Cu analog.

In evaluating these results care must be taken because in the experiments, the reaction took place with a high yield in the presence of a X= *t*Bu and Y= $\mathrm{CON}(i\mathrm{Pr})_2$ ligands (see Figure 2.2) under optimum conditions. However, this work is important in the sense that this is the first computational work on this potentially versatile and efficient process. Since the silver compounds represent a new form of potential catalyst, this study should be extended by considering the sterically demanding *N*,*N*-diisopropylamide and di-tert-butyl-phosphane substituted ligands which are substantial to improve reaction yield, at the same time computationally cumbersome. To elucidate the mechanism and the ligand effect in this promising reaction will help to increase its yield and the effectiveness of the AAC reaction with the Ag metal.

3. SYNTHESIS, REACTIONS AND DFT STUDY OF TROPOLONE DERIVATIVES[2]

3.1 Introduction

Tropolone is classified as a diosphenol, whose derivatives are known to act as medicaments. Stipitatic acid (1) [63], puberulonic acid (2)[64, 65], a commercially available drug [66, 67], colchicine (3) [68], and hinokitol (4) [69] are some examples of tropolone derivatives, which have been isolated from natural products and have antimitotic, antiviral, antibacterial, anticancer effects. Tropolone and its derivatives are also used in some reactions as a starting material for synthetic purposes [66, 70-72]. On the other hand, 3-mercaptotropone (3-mercapto 2,4,6-cycloheptatrien-1-one) is a member of troponoid family. While β derivatives are used in some synthesis, to our knowledge, no related record could be found for the 3-mercaptotropone in the literature [64, 65]. Therefore, finding new and easy synthetic methods for obtaining tropolone derivatives is a valuable task in synthetic organic chemistry (Figure 3.1). In this respect, we decided to apply a procedure to replace the enolic hydroxyl group on tropolone with -Cl, -Br, -I after converting to dimethylthiocarbamate derivative (10). For this purpose, an earlier study has been utilized with proper modifications for the examination of N,N-dimethylthiocarbamate of tropolone [73-75]. The synthesis and the reactions of diosphenol thiocarbamates (6) with some nucleophiles have been inspected in detail (Figure 3.2) [73, 74]. While replacement of the enolic oxygen of diosphenols (5) by chlorine or bromine were achieved by treating the dimethylthiocarbamate of 5 with lithium chloride or bromide in hot acetonitrile/acetic acid [74], treatment with lithium iodide gives replacement with hydrogen (Figure 3.2) [73].

---

[2] This chapter is based on the paper "Zaim, Ö., Tüzün, N. Ş.¸ Çevik, B., Özcan, H., Boz, E. (2015), Synthesis, reactions and DFT study of tropolone N,N-dimethylthiocarbamate. Tetrahedron, 71, 5391-5398. doi: 10.1016/j.tet.2015.05.100.

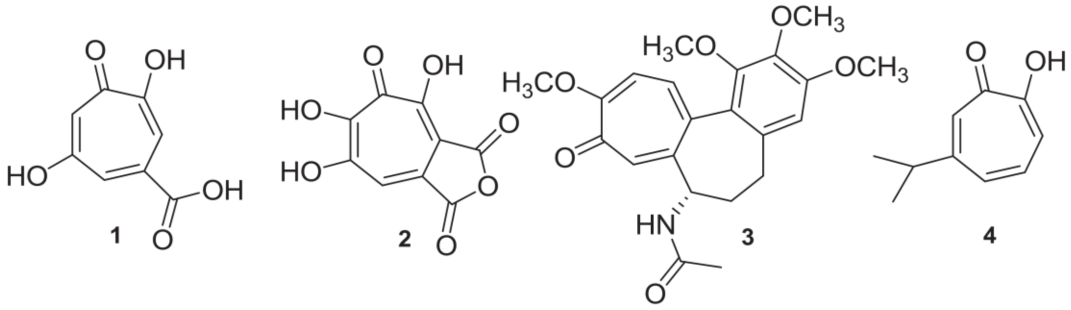
O
OH
HO
OH
O
1
O
OH
HO
HO
O
O
2
O
OCH$_3$
H$_3$CO
OCH$_3$
H$_3$CO
O
HN
O
3
O
OH
4

Figure 3.1 : Derivatives of tropolone.

Additionally, several 2-azido- and 2-thiocyanato-2,3-unsaturated cyclohexanones were prepared starting from 1,2-cyclohexanediones by using the same method [75]. In contrast to previous investigations [73-75], in this study seven membered tropolone ring (9) was converted to a 3-substituted-2,4,6-cycloheptatrien-1-one (11) by following the same experimental procedure.

Newman-Kwart rearrangement is also possible since thiocarbamates are involved in this reaction and an experiment was performed to observe if any related product formed [76].

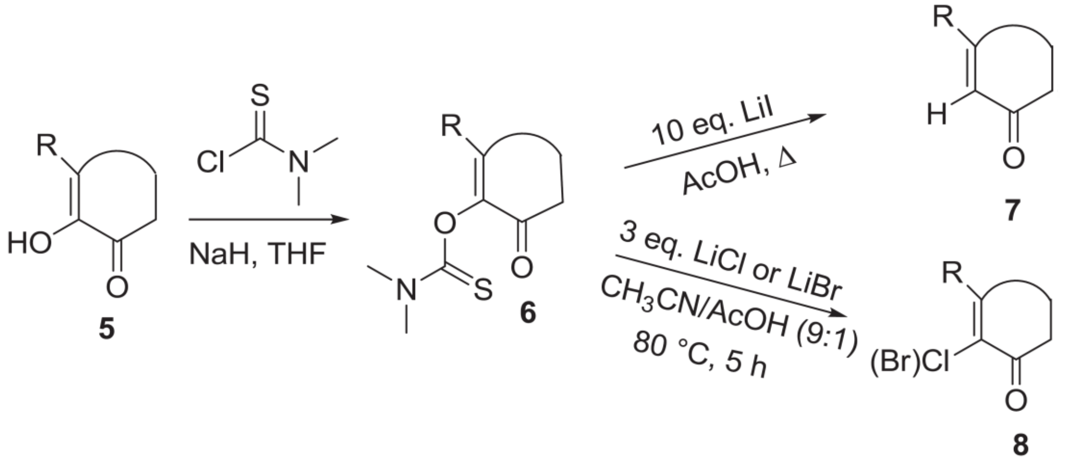
R
HO
O
5
S
Cl
N
NaH, THF
R
O
N
S
O
6
10 eq. LiI
AcOH, Δ
R
H
O
7
3 eq. LiCl or LiBr
CH$_3$CN/AcOH (9:1)
80 °C, 5 h
R
(Br)Cl
O
8

Figure 3.2 : Synthesis of diosphenol thiocarbamates with ClC(S)NMe$_2$ and reactions of thiocarbamates with halides.

As a part of this study, quantum mechanical calculations were performed in order to elucidate the dynamics in the five-membered diosphenols and seven-membered tropolone, which led to different regioselectivity. For this purpose, the key elimination steps are modeled for both reagents by using computational tools to account on the proposed reaction mechanism and to investigate the structural and electronic effects that caused the difference in these two cases.

3.2 Methods

Density functional theory (DFT) calculations employing B3LYP functional and 6-311++G** basis set have been carried out with the Gaussian 09 program [40, 77-79]. In the literature, a great number of theoretical studies on organic reaction mechanisms have been reported. B3LYP hybrid functional is the most widely used one and have proven to yield satisfactory results on energy and geometry.

More recent mechanistic studies showed that the Density functional theory (DFT) method employing B3LYP functional successfully explain mechanistic features of the organic systems [80, 81] as well. Despite the known shortcomings of B3LYP such as underestimation of barrier heights and less accurate determination of medium-ranged interactions, it gives satisfactory results for energy and geometry and good enough for our comparative study due to cancellation of errors. In order to investigate and verify the proposed mechanism, thermodynamic features of the elimination reactions were modeled in the gas phase and compared with the experimental data. Full geometry and transition states optimizations were carried out in the gas phase. All stationary points and transition states were verified using frequency calculations at the same level of theory. Intrinsic reaction coordinate (IRC) calculations were performed for all transitions states in order to validate stationary points of products and reactants in both directions [41, 42]. The energies given in text are free energies calculated at 298 K.

3.3 Results and Discussion

Tropolone (9), an analogous structure to the five- and six membered diosphenols (5), was used as the starting material in the experimental study. As a first step, N,N-dimethylthiocarbamate (10) was synthesized from tropolone with N,N-dimethylthiocarbamoyl chloride in dry THF (Figure 3.3). The product thiocarbamate was treated with LiCl, LiBr and LiI in CH_3CN/CH_3COOH (9:1) solvent system.

In contrast to the reactions of the halogens with diosphenol thiocarbamates, an identical compound was obtained from each reaction with halides. This compound was identified as 3-N,Ndimethylcarbamoylthio derivative (11), which is the rearranged product of the 2-N,N-dimethylthiocarbamate of tropolone (10).

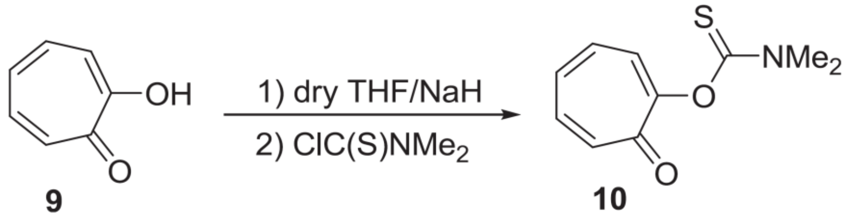
OH
O
9
1) dry THF/NaH
2) ClC(S)NMe$_2$
S
NMe$_2$
O
O
10

Figure 3.3 : Synthesis of tropolone thiocarbamate with ClC(S)NMe$_2$.

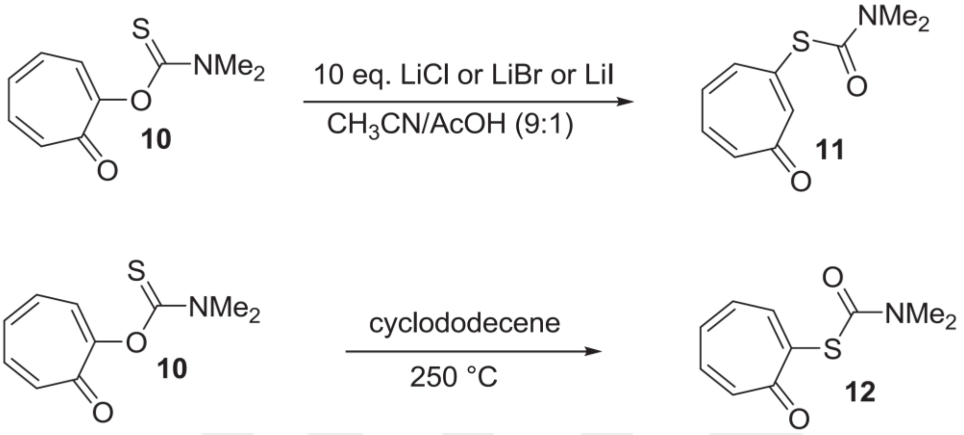
S
NMe$_2$
O
O
10
10 eq. LiCl or LiBr or LiI
CH$_3$CN/AcOH (9:1)
NMe$_2$
S
O
11
O
S
NMe$_2$
O
O
10
cyclododecene
250 °C
O
NMe$_2$
S
12
O

Figure 3.4 : Halide treatment and Newman-Kwart reaction of 10.

Next, N,N-dimethylthiocarbamate (10) was heated at 250 °C to compare the possible product of the Newman-Kwart reaction [76, 82, 83] with the experimentally obtained product. Spectroscopic and chromatographic analysis has shown that the product obtained from the procedure of Zaim et al. (11) and the product from Newman-Kwart rearrangement (12) were different (Figure 3.4). Product (11) was also hydrolyzed in NaOH solution and a new thiol derivative of tropolone (13) was obtained (Figure 3.5).

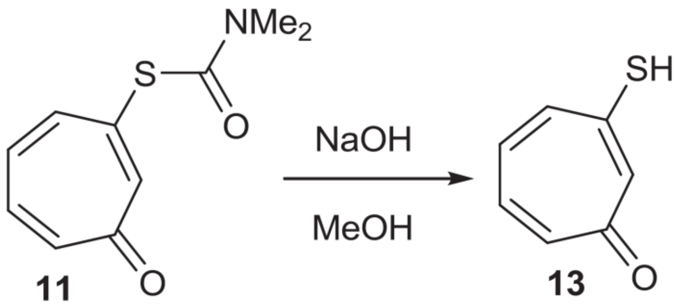
NMe$_2$
S
O
11
O
NaOH
MeOH
SH
13
O

Figure 3.5 : Hydrolysis of 11.

The regioselectivity observed in this reaction can be explained by the following mechanism (Figure 3.6). Comparison of the product with the products of earlier work has shown a significant difference. In the earlier work [73-75], enolic oxygen of five-

and six-membered diosphenols were replaced by Cl or Br after treating dimethylthiocarbamate with LiCl or LiBr in acidic media. In this work, following the same procedure, led to the substitution at 3-position rather than 2-position of tropolone.

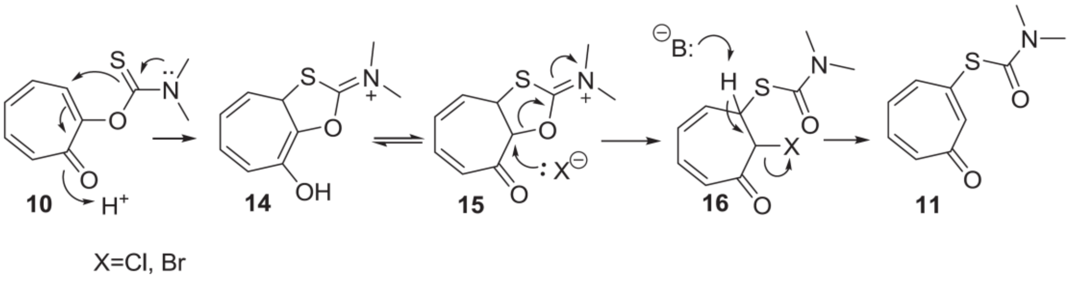

Figure 3.6 : A proposed mechanism for the formation of 11 from 10.

To account on this difference, quantum mechanical calculations are performed on both systems. The proposed pathways for the reactions of 10 and 17 when treated with LiCl (or LiBr), rendering different products, are shown in Figure 3.6 and Figure 3.7, respectively. The pathway shown in Figure 3.7 has been proposed in an earlier report on diosphenols and their hypothesis was confirmed by the observation that the substituents that are reluctant to undergo cyclization (i.e., brosylate, dimethylcarbamate) were unreactive. The difference in products was proposed to stem from the rearrangements followed by elimination products. While 10 leads to 11 possibly from 16, under the same reaction conditions 17 eliminates dimethylcarbanothioic-O-acid (immediately decomposes to dimethyl amine and carbon oxysulfide) from the system.

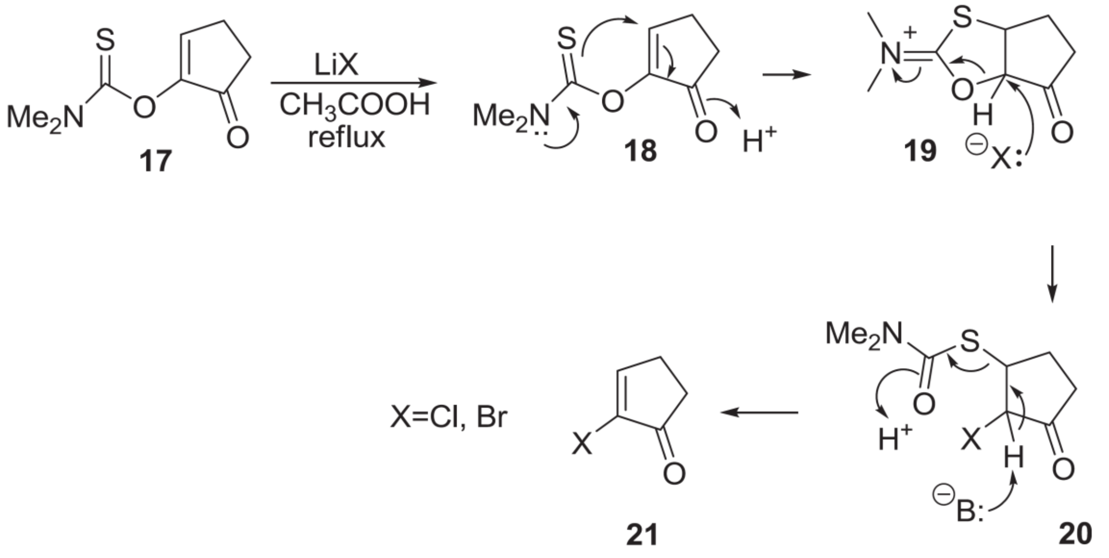

Figure 3.7 : A proposed mechanism for the formation of 21 from 17.

In order to elucidate the product distribution, elimination step was modeled for both 10 and 17 at the B3LYP/6-311++G** level. For both systems, possible configurations for 16 and 20 including their Z and E isomers were investigated. Diastereomer analysis has been conducted on both isomers and the minimum energy structures, shown in Figure 3.8, were obtained. For both reactions, E isomers were found as the minimum energy structures by an energy difference of 2.61 kcal/mol for 16 and 2.91 kcal/mol for 20.

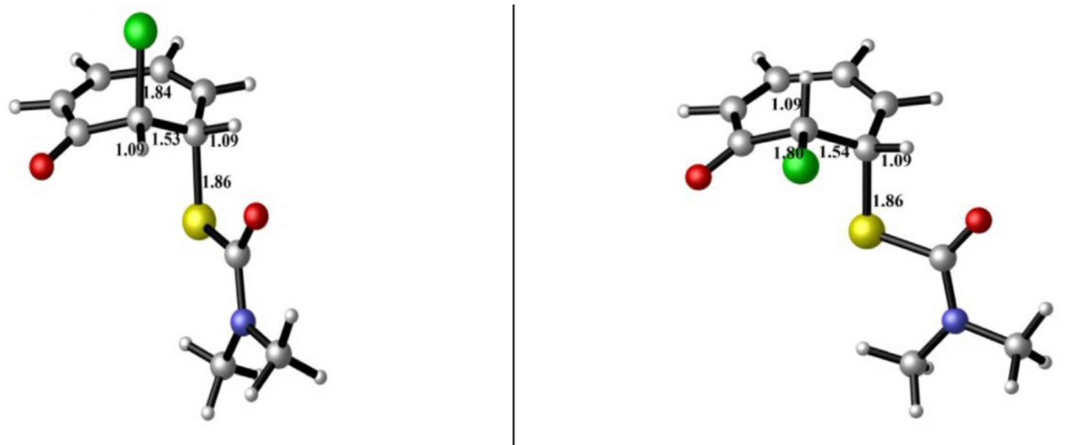

16_ *E* (0.0 kcal/mol) **16_*Z*** (2.61 kcal/mol)

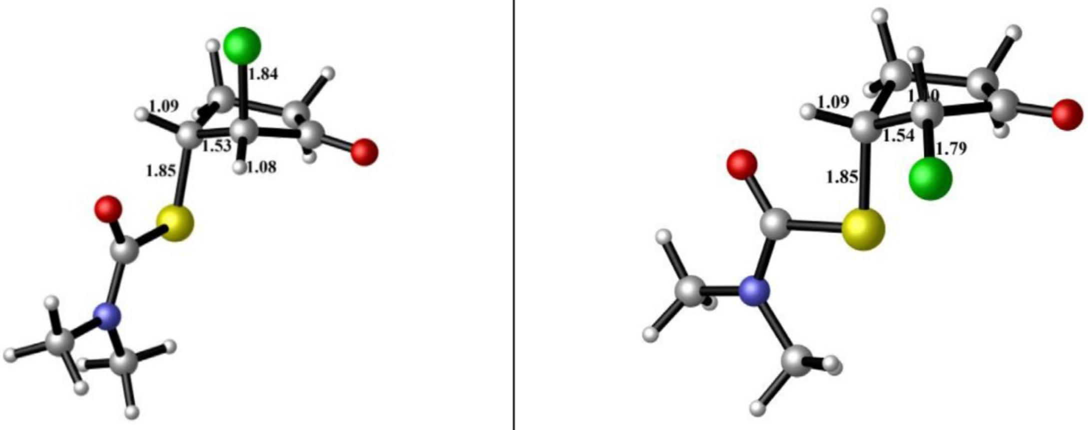

20_*E* (0.0 kcal/mol) **20_*Z*** (2.91 kcal/mol)

Figure 3.8 : 3D geometries, selected bond lengths (in Å) and relative free energies of E and Z isomers with minimum energy for 16 and 20.

In both cases, the E isomers, which have the Cl and dimethylcarbamoylthio substituents in pseudo-axial position are preferred over the Z orientation where the pseudo equatorial positioning of the bulky non-bonding orbitals of halogen created steric hindrance. Additionally, in the Z isomer, sulfur, chlorine and oxygen being directed towards the same point in space creates unfavorable electrostatic interactions and hence disfavors the Z orientation. In the E isomer, both in five- and seven-membered cases, chlorine atom is significantly more negatively charged than that of Z. The APT charge on chlorine atom is -0.37 in both 16 and 20 in E isomers whereas it is -0.27 and -0.28 in Z for 16 and 20, respectively (Figure 3.9). Thus, the E-orientation creates a more negatively charged halogen in the system.

The energy difference between the two isomers at room temperature creates a Boltzmann distribution of almost 99:1 of isomeric ratio. Thus, for modeling the elimination steps only the E-isomers have been used.

Reaction barriers for elimination are compared in the context of the experimentally observed elimination versus the alternative elimination. In modeling, chloride ion is considered as Lewis base for elimination. The least energetic transition state structures belonging to both paths of five and seven-membered rings are demonstrated in Figure 3.10. For five-membered system (20_E), activation barrier for the experimentally observed product is 10.45 kcal/mol, whereas the alternative elimination has a barrier of 12.79 kcal/mol (Figure 3.9).

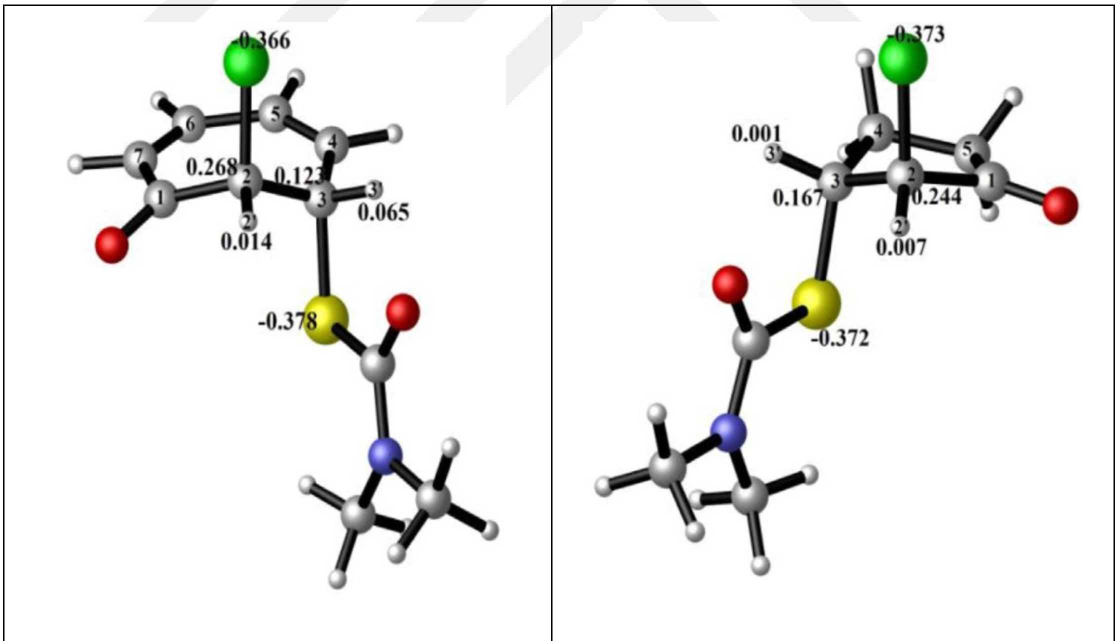

16_*E*

20_*E*

Figure 3.9 : APT charges on the selected atoms of 16_E and 20_E.

In the seven-membered case, experimentally observed product (11) has an even lower barrier than the alternative one (5.54 kcal/mol vs 12.76 kcal/mol). The reaction pathways of 16_E and 20_E, which led to different products are given in Figure 3.11 and Figure 3.12.

In the seven-membered system, among the hydrogens that can be abstracted, the one with higher positive charge is preferentially abstracted (Figure 3.9, 16_E). In the 20_E structure, there is no such difference in the charges of the hydrogens and their charges are relatively low as compared to that of 16_E.

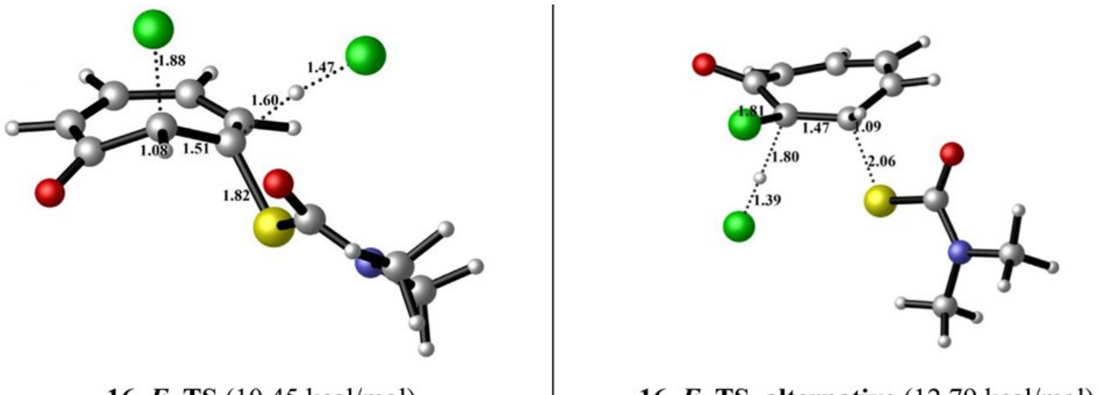

16_*E*_TS (10.45 kcal/mol) **16_*E*_TS_alternative** (12.79 kcal/mol)

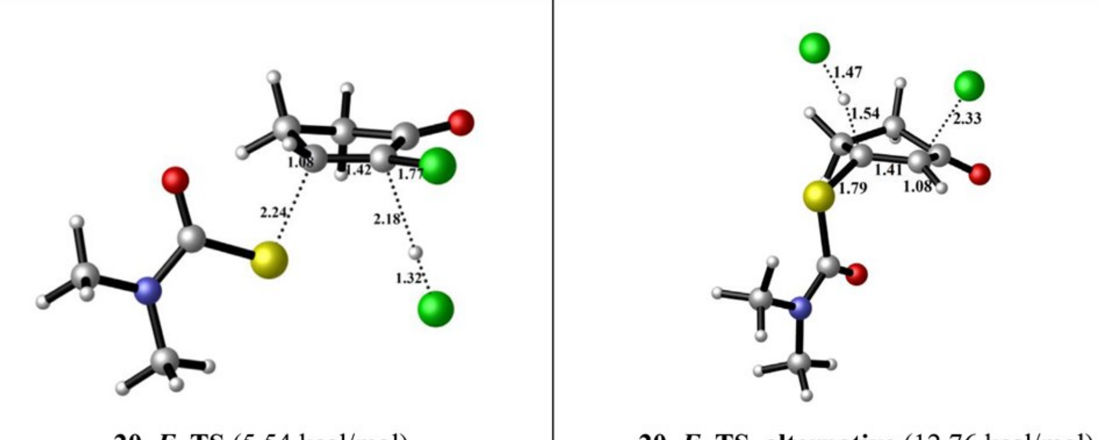

20_*E*_TS (5.54 kcal/mol) **20_*E*_TS_alternative** (12.76 kcal/mol)

Figure 3.10 : 3D geometries, free energies of activation and selected bond lengths (in Å) of transition states of E isomers with minimum energy for 16 and 20.

In 16_E_TS, there is an intramolecular H-bonding between the carbonyl oxygen and H on C2 at a distance of 2.39 Å, whereas in the five-membered analogous transition state structure, 20_E_TS_alternative, (The numbering in Figure 3.9 is used throughout the discussion) this distance does not imply a significant stabilization (3.21 Å). In 16_E_TS_alternative, the H-bonding between carbonyl and H on C3 is 2.34 Å, which acts to hinder the reaction. In the five-membered system, similar destabilization is present between the carbonyl oxygen and H on C3 at a slightly longer distance (2.40 Å in 20_E_TS_alternative). The Cl-H-C bond distances in 16_E_TS imply that it is an earlier transition state than 16_E_TS_alternative, thus requiring a lower barrier and giving the more exothermic product.

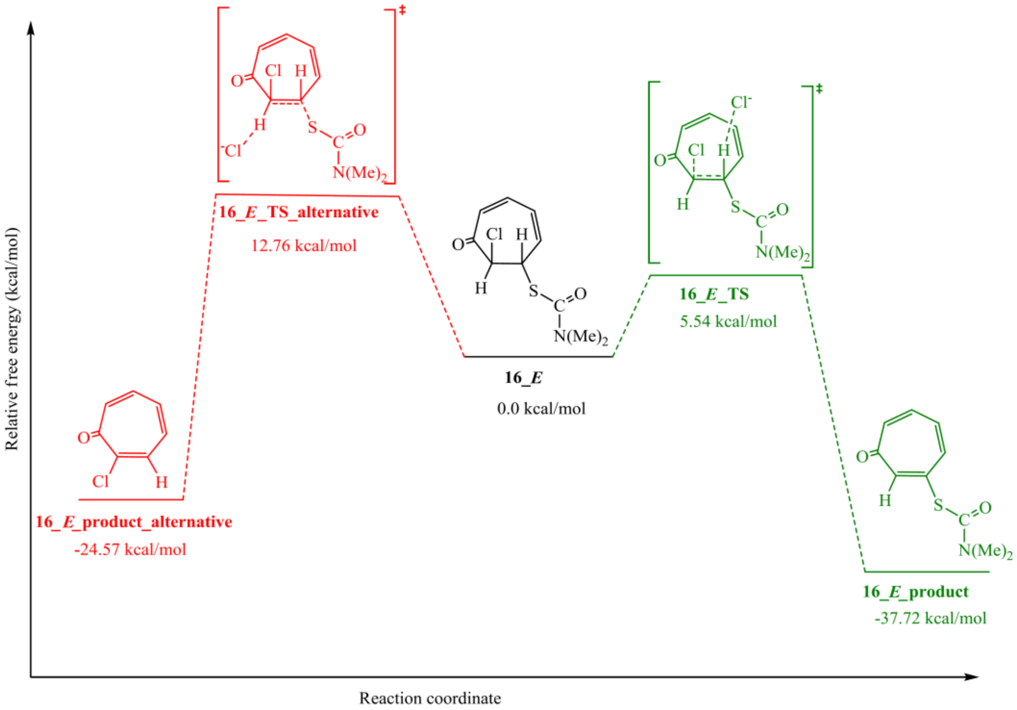

Relative free energy (kcal/mol)
Reaction coordinate
16_*E*_TS_alternative
12.76 kcal/mol
16_*E*
0.0 kcal/mol
16_*E*_TS
5.54 kcal/mol
16_*E*_product_alternative
-24.57 kcal/mol
16_*E*_product
-37.72 kcal/mol

Figure 3.11 : Reaction pathways of 16_E for two possible elimination products (Energies are not to scale).

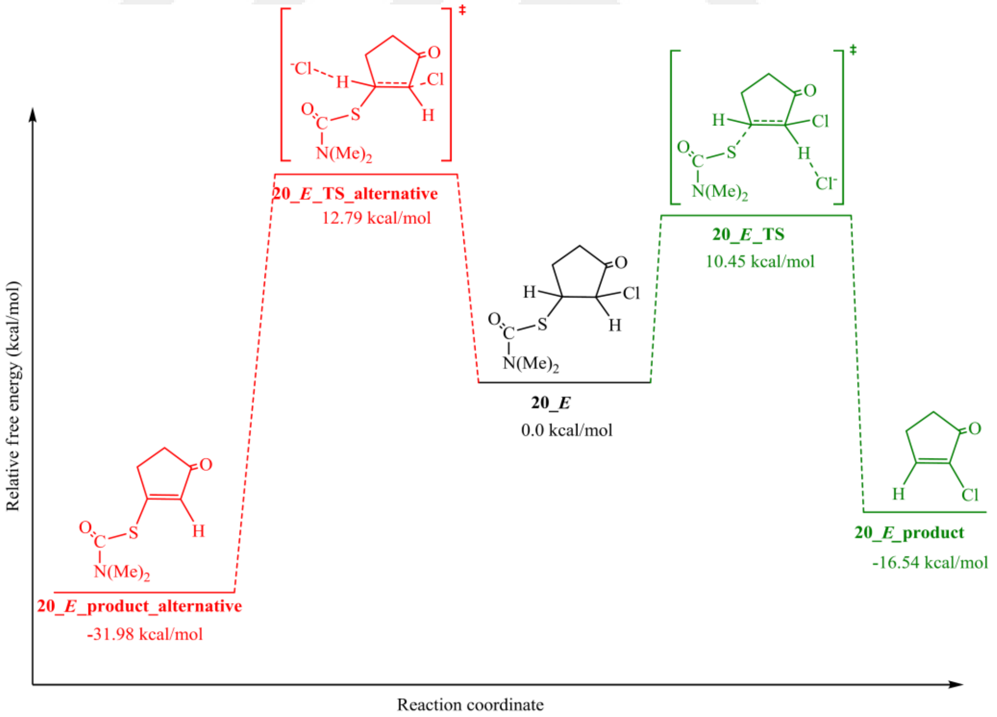

Relative free energy (kcal/mol)
Reaction coordinate
20_*E*_TS_alternative
12.79 kcal/mol
20_*E*
0.0 kcal/mol
20_*E*_TS
10.45 kcal/mol
20_*E*_product_alternative
-31.98 kcal/mol
20_*E*_product
-16.54 kcal/mol

Figure 3.12 : Reaction pathways of 20_E for two possible elimination products (Energies are not to scale).

This is also reflected in the changes of pyramidilization of the carbons (C2 and C3) that transform to sp^2 from sp^3 hybridization state. In 16_E_TS, the changes in dihedral angles defining pyramidilization of the carbons at the reaction center are significantly lower than that of the alternative path.

The geometries, electronics and the energetics of the transition state structures for two modes of elimination have demonstrated the preference for the experimentally observed product for both five and seven-membered systems.

3.4 Conclusion

A facile and efficient way to the synthesis of 3-mercapto-2,4,6-cycloheptatrien-1-one starting from tropolone has been devoleped by Zaim et al. It can be utilized for the synthesis of many new compounds as starting material or intermediate. The quantum mechanical calculations have provided insights into the synthetic pathway and regioselectivity of the reaction in comparison to analogous five-membered system. The elimination step for both five- and seven-membered systems, leading to two different products in each case, has been modeled at the B3LYP/6-311++G** level. The experimentally observed regioselectivity was correlated to the calculated activation barriers on five and seven-membered systems in the elimination step such that in both cases, experimentally observed product was favored over the alternative one. Steric effects, relative charges of the abstracted hydrogens and intramolecular H-bondings were found to rule the product formation dynamics. The proposed mechanisms have been confirmed for their key steps in the overall rearrangements, providing an additional confirmation for the reaction pathway and the experimentally observed regioselectivity.

4. REGIOSELECTIVITY PATTERNS IN RADICALIC CYCLIZATION OF DIOSPHENOL DERIVATIVES WITH DIFFERENT RING SIZE

4.1 Introduction

Radical cyclization reactions have opened a wide scope of possibilities in organic synthesis [84-88] and have been well documented [89, 90]. These reactions include the selective formation of cyclic structures. The regio- and stereoselectivity of radical cyclizations are often examined due to the highly reactive nature of the unstable carbon radicals which enables synthetic versatility. In this respect, tributyltin hydride (Bu_3SnH) has been reported to be a useful reagent since the initiator $Bu_3Sn\cdot$ radical can be formed very efficiently under mild conditions and can react with a variety of compounds to form carbon centered radicals [91-97]. A method for tin-mediated intramolecular aryl radical cyclization was reported by Beckwith in 1975 [98]. Since then, focusing on the synthesis of benzocyclic compounds with biarylic and heterocyclic structures, various methods based on intramolecular additions of aryl radicals onto aryl groups, CC double bonds and CN or CO double bonds, as well as the earlier discovery of photoinduced aryl-aryl couplings, have been developed [99, 100]. Zaim *et al.* and his co-workers have previously prepared oxabicycloalkanones via cyclization of radicals generated from diosphenol-ω-haloalkyl ethers (Figure 4.1) [101].

When the cyclization of diosphenol-ω-haloalkyl ethers 1 is compared with the results of Beckwith [102], it is found that a conjugated carbonyl group had affected cyclization over reduction substantially in these systems but there was almost no improvement in regioselectivity (exo : endo = 1.2 : 1). Then, we decided to examine the radical cyclization of a tropolone derivative. Tropolone is found structurally in naturally occurring compounds and may be considered as a diosphenole since it is an enolic 1,2- diketone system by the help of aromaticity.

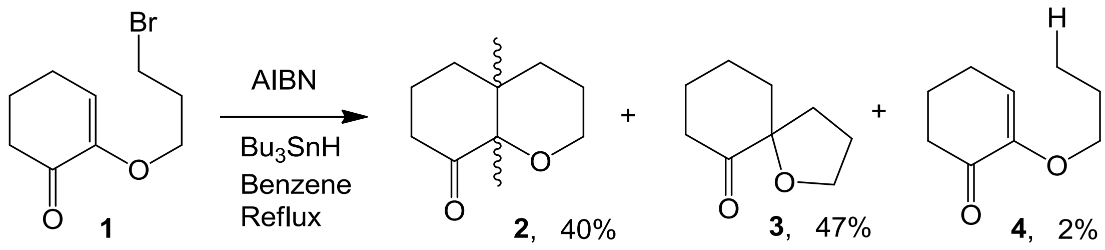

Figure 4.1 : Synthesis of oxabicycloalkanones via radicalic cyclization of diosphenol-ω-haloalkyl ethers.

Zaim et al. has synthesized a tropolone derivative, namely 2-(3-iodopropoxy) cyclohepta-2,4,6-trienone (6) [103]. The effect of moving from six membered diosphenol to seven membered ring system on reactivity and regioselectivity has been examined experimentally and theoretically in this study.

4.2 Computational Methods

Density functional theory (DFT) is utilized for all the calculations. Although this method is not the most precise choice to describe the absolute barrier heights, it is adequate for a comparative study since the errors in the barriers will be eliminated by means of comparison. Moreover, the correlation between the computational cost and the performance of the calculations is satisfactory. Thus, the relative barriers are presented and discussed rather than the exact barriers for 6- and 7-membered analogues.

All calculations have been carried out using Gaussian 09 quantum mechanical software [40]. The structures were optimized using unrestricted M05 functional, due to the radicalic character of the species, at the 6-311++G (d, p) level which is reported to present good performance for open shell systems [104, 105]. Vibrational frequency calculations have been performed on all the structures at the same level of theory.

Transition states were verified with a single imaginary frequency where all stationary points have positive frequency values. Intrinsic reaction coordinate (IRC) calculations have been carried out on the TS structures to verify the corresponding intermediates on both sides [42, 106, 107]. Gas phase optimizations were done at 298K, 1atm and followed by the solvent optimizations in benzene and toluene using unrestricted M05/6-311++G (d, p) and Polarizable Continuum Model (PCM) method for 6 and 7-membered systems, respectively [108].

Charge analysis on the optimized structures was performed using Atomic Polar Tensors (APT) at the same level of theory, written in light blue and the bond distances are given in units of Å written in black where appropriate [109].

For the termination step, butyl groups in the $(C_4H_{10})_3SnH$ are replaced by the methyl groups in order to reduce the conformational space and computational cost. In this case, effective core potential (ECP) has been utilized for the heavy atom Sn and MWB (46/4) basis set is specified for the core and valence electrons in the calculations [110]. The energies discussed through the manuscript are relative free energies (ΔG) in kcal/mol.

4.3 Results and Discussion

4.3.1 Experimental findings

Originating from the work of Beckwith, the features of the radicalic reaction of 7-membered tropolone analogue are examined. For this purpose, Zaim et al. synthesized 2-(3-iodopropoxy)cyclohepta-2,4,6-trienone from tropolone 5 and 1,3-diiodopropane in the presence of K_2CO_3 as base in boiling acetone (Figure 4.2).

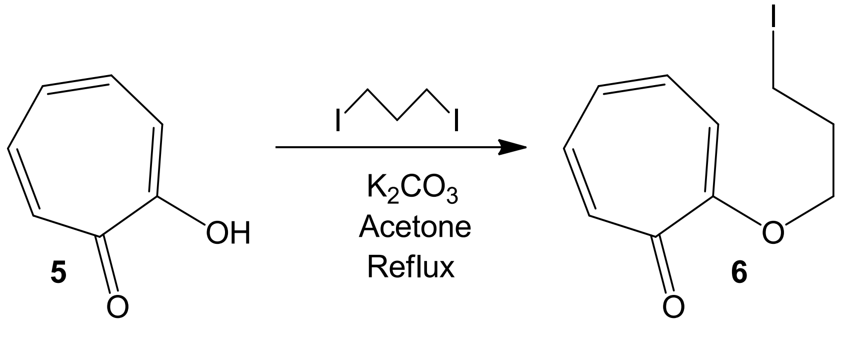

Figure 4.2 : Synthesis of 2-(3-iodopropoxy) cyclohepta-2,4,6-trienone from tropolone 5 in the presence of 1,3-diiodopropane and K_2CO_3 as base in boiling acetone.

Then, radical reactions were performed in boiling dry toluene with AIBN as initiator and tributyltin hydride as a hydride source (Figure 4.3). Only one product at the end of the reaction was observed after the purifications using column chromatography.

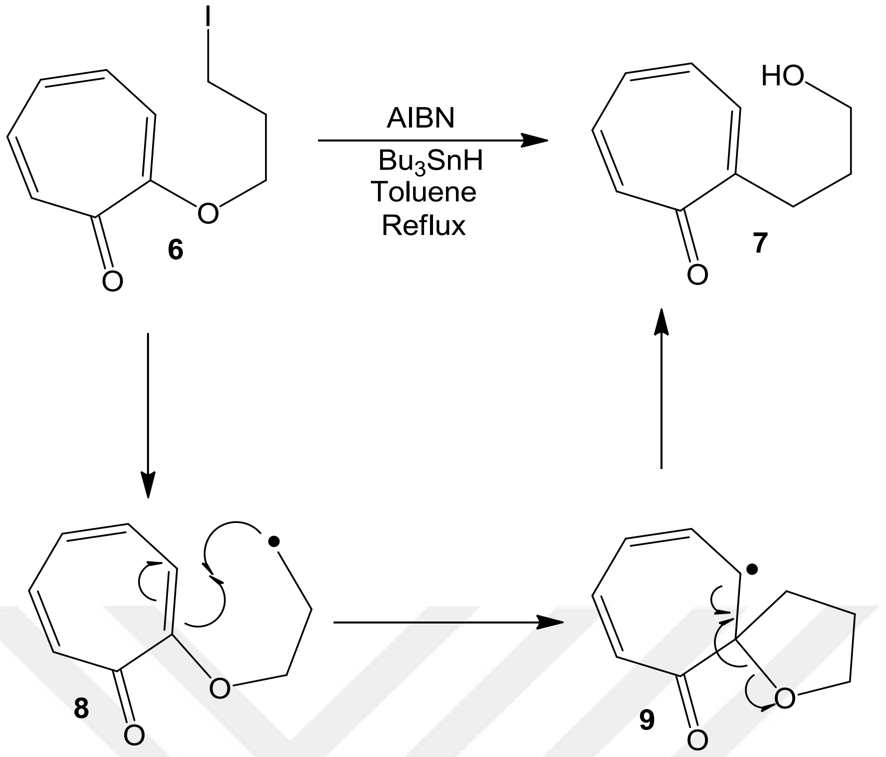

Figure 4.3 : Proposed mechanism for the synthesis of 2-(3-hydroxypropyl)cyclohepta-2,4,6-trienone.

After spectroscopic analyses, it is decided that compound 7, namely 2-(3-hydroxypropyl)cyclohepta-2,4,6-trienone is the only product of the reaction. Compound 7 is proposed to be produced via intermediates 8 and 9 (Figure 4.3). Results from the experiment suggest that exo cyclization is the only feasible process and a rapid aromatization follows the ring opening of 9, so that this transformation is enhanced by the stability of the final product.

Endo cyclization would give the radical intermediate 10 which results 11 after abstracting a hydrogen atom from tributyltin hydride (Figure 4.4). However, compound 11 has not been observed in the final product mixture and spectroscopic results show that 7 is the only product of the reaction. To prove the structure of 7, HMBC which shows a cross coupling between 188.1 (from C=O carbon of the ring system) and 2.79 (triplet from CH_2 of side chain C-1) was employed. This correlation is only possible at compound 7, not at compound 11. Besides, the stability of two possible radical intermediates 9 and 10 also implies the same outcome. 9 is more likely to be more stable than 10 because it is allylic and has an extended conjugation up to the carbonyl group on the ring.

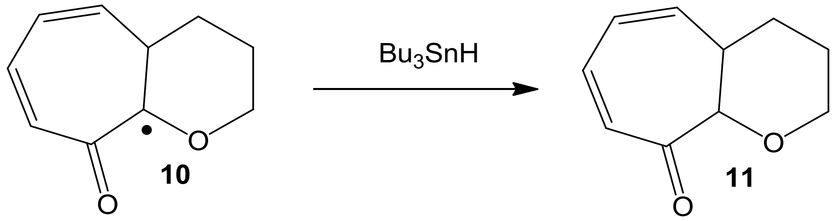

Figure 4.4 : Formation of 11 via H-abstraction.

However, neighboring carbonyl and etheric oxygen to the radical center do not support the stability of 10 as much as the conjugation does to radical 9. This is reflected in the calculated energies (the details will be discussed in the following part) such that intermediate 9 is 10.11 kcal/mol more stable than 10.

4.3.2 Computational results

In order to reveal the dynamics that are responsible at the regioselectivity step of product formation, quantum chemical calculations were performed on both 6- and 7-membered diosphenol systems. Calculations on the 6-membered ring is expected to serve in two ways: *i.* It will be possible to compare its results and features with that of 7-membered ring. *ii.* It will help us to validate the theoretical methodology involved in this manuscript.

The experimental studies show that there is no regioselectivity in the cyclization generated from 6-membered diosphenol-ω-haloalkyl ethers 1, due to the competition between endo and exo products. Moreover, the activation barriers calculated in solvent by DFT methods indicate that formation of endo (2) and exo (3) products are dominated over H-abstraction (4) (Table 4.1). The absolute charge difference of the involved atoms in TS_{endo} and TS_{exo} are (0.29 vs. 0.35) almost similar and also consistent with the attraction provided between the reactive centers and resulting in 40 vs. 47% product formation ratio. The methodology employed here is quite successful to reproduce the experimental regioselectivity, both qualitatively and quantitatively.

In the case of 7-membered system, the experiments performed herein lead to a single product 7, regioselectively. In order to put a theoretical aspect and comment on this observation, all possible pathways for exo, endo cyclization and H-abstraction were scanned which are proposed in Figure 4.5.

Table 4.1 : Activation barriers calculated at UM05/6-311++G(d,p) level in benzene with PCM for the cyclization of 1 leading to different products. ($\Delta G^{\ddagger}$: Free energy of activation, in kcal/mol).

Reaction	*Energy*	
	$\Delta G^{\ddagger}$	*Relative* $\Delta G^{\ddagger}$
Cyclization-Exo	*7.60*	*0.0*
Cyclization-Endo	*7.45*	*0.95*
Termination by H-abstraction	*12.20*	*4.60*

Mechanistically, all the possible formations were suggested to initiate once the radical 8 forms after the attack of Bu_3SnH and product distribution will be determined by the relative energies of transition state structures leading to exo and endo cyclization or H-abstraction.

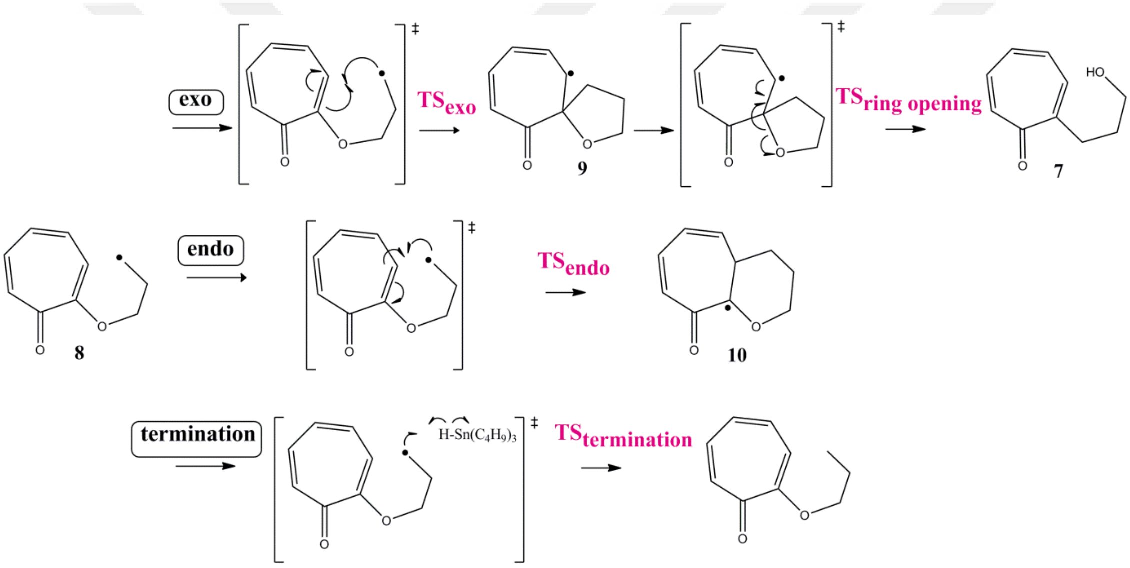

Figure 4.5 : TS’s and intermediates leading to possible products after the radicalic initiation step.

The free energy of activation barrier, ($\Delta G^{\ddagger}$, Table 4.2) for exo cyclization is much lower than that of endo cyclization and H-abstraction (3.47 vs. 11.47 and 13.27 kcal/mol). This is in accordance with the experimentally non-observed endo and H-abstraction products. Then, having not observed any exo product from the spectroscopic analyses has invoked us to the idea of a completely different route for ring opening of compound 9 which subsequently rearranges to product 7. Thus, the facility of this ring opening was also further investigated theoretically. The free energy activation barrier for the exo cyclization is 3.47 kcal/mol which is the lowest among the possible pathways (exo, endo, H-abstraction) in the reaction medium and the cyclization will be followed by a facile rearrangement of 9 to 7 via a barrier of 4.35 kcal/mol.

Table 4.2 : Activation barriers calculated at UM05/6-311++G(d,p) level in toluene with PCM for the cyclization of 6 leading to different products. ($\Delta G^{\ddagger}$: Free energy of activation, in kcal/mol).

Reaction	*Energy*	
	$\Delta G^{\ddagger}$	*Relative* $\Delta G^{\ddagger}$
Cyclization-Exo	*3.47*	*0.0*
Cyclization-Endo	*11.47*	*8.0*
Termination by H-abstraction	*13.27*	*9.8*
Ring opening	*4.35*	*0.88*

This energetic profile supports the experimental proposal that starts with exo-cyclization of 8 via TS_{exo} and is followed by ring opening pathway (via $TS_{ring\_opening}$) and produces 7 as a single product via a facile pathway (Figure 4.5). This trend is also reflected in the absolute charge differences on the involved atoms causing attractive force in TS_{endo} and TS_{exo} (0.28 *vs.* 0.59) which is giving rise to exo formation instead of endo. Ring opening is a facile route following the exo formation due to the negative charges on the involved atoms (-0.22 and -0.19 in $TS_{ring\_opening}$) in the transition state structure.

In the literature, there are several aspects to justify the possible contribution of different products to the overall product distribution in radicalic systems [89, 111, 112]. They are mainly focused on the electronic and steric effects leading the transition state and the forming product. These effects include the stability of the radical intermediates, substitution of stabilizing groups, as well as the ring size, conjugation of the reactive double bond, distortion type of the ring in the TS structure into a boat or chair like geometry, torsion angles between the reacting centers. Here, both 6- and 7-membered systems (1 and 6) are consisted of a carbonyl group conjugated with a double bond in the ring and they have similar steric environments. Comprehensive analysis of the data shows that, in both systems cyclization is dominated over the simple reduction product (via termination) due to the low stability of the initially formed radical and the facileness of low entropic nature of the intramolecular cylization. However, in the 6-membered system, the energy required to distort the radicalic center onto the functionalized double bond for endo and exo product formation is presumably similar.

6-membered system	7-membered system

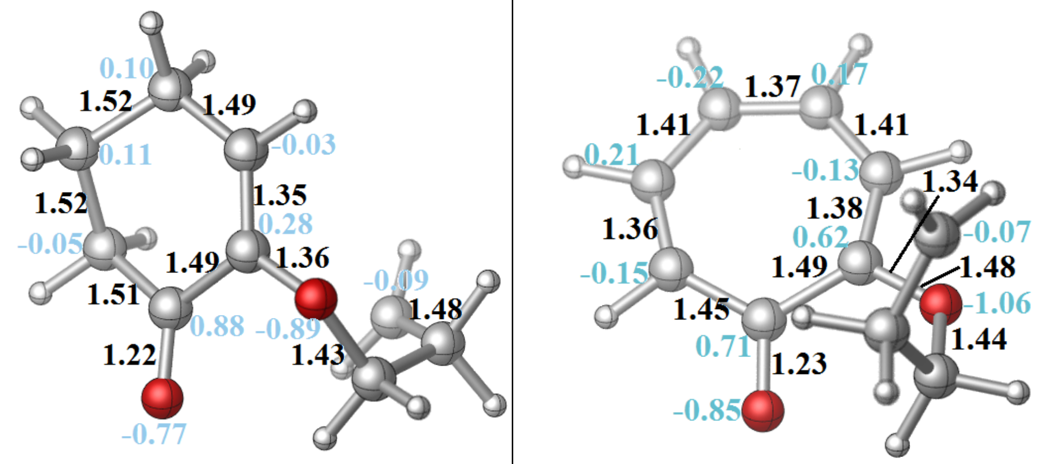

6-mem_initial_radical

7-mem_initial_radical

0.10
1.52
1.49
-0.03
0.11
1.52
1.35
0.28
-0.05
1.49
1.36
-0.09
1.51
1.48
0.88
-0.89
1.22
1.43
-0.77
-0.22
1.37
0.17
1.41
1.41
0.21
-0.13
1.34
1.38
-0.07
1.36
0.62
1.49
1.48
-0.15
-1.06
1.45
0.71
1.44
1.23
-0.85

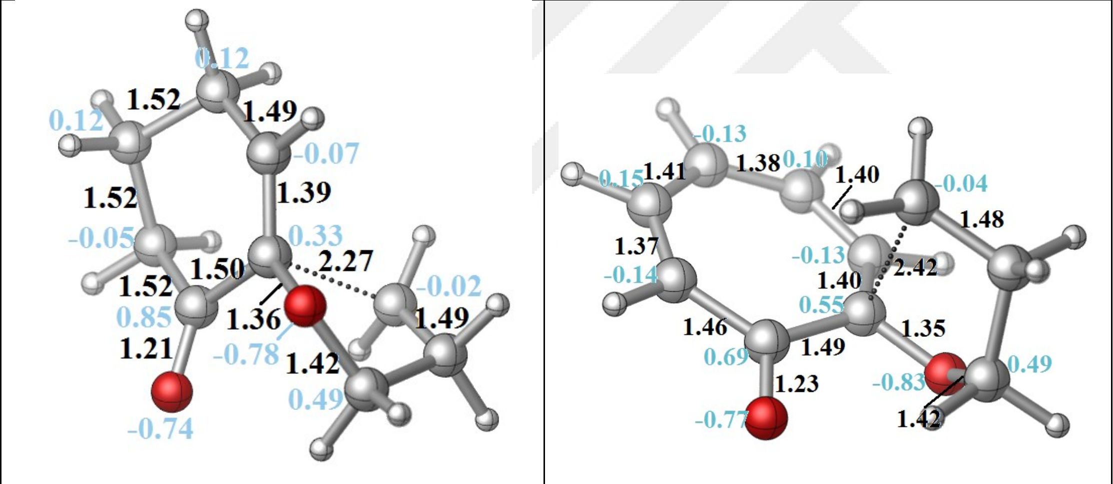

6-mem_TS$_{exo}$

7-mem_TS$_{exo}$

0.12
1.52
1.49
0.12
-0.07
1.52
1.39
-0.05
0.33
2.27
1.50
-0.02
1.52
1.36
1.49
0.85
1.21
-0.78
1.42
0.49
-0.74
-0.13
1.38
0.10
0.15
1.41
1.40
-0.04
1.48
1.37
-0.14
-0.13
2.42
1.40
0.55
1.46
1.35
0.69
1.49
0.49
1.23
-0.83
-0.77
1.42

Figure 4.6 : Critical bond lengths (in Ǻ, black) and APT charges (blue) on the TS structures and intermediates.

Dihedral torsion angle between the radicalic center and functionalized double bond is 88° and 128° in TS$_{exo}$ and TS$_{endo}$ in 6-membered system, whereas; 87° and 179° in 7-membered system, respectively. This difference in the torsion angle confirms the need for the extra energy in 7-membered system, in order to distort the geometry where radical carbon and alkene terminus will form the endo product. Moreover, the planarity of the aromatic ring in 7-membered system is constraining the perpendicular attack of the radicalic center to the double bond for the endo cyclization which is much more facile in 6-membered case due to the distorted geometry of the ring. This fact also justifies why TS$_{endo}$ is disfavored by 8 kcal/mol relative to the exo production in 7-membered system.

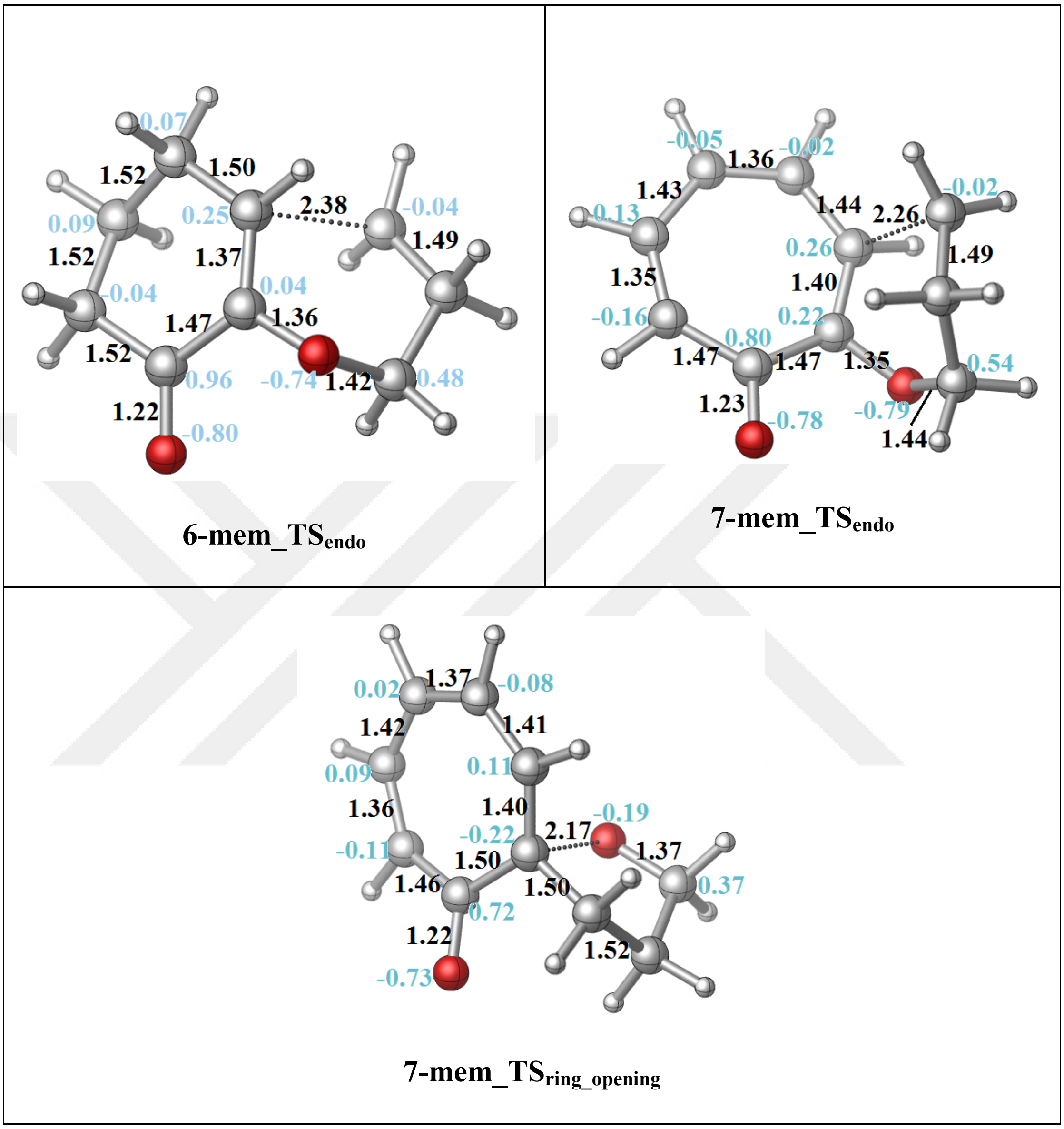
0.07
1.52
1.50
0.09
0.25
2.38
-0.04
1.52
1.37
1.49
0.04
-0.04
1.47
1.36
1.52
0.96
-0.74
1.42
0.48
1.22
-0.80
-0.05
1.36
-0.02
1.43
1.44
2.26
-0.02
0.13
0.26
1.49
1.35
1.40
-0.16
0.22
0.80
1.47
1.47
1.35
0.54
1.23
-0.78
-0.79
1.44
0.02
1.37
-0.08
1.42
1.41
0.11
0.09
1.36
1.40
-0.19
-0.22
2.17
1.37
-0.11
1.50
0.37
1.46
1.50
0.72
1.22
1.52
-0.73

6-mem_TS$_{endo}$

7-mem_TS$_{endo}$

7-mem_TS$_{ring\_opening}$

Figure 4.7 : Critical bond lengths (in Å, black) and APT charges (blue) on the TS structures and intermediates.

On the other hand, it is also claimed that the conjugation of the carbonyl double bond in the aromatic ring might play a role in the product distribution. In order to clarify the effect of aromaticity, planarity and charge features; 3D-geometries, bond lengths and charges on the reaction center of transition states leading to products and pre-intermediates were investigated (Figure 4.6 and Figure 4.7). An overall look at the transition states of 7-membered system shows that first, the transition state with a low entropy path is preferred via cyclization (endo-exo vs. H abstraction) and then followed by the formation of fully aromatic ring seen in 7 but not in 11. Conversely, the aromatization factor is lacking in 6-membered system and the reaction is only driven by less entropy pathway which results in an endo-exo mixture.

4.4 Conclusions

In this study, the radicalic reactions of 6- and 7-membered diosphenol derivatives differing in reactivity, ring size, aromaticity and stability were reported both experimentally and with DFT calculations. The experimental investigations performed in this study have shown that 7-membered tropolone 5 has regioselectively yielded 2-(3-hydroxypropyl)cyclohepta-2,4,6-trienone 7 via a radicalic mechanism. On the other hand, we have previously reported formation of a set of oxabicycloalkanones via cyclization of radicals generated from a similar 6-membered derivative of diosphenol-ω-haloalkyl ethers. Here, formation of 2-(3-hydroxypropyl)cyclohepta-2,4,6-trienone as product is proposed to take place via radicalic intermediates 8 and 9.

In order to test this proposal quantum mechanical calculations were performed for possible intramolecular cyclizations of the forming radical in exo and endo modes and also for termination by H-abstraction. For this purpose, both 6 and 7-membered were used in the calculations which would allow us to validate the methodology used in this study and provide a wide perspective to understand the origins of the regioselectivity in a comparative sense. The UM05/6-311++G(d,p) calculations on radicalic cyclization of a 6-membered tropolone derivative 1 have shown that the barriers to both endo and exo products are similar whereas termination by H-abstraction is energetically unfavorable. The non-regioselectivity of the process is attributed to the non-planar geometry of the ring which provides flexibility to the radicalic chain and eases the attack for the endo and exo formation at the same time. Besides that, lack of stabilizing effect of aromaticity in the final products disables the regioselectivity of this process. In the 7-membered system, radical 8 is produced by the radicalic initiation of 2-(3-iodopropoxy) cyclohepta-2,4,6-trienone 6. Following this radicalic species, it is proposed and supported by spectroscopic calculations that structure 7 has been obtained as a single product instead of a product mixture. The possible existence of different products are investigated by modeling three different pathways by quantum mechanical calculations. The calculated barriers show that the formation of 7 is energetically the most favored product to occur. Explanations for the different selectivity patterns are mostly based on entropy factors, variation of dihedral torsion angle between the radicalic center and functionalized double bond, aromatization of the ring and the charge distribution at the reactive atoms.

5. CONTROL OF THERMODYNAMICS AND MICROKINETICS OF THE REDUCTIVE AMINATION REACTION BY ASSISTANCE OF SOLVENT AND CO-CATALYST

5.1 Introduction

A green chemistry approach and the utilization of natural products from sustainable sources is becoming more significant in industrial applications. Amines represent an important class of fundamental chemicals which are used as intermediates in a range of applications including pharmaceuticals, agricultural chemicals, rubber chemicals, water treatment chemicals, and solvents [113]. The transformation of industrially available fatty acids from sustainable sources into long chain amines via an environmentally friendly and sustainable way has recently gained significant importance (Figure 5.1) [114].

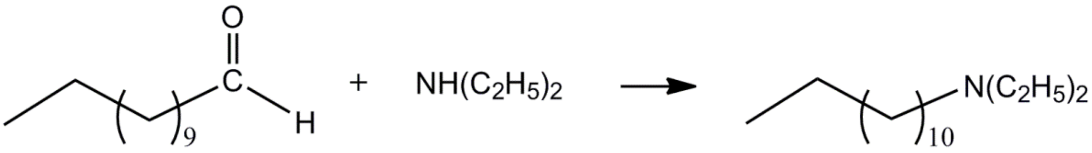

Figure 5.1 : Production of long chain diethylamines from aldehydes via reductive amination.

Indeed, the process of reductive amination has been stated to be one of the most relevant challenges of process design for the pharmaceutical industry [115]. The sequential or tandem coupling of industrial chemistry reactions [116] gives access to these classes of compounds, for example, by coupling a hydroformylation reaction, followed by an amination of the obtained aldehyde and finally hydrogenation of the enamine to produce saturated, long chain primary, secondary or tertiary amines [117]. Starting from n-undecene, first n-dodecanal (lauryl aldehyde, a fragrance) is being produced which is then converted into N,N-diethyltridecane-1-amine ($C_{15}H_{33}N$, an anti infective; Figure 5.1). Such a facile and more efficient route for a hydroaminomethylation process is of great interest to the chemical and pharmaceutical industry [118, 119].

The reductive amination initiates with the addition of an amine to the carbonyl group of the aldehyde/ketone and forms a hemiaminal as intermediate (Figure 5.2).

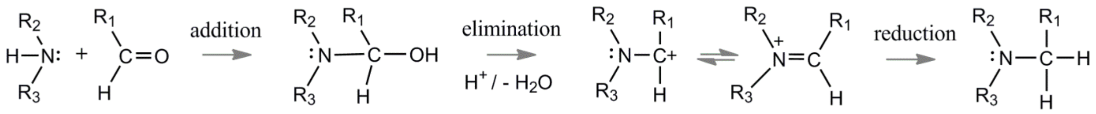

Figure 5.2 : Proposed mechanism for the reductive amination of aldehydes.

The subsequent condensation reaction results in an imine or an iminium ion depending on the pH of the reaction medium. The equilibrium between aldehyde/ketone and imine can be controlled by continuous removal of the released water. At the final step, the desired amine is obtained by a reduction of the C=N bond. However, reduction of the C=N bond in an efficient, industrially applicable and non-toxic way is still a challenging subject. Due to their great importance, there are numerous synthetic approaches to form amines. These methods are generally classified as ‘direct’ and ‘indirect’ according to the subsequent addition of the reducing agent [120]. The reaction is described as ‘direct’, when aldehyde, amine and reducing agent are reacting in a one pot process [117]. The drawback of the direct reduction process is the competition between reduction of the C=O carbonyl group of the aldehyde and the C=N unsaturated bonds of imine which might lead to a number of side products. Thus, the appropriate choice of the reducing agent becomes more critical. In order to obtain an amine as a final product, the reducing agent must react selectively with the imine (or enamine, when secondary amines are used) or iminium ion rather than the carbonyl group of the aldehyde.

Usually, direct reductive amination is preferred to an ‘indirect’ process, because it is more convenient and a more efficient process, especially in large scale applications [116]. The use of borohydrides, for example sodium triacetoxyborohydrid [120-122], are used as one example of a simple and cheap choice of reducing agents because of its different selectivity at different pH, its stability in acidic conditions (pH=3) and its solubility in polar solvent. However, the toxicity of the reducing agent and its low conversion rate in case of unreactive ketones hamper the large scale application [123]. Recently, a silane-based reductant was reported for the direct reductive amination as a representative of the organosilane family [124]. This reducing reagent is not only cheap and metal free which provides a sustainable green process; but it also shows a high selectivity to several unsaturated functional groups which prevents the formation of undesired side products.

Heterogeneous catalytic reductive amination with suitable transition metals is an efficient and economical way and used frequently on industrial scale [125]. One drawback of this approach is the need for elevated H_2 pressure during the process. This procedure is successful with noble metal complexes such as Rh, Ru, and Pd/C systems, however reduction by the Ni and Co metals seems to be limited to the production of primary amines [126].

Homogeneous transition metal catalysts such as Rh(I), Ru(II) and Ir(I-III) [127-129] are also successful tools for asymmetric reduction of imines/enamines which are in complex with variety of ligands [130]. These reducing agents are particularly used for an enantioselective synthesis of amines.

Most of the reduction methods are established for the synthesis of primary and secondary amines. However, production of a tertiary amine is more challenging due to the steric demand of two nitrogen-bound organic rests (R_2 and R_3 in Figure 5.2) and the strained formation of the imine/enamine intermediates. Several metal-based catalyst systems (such as Co_3O_4/H_2 and $SnCl_2$/reducing agent) are especially highlighted in the literature as good candidates for this process [124, 131, 132]. There are also several successful experimental and computational reports on the functionalization of several amines via intra- and intermolecular cyclization reactions in a redox neutral way [133-135]. In addition, they give some evidence for the formation of ylide intermediates which suggests that the reaction can also proceed via an alternative route and not necessarily be forming the iminium ions, particularly in case of intramolecular transformations of cyclic structures.

Here, we present a computational study on the thermodynamics and full mechanism of the reductive amination reaction in an organic solvent in the absence and presence of the co-catalyst acid using a combination of an explicit cluster model of solvation and an implicit solvent model to account for long range effects. Information about the thermodynamics, the non-ideality of reaction media and the rate-determining step are required for the design of a reaction network model of the reductive amination of sustainable long-chain aldehydes such as tridecanal which can elegantly be generated from a Rh-based hydroformylation reaction of 1-dodecene in a thermomorphic multicomponent solvent system (TMS) [136-139] or directly in a hydroaminomethylation reaction in a TMS [140].

5.2 Computational Methods

In the scope of this work, a representative reaction between a long chain aldehyde and a secondary amine has been studied in terms of neutral and co-catalyst assisted reaction conditions. The computational set consists of propanal (C_3H_6O) and diethylamine ($(C_2H_5)_2NH$). In order to simplify the system and reduce the conformational space, propanal was chosen instead of dodecanal ($C_{12}H_{24}O$) in the calculations which is shorter in chain length. The calculation of the Gibss free energy of the reaction shows that the shortening of the carbon chain length does not significantly affect the thermodynamics of the reaction.

The reductive amination process has been investigated in terms of computational calculations by use of ab initio Møller–Plesset perturbation theory (MP). The correlation of the movement of electrons is crucial to describe the electronic structure of such a system correctly and has to be taken into account which is lacking in most of the popular density functionals. The barrier heights of an enamine formation calculated at Density Functional Theory (DFT) and the second order Møller-Plesset perturbation theory (MP2) levels were shown to differ by up to 4 kcal/mol [141] which is larger than ‘chemical accuracy’ and shows the necessity of full geometry optimization with a wavefunction-based approach. Additionally, the computed energy barriers in an implicit solvent were found to be lower by 14 kcal/mol than in gas phase [141]. This is also emphasizing the importance of the stabilizing effect of the explicitly coordinating solvent molecules on the charge distribution and that solvent effects should be taken into account to refine the computed barriers.

All the intermediates and transition state structures were fully optimized by using MP2(full) with a 6-311+g (d,p) basis set [142] in Gaussian 09 [40]. Optimized structures were verified by calculation of second derivatives to correspond to minima, whereas a single imaginary frequency indicates a saddle point, presumably a transition state. In order to verify the transition state structures, intrinsic reaction coordinate (IRC) calculations were done along the reaction coordinate by following the gradient in both directions [41, 42].

During the reaction, water is released in the condensation step (see above). The role of the explicit water molecules which are coordinating to the substrates on the reaction mechanism was investigated. Additionally, the role of the co-catalyst acid was explored particularly on the coupling step, since it is stated to be unclear in the literature. A mixed cluster-continuum solvation model was used particularly for 'Explicit Water-Coordination' (see section 5.3.2.2) by considering explicit water molecules to form a hydrogen bond network and additionally treated with an implicit solvation model. Single point implicit solvent calculations were carried out on the optimized geometries at the same level of theory in order to estimate the effect of the solvent on the reaction profile. The solvent effects were included using the solvation model based on density (SMD) method for N,N-dimethylformamide (DMF) as polar and decane as apolar solvent to mimic the polarity effect ($\varepsilon = 36.7$ and 2, respectively) [143]. The choice of solvents correspond to that used in the experiments for the hydroformylation reaction of dodecene [137, 138].

All the energies reported through this work are Gibbs free energies at standard conditions of 298 K and 1 bar. Thermodynamic corrections were taken from MP2 frequency calculations at 298 K and added to the single point SMD MP2 energies. Charge analysis on the optimized structures was performed using the Natural Bond Orbital (NBO) method [144, 145]. The bond distances are given in units of Å written in black and NBO charges in blue where appropriate.

5.3 Results and Discussion

5.3.1 Reaction thermodynamics

The thermodynamics of a reaction are critical parameters for simulation of chemical reaction networks [146] and an entire process [147]. Standard thermodynamic parameters such as reaction enthalpy and Gibbs free energy of the ideal system are often not available in the literature but can be obtained computationally and then later combined with other thermodynamic approaches to account for the non-ideality of complex reaction mixtures at process conditions. Solvent effects on the kinetics [148] and thermodynamics [149] of the hydroformylation reaction of 1-dodecene were already investigated experimentally and combined with the Perturbed Chain Polar Statistical Associating Fluid Theory (PCP-SAFT) to model the reaction of dodecene with syngas (CO/H_2) in a solvent mixture of DMF/decane at 90 °C and 21 bar. Quantum chemical calculations of thermochemical data pose a challenge in terms of accuracy and standard DFT functionals were not suitable to obtain accurate data for the hydroformylation of long chain olefins but MP2 calculations gave reliable thermodynamic equilibrium constants K_f [149].

The reaction thermodynamics $\Delta G°r$ of the reductive amination reaction of aldehydes of various carbon chain lengths and diethylamine were calculated in the gas phase and in an implicit solvent environment. The free energy of the reaction was -14.7 kcal/mol and only slightly affected by presence of a solvent at -15.1 and -15.3 kcal/mol in either DMF or decane (see Table 5.1).

Then, the effect of the chain length of the aldehyde on the thermodynamics of the reductive amination reaction has been investigated. The free energy of the reaction was almost independent of chain length and only slightly fluctuating (-14.3 to -14.7 kcal/mol) with the chain length, and again the effect of the solvent is only minor. One can thus conclude that the thermodynamics of the reaction is independent from the chain length of the aldehyde. Thus, we investigated the mechanism of the reductive amination only for the short chain aldehyde, e.g. for the reaction of propanal and diethylamine.

Table 5.1 : The thermodynamics and solvent effects of the reductive amination reaction of various aldehydes with diethylamine ($(C_2H_5)_2NH$), ($\Delta G°r$, kcal/mol).

Chain Length	*Free Energy of Reaction*		
	Gas phase	*DMF*	*Decane*
C_3H_6O	*-14.7*	*-15.1*	*-15.3*
$C_5H_{10}O$	*-14.5*	*-15.4*	*-15.2*
$C_9H_{18}O$	*-14.5*	*-15.3*	*-15.1*
$C_{10}H_{20}O$	*-14.4*	*-15.3*	*-15.1*
$C_{11}H_{22}O$	*-14.3*	*-15.2*	*-15.0*

5.3.2 Reaction mechanism

Reductive amination of an aldehyde starts with a nucleophilic addition of the amine to the carbonyl group of the aldehyde. The initial step of the reaction leads to the formation of a carbinolamine intermediate. In an intramolecular condensation reaction, an imine or an iminium ion are formed depending on the chosen reaction conditions (in particular the pH of the reaction medium). This imine formation is an equilibrium reaction and can be controlled by H_2O addition or removal in a chemical process. The equilibrium can be shifted towards both directions, preferably to the completion by the continuous removal of water [125]. At the final step, the product amine is generated by reduction of the enamine. Throughout the reaction process, there are several key structures and the reaction is proceeding via multiple transformations in order to form the long chain amine as a final product. These chemical transformations are controlled by several factors like the pH of the reaction medium (see above), polarity of the solvent, explicit formation of hydrogen bonds by polar reaction media, and activation of the intermediates by Lewis base/Brønsted acid addition.

We here investigate in detail the reductive amination mechanism of propanal by diethylamine to yield N,N-diethylpropan-1-amine under varying reaction conditions:

a) The uncatalyzed reaction in neutral media with an implicit solvent model.

b) The uncatalyzed reaction in the presence of explicitly considered solvent molecules (here water) to form a hydrogen bond network between electrophilic and nucleophilic sites plus an implicit solvation model.

c) The effect of the co-catalyst acid on the reaction profile.

5.3.2.1 The uncatalyzed reaction in neutral media

In neutral media, the aldehyde (1) and the amine (2) form a pre-complex before the nucleophilic addition of the lone pair of the nitrogen to the positively polarized carbon atom of the aldehyde occurs (Figure 5.3) in a barrierless process. This pre-complex is a stable intermediate and 9.1 vs. 7.6 kcal/mol higher in energy than the substrates. Patil and Sunoj also report a barrierless nucleophilic attack from DFT mPW1PW91 calculation and an increase by 5 kcal/mol upon pre-complex formation [141]. A hemiaminal intermediate (4) is formed via an intramolecular proton transfer from the amine to the carbonyl oxygen in a concerted fashion (TS_1) with an activation barrier of 33.3 kcal/mol (see Table 5.2) in the gas phase and 32.4 vs. 34.1 kcal/mol in DMF and decane, respectively, which agree with the 38 kcal/mol in the gas phase (24 kcal/mol in THF) [141]. The polar solvent DMF slightly stabilizes the transition state. The coupling is followed by an intramolecular release of a water molecule, formed by the -OH group with a proton from the hemiaminal (4).

In the condensation step, a proton from either an α– or a β carbon atom can be eliminated. Abstraction of the proton at α position via TS_2a leads to forming the imine 5a intermediate whereas when the β-proton is eliminated via TS_2b the enamine intermediate 5b is formed. The activation barriers for both routes are 48.9 kcal/mol high in gas phase. They are lowered 5-10 kcal/mol by solvent calculations (still > 40 kcal/mol in both DMF and decane) with the α-pathway being slightly favoured.

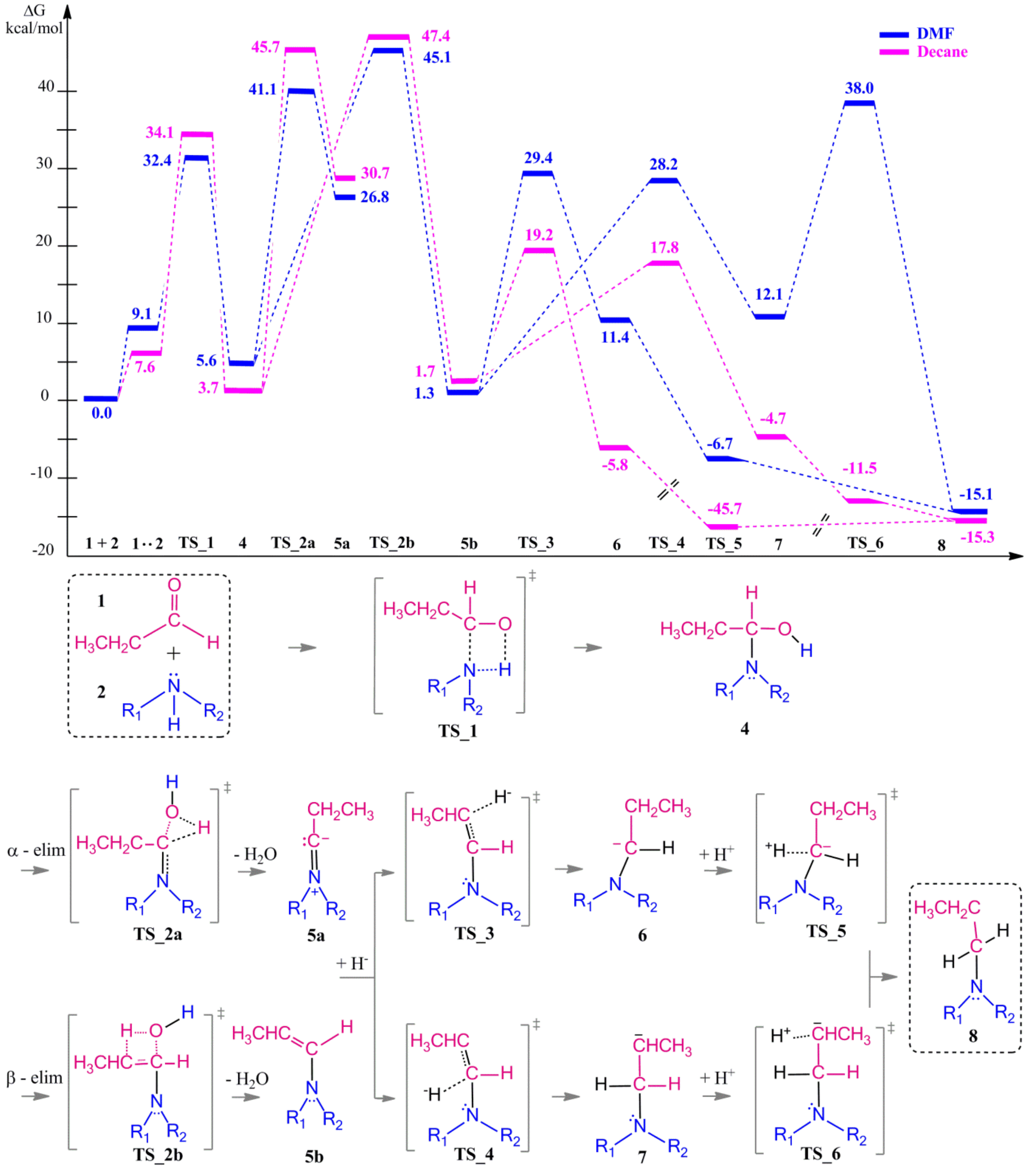
ΔG
kcal/mol
40
30
20
10
0
-10
-20
DMF
Decane
0.0
9.1
7.6
34.1
32.4
5.6
3.7
45.7
41.1
30.7
26.8
47.4
45.1
1.7
1.3
29.4
19.2
11.4
-5.8
28.2
17.8
-6.7
-45.7
12.1
-4.7
-11.5
38.0
-15.1
-15.3
1 + 2
1··2
TS_1
4
TS_2a
5a
TS_2b
5b
TS_3
6
TS_4
TS_5
7
TS_6
8
1
2
TS_1
4
α - elim
β - elim
- H₂O
+ H⁻
+ H⁺
TS_2a
5a
TS_3
6
TS_5
TS_2b
5b
TS_4
7
TS_6
8

Figure 5.3 : Reaction mechanism including transition state and intermediate structures (top) and the energy profile for reductive amination reaction in neutral media (bottom), ($R_1 = R_2 = -CH_2CH_3$).

Table 5.2 : Relative Gibbs free energies (in kcal/mol) of the transition state and intermediate structures for reductive amination reaction in neutral media, in neutral media with explicit water assistance and in acidic media, respectively.

	1 .. 2	**TS_1**	**4**	**TS_2a**	**TS_2b**	**5a**	**5b**	**TS_3**	**TS_4**	**6**	**7**	**TS_5**	**TS_6**	**8**
Gas phase	4.2	33.3	2.1	48.9	48.9	33.4	2.1	0.2	-1.2	-28.1	-25.9	-134.9	-125.2	-14.7
DMF	9.1	32.4	5.6	41.1	45.1	26.8	1.3	29.4	28.2	11.4	12.1	-6.7	38.0	-15.1
Decane	7.6	34.1	3.7	45.7	47.4	30.7	1.7	19.2	17.8	-5.8	-4.7	-45.7	-11.5	-15.3

	1_w..2	**TS_0_w**	**1w_2**	**TS_1_w**	**4_w**	**TS_2a_w**	**TS_2b_w**	**5a_w**	**5b_w**	**8**
Gas phase	2.5	7.3	8.6	24.3	0.9	34.0	49.6	30.4	-2.1	-21.5
DMF	7.5	10.6	8.4	26.2	4.2	33.1	45.2	27.2	-3.1	-27.3
Decane	9.6	13.7	13.6	30.2	7.4	38.6	53.2	34.1	2.5	-19.3

	3 .. 2	**TS_7**	**9**	**TS_8**	**TS_9**	**10**	**5b**	**TS_3**	**TS_4**	**6**	**7**	**TS_5**	**TS_6**	**8**
Gas phase	4.3	61.3	60.3	46.9	57.4	42.8	-9.0	-10.9	-12.4	-39.2	-37.0	-146.1	-136.4	-25.8
DMF	6.6	55.3	50.0	37.1	52.5	29.6	-10.2	17.8	16.7	-0.1	0.6	-6.8	26.5	-26.7
Decane	5.1	59.5	57.0	43.2	55.4	38.1	-9.7	7.8	6.4	-17.3	-16.1	-62.9	-22.9	-26.8

This is significantly lower than the 58-60 kcal/mol reported in the literature [141]. The resulting intermediates 5a (imine) and 5b (enamine) are very different in stability (Figure 5.3, bottom). The instability of the 5a by 25-29 kcal/mol compared to 5b can be attributed to the larger charge separation in the structure and the re-hybridization character of the C_{α}.

Whereas in 5b, formed double bond has a planar geometry with trans orientation of the alkyl groups and a charge density that is evenly distributed through the structure which are stabilizing 5b in comparison to 5a (Figure 5.4).

The final step in the reductive amination, is the hydrogenation (reduction) of either intermediate 5a and 5b to generate the desired tertiary amine. Besides the conventional boro hydride derivatives, there are several novel approaches for a mild and selective reduction and most of them consider a transition metal catalyst splitting H_2 into H^- and H^+ species for the addition to the double bond.

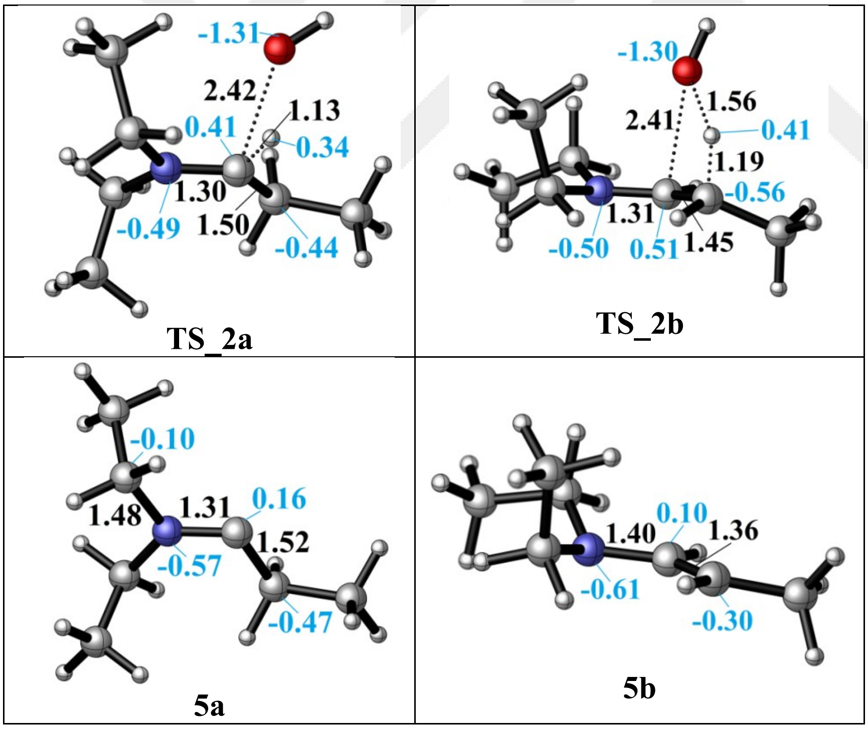

Figure 5.4 : Details of the formation of the imine 5a and enamine 5b intermediates after proton abstraction to release water via TS_2a (C_{α} position) and via TS_2b (C_{β} position).

In this work, we used a sequential approach for hydrogenation since that reflects also the procedure when an external hydride donor or an activated hydrogen molecule bound to a transition metal catalyst is used. We did not consider the hydride donor or the catalyst in molecular details since this is highly dependent on each experimental set-up and the choice of the reducing agent.

Depending on the proton abstraction step, either the imine 5a or the enamine 5b can be hydrogenated. Since the enamine is 25 - 29 kcal/mol lower in energy, only reduction of the enamine was investigated via the addition of first H^- and then H^+ species. The hydride addition to the enamine 5b structure was investigated for both carbon atoms in the C=C double bond (C_β via TS_3 to give 6 and C_α via TS_4 to give 7). The C_α atom in 5b has a charge of 0.10, where C_β is negatively charged (Figure 5.4). Thus, the attack of the H^- to the positively charged C_α carbon via TS_4 to generate 7 is found to be kinetically favourable with a difference in transition state barrier of 1.2-1.4 kcal/mol but thermodynamically less preferred by 0.7-1.1 kcal/mol. Thus, we consider both intermediates 6 and 7 in the final protonation step to give the product 8. Formation of the intermediates 6 and 7 was followed by the H^+ addition as the last part of the reduction. Intermediate 6 has a higher proton affinity by 44 – 47 kcal/mol than that of 7 and consequently the proton addition via TS_5 is preferred due to its highly exergonic fashion.

5.3.2.2 Explicit water-coordination

Water as a green solvent was shown to accelerate the reductive amination reaction itself [127]. It is also observed that H_2O addition has a positive influence to avoid the byproduct formation and catalyst poisoning, and also promotes the reduction [126, 150]. At the same time, the presence of an excess of water might lead to an unwanted hydrolysis of the enamine intermediate.

It is reported that the direct reductive amination reaction can be catalysed by non-aqueous hydrogen bonding solvents e.g. via thiourea coordination by means of the imine activation solution in the absence of an acid [151]. Moreover, kinetic studies on the system revealed that the added amount of the H-bond donor had no effect on the rate- determining step and only needed to be used in catalytic amounts. Additionally, the role of a hydrogen bond network has been shown to facilitate the nucleophilic addition and stabilize intermediates [141, 152]. Also the activation barrier of the nucleophilic attack of an amine decreased by explicit coordination of an additional amine or a solvent methanol [141].

We here investigate the catalytic effect and mechanistic role of explicitly coordinating water molecules on the kinetics (transition state barriers) in the reductive amination. For this purpose, two explicit water molecules were introduced into the initially investigated system.

Propanal was coordinated by two assisting water molecules which form hydrogen bonds to the oxygen lone pairs. The resulting aldehyde complex (1_w) was used as the starting structure (see Figure 5.5). Subsequently, the entire reaction pathway including transition state localizations was elucidated in detail.

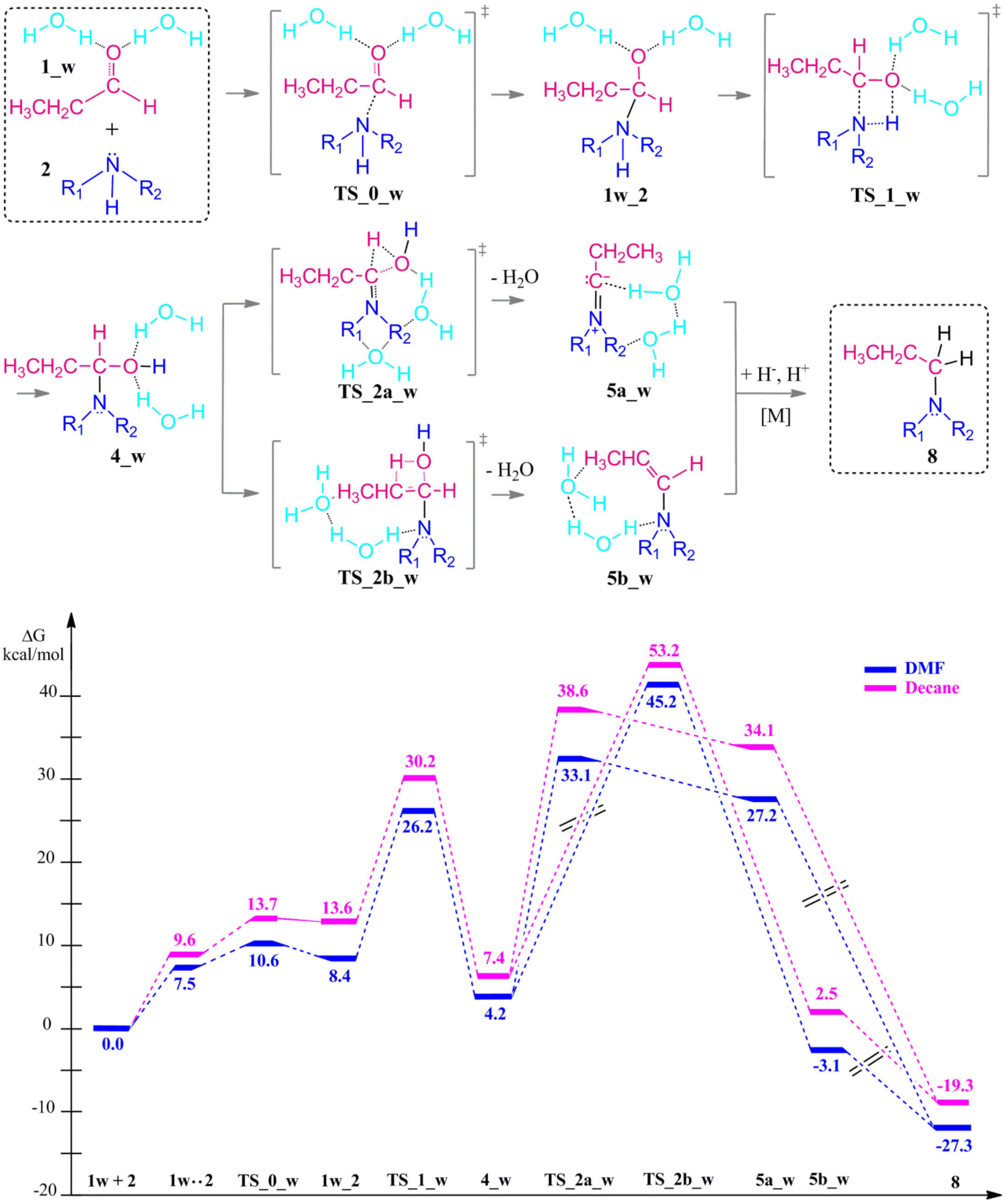

1_w
2
+
TS_0_w
1w_2
TS_1_w
4_w
TS_2a_w
TS_2b_w
5a_w
5b_w
8
- H2O
- H2O
+ H-, H+
[M]
ΔG
kcal/mol
40
30
20
10
0
-10
-20
DMF
Decane
0.0
9.6
7.5
13.7
10.6
13.6
8.4
30.2
26.2
7.4
4.2
38.6
33.1
53.2
45.2
34.1
27.2
2.5
-3.1
-19.3
-27.3
1w + 2
1w··2
TS_0_w
1w_2
TS_1_w
4_w
TS_2a_w
TS_2b_w
5a_w
5b_w
8

Figure 5.5 : Reaction mechanism including transition states and intermediates and the energy profile for reductive amination reaction with explicit water assistance, ($R_1 = R_2 = -CH_2CH_3$).

Upon hydrogen bonding, the electrophilicity of the carbonyl carbon atom in 1_w structure increases due to the increase in charge on the oxygen atom (from -0.62 to -0.70, see Figure 5.6, top). In the aldehyde-amine pre-complex, this leads to an extra stabilization by 10.6 - 6 kcal/mol in DMF and decane due to water molecule mediated interaction between aldehyde and amine (see Figure 5.6, bottom).

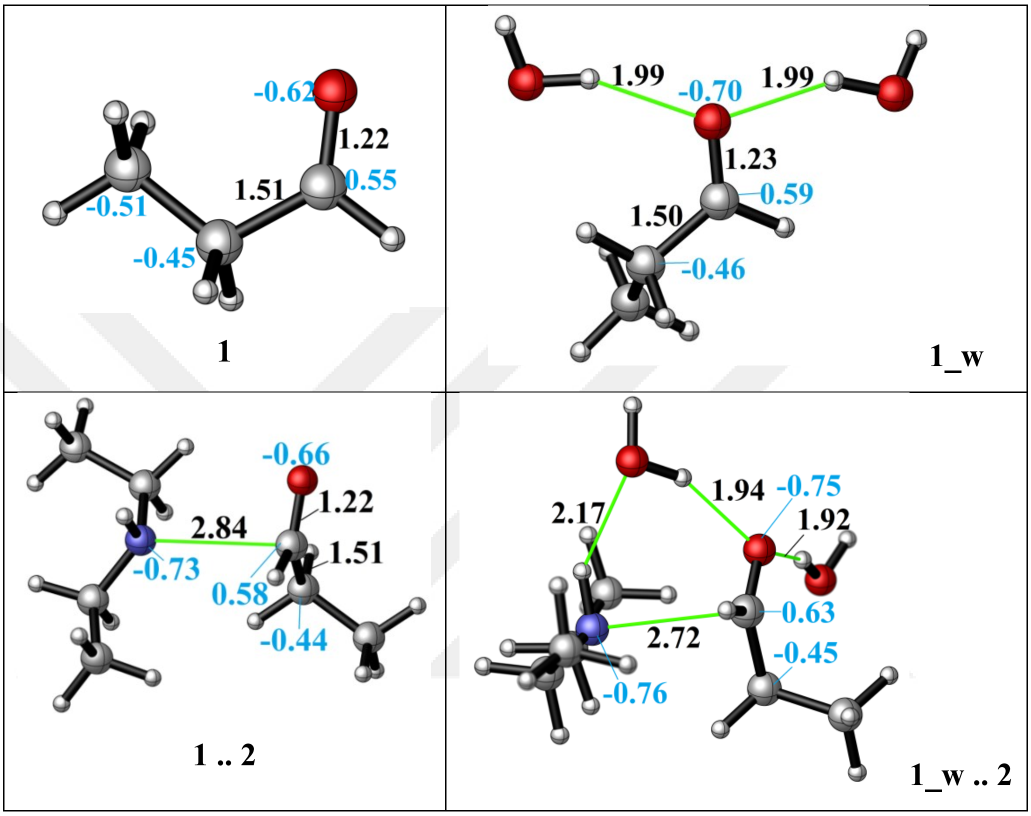

Figure 5.6 : The effect of the water assistance on pre-complex formation, (Distances are given in Å, black; NBO charges are presented in blue).

Complex 1_w .. 2 is more tightly bound and the N…C distance decreases from 2.84 Å to 2.72 Å. Coordination by water molecules leads to a different stepwise nucleophile attack pathway which now proceeds via TS_0_w (amine addition) to give 1w_2 and TS_1_w (proton transfer) to 4w. Here, the addition proceeds in a stepwise fashion whereas in the absence of water it showed a concerted fashion (TS_1, Figure 5.3). Explicit water coordination lowered the barrier of activation by 5.5 - 9.9 kcal/mol which is in agreement with the 20 kcal/mol in the case of one methanol and 28 kcal/mol for two coordinating methanol molecules with implicit THF in DFT calculations [141].

The water elimination step by proton abstraction from the C_α carbon is facilitated by the explicit water coordination. This solvent cage lowers the barrier of the condensation reaction, particularly for the imine transition state TS_2a_w (by 8 - 7.1 kcal/mol) where one solvent water coordinates to the leaving water molecule.

On the other hand, water coordination disfavors elimination from C_β of the enamine TS_2b_w by 0.1 - 5.8 kcal/mol. As a result, explicit solvation changes the preference of reaction path of the water condensation reaction. In the absence of explicit solvation, the α-pathway via the imine was slightly favoured. When solvent molecules are considered, water release via C_α proton abstraction from the enamine is kinetically favored over C_β (TS_2a_w *vs.* TS_2b_w). However, the relative thermodynamic stabilities of the intermediates 5a and 5b and 5a_w and 5b_w are preserved in neutral and water coordinated systems and are still in favor of 5b and 5b_w formation.

We can thus show that the choice of an explicitly coordinating hydrogen-bonding solvent (here water) changes the control of the reductive amination in that C_β elimination from the enamine becomes kinetically favoured while C_α elimination from the imine is still thermodynamically preferred.

5.3.2.3 The role of an acid as a co-catalyst

Experimentally, the presence of an acid as a co-catalyst was found to favorably influence the reductive amination reaction. An optimum pH range is 2.5 - 3.5 in aqueous solution to achieve the best performance with cyclometallated iridium complexes in a formic acid/formate buffer solution [127]. In the literature, different aspects of the role of the acid addition in the reductive amination reaction are discussed. Some of the studies suggest that the presence of a weak acid will facilitate and promote the first addition step whereas strongly acidic solutions prevent further reactions of the initially formed primary amine by formation of the ammonium salt [126]. It was also shown that the pH level of the reaction media can affect the catalyst activity during the reduction step as well as the enantioselectivity of the intermediates and kinetics of the process by a rate increase about six times [127]. The pH value is particularly relevant for an optimization of the catalytic selectivity and the yield of the reaction. Another work suggested an imine/enamine tautomerization in the presence of an acid [153]. Several experiments on reductive amination showed that the addition of phosphoric acid was essential for a successful reduction with Hantzsch esters. This was also investigated in computational works [154, 155] which focused on the final hydrogenation step of the imine and concluded that phosphoric acid played a crucial role in the imine activation and was controlling the enantioselectivity. An acid and H-bond assistance were shown to influence the equilibrium between iminium ion and enamine intermediate structures which can control the yield of the reaction [156].

We here investigate the effect of an acid which acts as a co-catalyst in the reductive amination reaction at mildly acidic conditions (pH 4 or 5; for example acetic acid or formic acid). In the presence of an acid, the carbonyl oxygen can be protonated and the protonated form is in equilibrium with the enol or enolate structure which is formed via enolization (Figure 5.7).

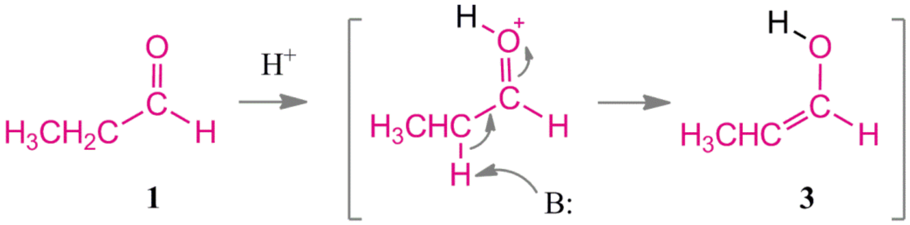

Figure 5.7 : Formation of the enol structure (3) from the aldehyde (1) in acidic conditions via protonation of the carbonyl oxygen and keto-enol tautomerization.

After a keto-enol tautomerization, the reaction between the enol and the substrate diethylamine was investigated (Figure 5.8). In the presence of the co-catalyst, two different pathways which both lead to the enamine intermediate can be distinguished. The first route is following the nucleophilic attack via TS_7 (> 55 kcal/mol) which then leads to the high energy adduct 9 which is 50-57 kcal/mol higher in energy than the substrates. From 9, C_α proton abstraction and water elimination may proceed. Here, the leaving -OH group is stabilized by interactions with the nearby methyl hydrogen atoms of the alkyl chain. This stabilization makes the elimination from the alpha position (TS_8) more favorable (by 4 - 2.5 kcal/mol compared to the neutral path, Figure 5.3) to give the enamine zwitter ion 10.

The second route is the nucleophilic addition of the amine and intramolecular water elimination by proton abstraction from the positively charged nitrogen atom via TS_9. This transition state barrier is comparable to TS_7 in the absence of the co-catalyst (within 3-4 kcal/mol) but the formation of the intermediate 5b is thermodynamically more favorable and it is significantly more stable compared to 10 by 40-48 kcal/mol.

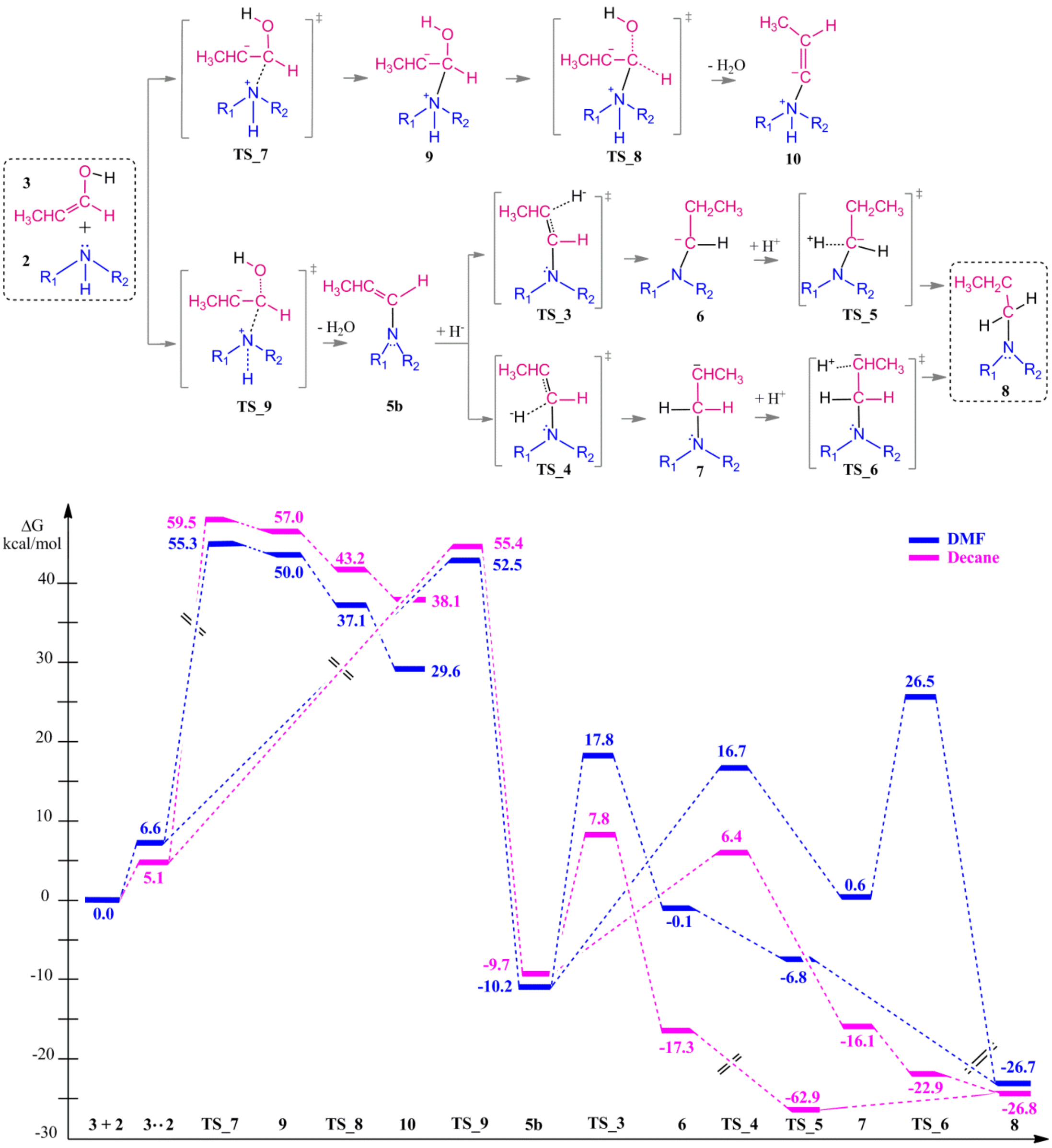

Figure 5.8 : Reaction mechanism including identified transition state and intermediate structures and the energy profile for reductive amination reaction in the presence of an acid as a co-catalyst, ($R_1 = R_2 = -CH_2CH_3$).

After the formation of 5b, hydrogenation proceeds in analogy to the neutral pathway by first hydride binding to C_α or C_β and subsequent protonation of the remaining carbon atom. Here, C_β reduction via TS_3 to give 6 is both kinetically and thermodynamically less preferred than C_α reduction via TS_4 to yield 7. The final protonation of 7 via TS_6 gives the desired product 8. TS_6 was found to be lower in energy than TS_5 in decane but upshifted by around 40 kcal/mol in DMF. This destabilization creates a barrier around 26 kcal/mol for TS_6 in DMF which was exothermic in case of TS_5.

The large effects of destabilization of the transition states TS_5 and TS_6 in polar media such as DMF indicate the need for a careful design of a suitable solvent which thermodynamically and kinetically enables the reaction.

The main difference between the pathways in neutral and acidic media was observed in the first addition step. The enol compound which was formed by tautomerization has a different atomic partial charge distribution. Protonation of the oxygen atom decreases the electrophilicity of the carbon atom from an atomic charge of 0.55 for the aldehyde compound to 0.23 for the enol. Thus, the reactivity of the carbon center towards the nucleophilic attack of the amine is lowered and renders this reaction pathway inaccessible. This effect is also reflected in the activation barriers of this step in each path (TS_7 vs. TS_1) which show a difference of 22.9 - 25.4 kcal/mol and an elongation of the N…C distance from 1.58 to 1.73 Å in the transition state (Figure 5.9).

For the second part of the reaction, hydrogenation of the enamine intermediate is following the same route as in the neutral route. However, the stability of the enamine is different with respect to the initial reactants of the co-catalyst route. 5b intermediate is thermodynamically more stable than that of the neutral reaction by 11 kcal/mol here. Although the barrier heights are the same for the hydrogenation step in the neutral and co-catalyst assisted pathways, the reaction can thus be driven easily due to the enchanced thermodynamic stability of the 5b.

5.4 Conclusion

We have carefully investigated the mechanism of the reductive amination reaction between an aldehyde and a secondary amine to give a tertiary amine. This family of products is of great relevance to the pharmaceutical and chemical industries [113-115].

Three different reaction route scenarios (unassisted, explicitly water-assisted and with an acid as a co-catalyst) were followed along the pathways. Relevant structures for each case were modelled and the energetic reaction profiles of all were compared. The thermodynamics of a reductive amination of an aldehyde was found to be exergonic around -15 kcal/mol, independent of the carbon chain length and consideration of an organic solvent has a negligible effect on the free energy of reaction.

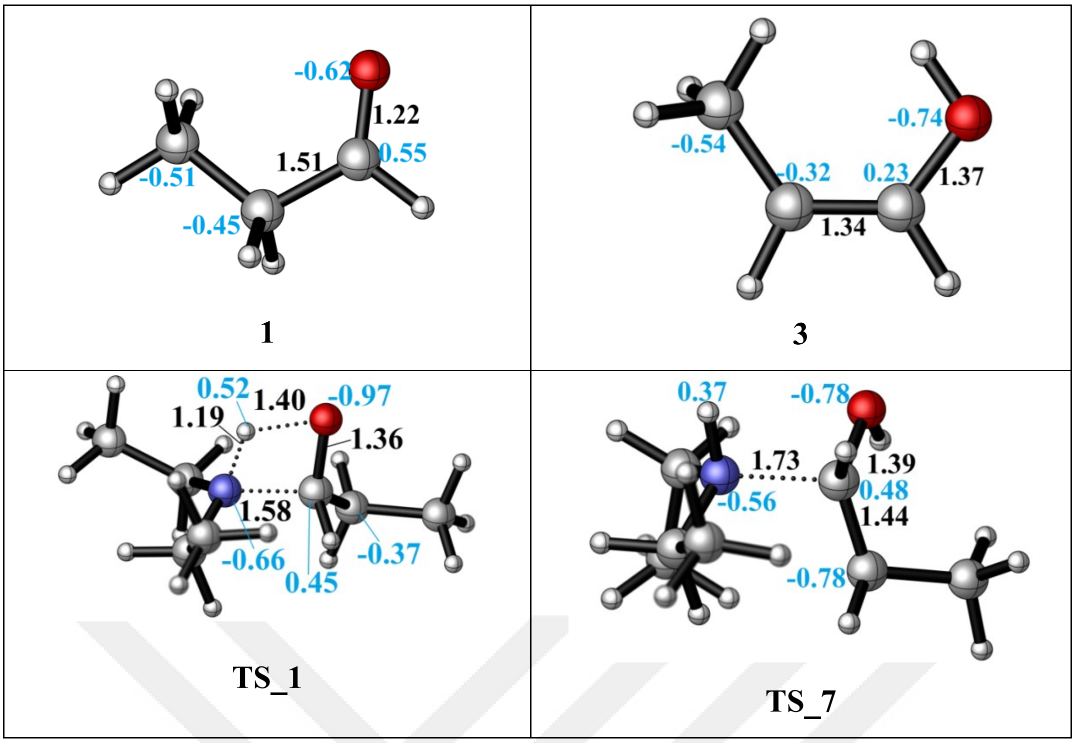

Figure 5.9 : Details of the role of the co-catalyst in the amine addition step. The first transition states (TS_1 and TS_7) from different precursors (1 and 3) via neutral and co-catalyst routes.

In the presence of water which is released during the condensation reaction, the first part of the reaction is strongly affected. Water coordination is increasing the electrophilicity of the substrate aldehyde. Thus, the activation barrier for the nucleophilic addition is significantly lowered via formation of hydrogen bond and the former concerted addition step turns into a stepwise fashion with lower energy barriers. Explicit water assistance drives the reaction pathway from an imine- to an enamine-based intermediate preferred one. Such insight is of relevance for the design of a suitable solvent in a large-scale production of tertiary amines from long-chain substrates from sustainable sources and the continuous removal of water during the process in order to minimize product loss due to hydrolysis.

Addition of an acid as a co-catalyst changes both parts of the reaction, the addition and hydrogenation steps. First, the neutral and co-catalyst assisted pathways are already diverting at the nucleophilic addition step of the cycle because the initial reactants (aldehyde vs. enol) have different electronic properties. The presence of an acid here increases the activation barrier and decelerates the rate of the reaction. However, the intramolecular release of water in the condensation reaction strongly affects the thermodynamics of the enamine formation and clearly renders this pathway the preferred one. After the water elimination step and formation of the enamine 5b, both pathways are converging to the final product via the same hydrogenation route. Thus, the presence of an acid as a co-catalyst strongly enhances the relative stability of the enamine intermediate 5b and drives the reaction forward.

In conclusion, explicit coordination of solvent water and the co-catalyst acid assistance provide extra stabilization to different intermediates of the reductive amination of aldehydes with diethylamine and drive the reaction along different pathways. Thus, by choice of solvent and pH the microkinetics of different steps will strongly be affected and allow control of kinetics and thermodynamics of the ‘step of interest’ through the reaction. Until now, the effect of the addition of acids, bases, or water on the activity and selectivity of catalysts were not resolved yet [126]. This computational work, for the first time, provides a detailed insight into these process control parameters and will aid the design of an appropriate reaction medium as well as a suitable catalyst for the hydrogenation step which is the focus of currently ongoing work.

6. CONCLUSIONS AND RECOMMENDATIONS

Since Click chemistry achieved a significant breakthrough in synthetic organic chemistry, further experimental and computational studies on this area are valuable contributions. The success of the CuAAC reaction led the researchers to investigate several transition metals to enhance this process. As a result of these efforts, efficient application of Ag metal in this cycloaddition has been presented. In the first part of this study, AgAAC reaction has been investigated by computational tools which is the nontoxic successor of the Cu catalyzed reaction. The mechanism for AgAAC reaction has been modelled for the first time with quantum mechanical calculations in this thesis by considering the experimental proposal and the general CuAAC pathway. The calculations herein show that once the proposed silver acetylide structures form, their cycloaddition with azide following the proposed path is a facile reaction in terms of energetics. The number of metal atoms involved in a Click reaction is one of the main questions considered in mechanistic studies. In AgAAC reaction, comparison of mononuclear and binuclear paths shows that the barrier for binuclear cases are lower than that of mononuclear by 4.5 to 7.2 kcal/mol in all systems. Although this energy difference does not look so high, it has a significant effect on the relative reaction rates of mono and dinuclear cases. This difference will move the dinuclear process further almost 10^3 - 10^4 times faster than the mononuclear in the current reaction conditions. A similar trend is seen in the CuAAC where dinuclear complex is kinetically favored among the active mono- and bis-copper species. One can conclude that the second metal atom has a critical role not only in AgAAC but also in CuAAC reaction which cause the superiority of dinuclear mechanism to the mononuclear one. The role of the ligands in the Ag catalyst is a substantial parameter for the reaction performance. The choice of the ligand in the catalyst complex is not only affecting the yield but also controls the regioselectivity of the process. This work is important in the sense that this is the first computational work on this potentially versatile and efficient process. Since the silver complexes represent a new form of high potential catalyst, this study should be extended by considering the sterically demanding ligands such as N,N-diisopropylamide and di-tert-butyl-phosphane. Although the steric ligands are computationally cumbersome, extension of the current work might enlighten the role of the highly potent ligands in the catalyst. Thus, elucidating the mechanism and the role of the ligands will help to increase the reaction yield and the effectiveness of the promising AAC reaction with the Ag metal.

Tropolone and diosphenol derivatives are substantial natural products which can be converted into medicaments and be used as a starting material for synthetic purposes. One of the easy and robust methods for obtaining tropolone derivatives is cyclization reactions. Therefore, convertion of tropolones into its derivatives via several cyclization reactions is a valuable task in organic chemistry. In the second chapter of the thesis, quantum mechanical calculations have been performed in order to provide insights into the synthetic pathway and regioselectivity of the reaction of a tropolone derivative in comparison to analogous five-membered system. The proposed mechanisms have been confirmed for their key steps in the overall rearrangements, providing an additional confirmation for the reaction pathway and the experimentally observed regioselectivity. The elimination step of the reaction has been modeled at the B3LYP/6-311++G** level and discussed in detail which is responsible for the regioselectivity. In conclusion, steric effects, relative charges of the abstracted hydrogens and intramolecular H-bonds were found to rule the dynamics of product formation. Moreover, these parameters are leading the ease of the elimination and determining the difference in activation barrier during the formation of various products. In both systems, experimentally observed product was favored over the alternative one, also in terms of energetics. In the third chapter, the radicalic reactions of 6- and 7-membered diosphenol derivatives differing in reactivity, ring size, aromaticity and stability were reported both experimentally and with DFT calculations. While the former is producing a mixture of products, the latter is resulting with a single product, regioselectively. DFT calculations were performed following the experimental studies in order to describe the outcomes correctly. First, quantum mechanical calculations were performed for possible intramolecular cyclizations of the forming radical in exo and endo modes and also for termination by H-abstraction. Consequently, the activation barriers for both endo and exo production of 6-membered diosphenole derivative are similar whereas termination by H-abstraction is energetically unfavorable. The non-regioselectivity of the process is attributed to the non-planar geometry of the ring which provides flexibility to the radicalic chain and eases the attack for the endo and exo formation at the same time. Besides that, lack of stabilizing effect of aromaticity in the final products disables the regioselectivity of this process. Explanations for the different selectivity patterns of 6- and 7-membered analogues are mostly based on entropy factors, variation of dihedral torsion angle between the radicalic center and functionalized double bond, aromatization of the ring and the charge distribution at the reactive atoms.

Amines represent an important class of fundamental chemicals which are used as intermediates in a wide range of applications. Finding an environmentally friendly and sustainable way to produce long chain amines from industrially available fatty acids has recently gained significant importance. Indeed, the process of reductive amination has been stated to be one of the most relevant challenges of process design for the pharmaceutical industry. In the fourth chapter, the mechanism of the reductive amination reaction between an aldehyde and a secondary amine to give a tertiary amine has been carefully investigated. Relevant structures for unassisted, explicit water-assisted and acid as a co-catalyst assisted routes were modeled and the energetic profiles of all reactions were compared. The thermodynamics of a reductive amination of an aldehyde was found to be exergonic and independent of the carbon chain length. In the presence of water which is released during the condensation reaction, the first part of the reaction is strongly affected because water coordination is increasing the electrophilicity of the substrate aldehyde. Thus, the activation barrier for the nucleophilic addition is significantly lowered via formation of hydrogen bond and the former concerted addition step turns into a stepwise fashion with lower energy barriers. Addition of an acid as a co-catalyst changes both parts of the reaction, the addition and the hydrogenation steps. The presence of an acid increases the activation barrier and decelerates the rate of the reaction. However, the intramolecular release of water in the condensation reaction strongly affects the thermodynamics of the enamine formation and clearly renders this pathway the preferred one. In conclusion, explicit coordination of water and the co-catalyst acid assistance provide extra stabilization to different intermediates and drive the reaction along different pathways. Thus, by choice of solvent and level of pH, the microkinetics of different steps will strongly be affected. This information can direct the kinetics and thermodynamics of the ‘step of interest’ through the reaction. This computational work, for the first time, provides a detailed insight into the synthetic pathway and valuable contribution in sense of process control.

This Ph.D. thesis demonstrates several computational modeling applications in organometallic, radicallic and organic reaction fields. In each chapter, the detailed mechanisms and critical steps of the reactions have been illuminated. Moreover, various parameters such as thermodynamic driveability, the key step for regioselectivity, the effect of the polarity of the solvent, the critical role of the available H-bonds in the system, effect of the co-catalyst have been investigated which are substantial factors for a rational reaction design. As a future work, important findings and conclusions from this computational study can be tested experimentally. This may aid the design of an appropriate reaction medium by providing insight into the parameters for process control.

REFERENCES

[1] **Alvarez, R., Velazquez, S., San-Felix, A., Aquaro, S., Clercq, E. D., Perno, C. F., . . . Camarasa, M. J.** (1994). 1, 2, 3-Triazole-[2, 5-Bis-O-(tert-butyldimethylsilyl)-. beta.-D-ribofuranosyl]-3'-spiro-5"-(4"-amino-1", 2"-oxathiole 2", 2"-dioxide)(TSAO) Analogs: Synthesis and Anti-HIV-1 Activity. *Journal of Medicinal Chemistry, 37*, (24), 4185-4194.

[2] **da Silva, F. C., de Souza, M. C. B., Frugulhetti, I. I., Castro, H. C., Silmara, L. d. O., de Souza, T. M. L., . . . Passamani, F.** (2009). Synthesis, HIV-RT inhibitory activity and SAR of 1-benzyl-1H-1, 2, 3-triazole derivatives of carbohydrates. *European Journal of Medicinal Chemistry, 44*, (1), 373-383.

[3] **Buckle, D. R., Rockell, C. J., Smith, H., Spicer, B. A.** (1986). Studies on 1, 2, 3-triazoles. 13.(Piperazinylalkoxy)-[1] benzopyrano [2, 3-d]-1, 2, 3-triazol-9 (1H)-ones with combined H1-antihistamine and mast cell stabilizing properties. *Journal of Medicinal Chemistry, 29*, (11), 2262-2267.

[4] **Fung-Tomc, J. C., Huczko, E., Minassian, B., Bonner, D. P.** (1998). In vitro activity of a new oral triazole, BMS-207147 (ER-30346). *Antimicrobial Agents and Chemotherapy, 42*, (2), 313-318.

[5] **Genin, M. J., Allwine, D. A., Anderson, D. J., Barbachyn, M. R., Emmert, D. E., Garmon, S. A., . . . Hutchinson, D. K.** (2000). Substituent Effects on the Antibacterial Activity of Nitrogen−Carbon-Linked (Azolylphenyl) oxazolidinones with Expanded Activity Against the Fastidious Gram-Negative Organisms Haemophilus influenzae and Moraxella c atarrhalis. *Journal of Medicinal Chemistry, 43*, (5), 953-970.

[6] **Périon, R., Ferrières, V., Garcia-Moreno, M. I., Mellet, C. O., Duval, R., Fernández, J. M. G., Plusquellec, D.** (2005). 1, 2, 3-Triazoles and related glycoconjugates as new glycosidase inhibitors. *Tetrahedron, 61*, (38), 9118-9128.

[7] **Shen, J., Woodward, R., Kedenburg, J. P., Liu, X., Chen, M., Fang, L., . . . Wang, P. G.** (2008). Histone deacetylase inhibitors through click chemistry. *Journal of Medicinal Chemistry, 51*, (23), 7417-7427.

[8] **Hou, D. R., Alam, S., Kuan, T. C., Ramanathan, M., Lin, T. P., Hung, M. S.** (2009). 1, 2, 3-Triazole derivatives as new cannabinoid CB1 receptor antagonists. *Bioorganic & Medicinal Chemistry Letters, 19*, (3), 1022-1025.

[9] **Jordão, A. K., Ferreira, V. F., Lima, E. S., de Souza, M. C., Carlos, E. C., Castro, H. C., . . . Cunha, A. C.** (2009). Synthesis, antiplatelet and in silico evaluations of novel N-substituted-phenylamino-5-methyl-1H-1, 2, 3-triazole-4-carbohydrazides. *Bioorganic & Medicinal Chemistry, 17*, (10), 3713-3719.

[10] **Thompson, A. M., Blaser, A., Anderson, R. F., Shinde, S. S., Franzblau, S. G., Ma, Z., . . . Palmer, B. D.** (2008). Synthesis, reduction potentials, and antitubercular activity of ring A/B analogues of the bioreductive drug (6 S)-2-nitro-6-{[4-(trifluoromethoxy) benzyl] oxy}-6, 7-dihydro-5 H-imidazo [2, 1-b][1, 3] oxazine (PA-824). *Journal of Medicinal Chemistry, 52*, (3), 637-645.

[11] **Hoshino, M.** (1960). Effect of 3-amino-1, 2, 4-triazole on the experimental production of liver cancer. *Nature, 186*, (4719), 174.

[12] **Hein, J. E., Fokin, V. V.** (2010). Copper-catalyzed azide–alkyne cycloaddition (CuAAC) and beyond: new reactivity of copper (I) acetylides. *Chemical Society Reviews, 39*, (4), 1302-1315.

[13] **Gothelf, K. V., Jørgensen, K. A.** (1998). Asymmetric 1, 3-dipolar cycloaddition reactions. *Chemical Reviews, 98*, (2), 863-910.

[14] **J. Mulzer, H. J. A., M. Braun, K. Krohn, and H.U. Reissig,** *Organic Synthesis Highlights*. VCH: Weinheim, 1991; p 410.

[15] **Rostovtsev, V. V., Green, L. G., Fokin, V. V., Sharpless, K. B.** (2002). A stepwise huisgen cycloaddition process: copper (I)-catalyzed regioselective "ligation" of azides and terminal alkynes. *Angewandte Chemie, 114*, (14), 2708-2711.

[16] **Kolb, H. C., Finn, M., Sharpless, K. B.** (2001). Click chemistry: diverse chemical function from a few good reactions. *Angewandte Chemie International Edition, 40*, (11), 2004-2021.

[17] **Jin, L., Tolentino, D. R., Melaimi, M., Bertrand, G.** (2015). Isolation of bis (copper) key intermediates in Cu-catalyzed azide-alkyne "click reaction". *Science Advances, 1*, (5), e1500304.

[18] **Worrell, B., Malik, J., Fokin, V. V.** (2013). Direct evidence of a dinuclear copper intermediate in Cu (I)-catalyzed azide-alkyne cycloadditions. *Science*, 1229506.

[19] **Buckley, B. R., Dann, S. E., Heaney, H.** (2010). Experimental evidence for the involvement of dinuclear alkynylcopper (I) complexes in alkyne–azide chemistry. *Chemistry-A European Journal, 16*, (21), 6278-6284.

[20] **Iacobucci, C., Reale, S., Gal, J. F., De Angelis, F.** (2015). Dinuclear Copper Intermediates in Copper (I)-Catalyzed Azide–Alkyne Cycloaddition Directly Observed by Electrospray Ionization Mass Spectrometry. *Angewandte Chemie International Edition, 54*, (10), 3065-3068.

[21] **Ahlquist, M., Fokin, V. V.** (2007). Enhanced reactivity of dinuclear copper (I) acetylides in dipolar cycloadditions. *Organometallics, 26*, (18), 4389-4391.

[22] **Straub, B. F., Bessel, M., Berg, R.** (2011). Dicopper catalysts for the azide alkyne cycloaddition: a mechanistic DFT study. *Modeling of Molecular Properties*, 207-214.

[23] **Ikhlef, D., Wang, C., Kahlal, S., Maouche, B., Astruc, D., Saillard, J.-Y.** (2015). Reaction mechanisms of transition-metal-catalyzed azide–alkyne cycloaddition "click" reactions: A DFT investigation. *Computational and Theoretical Chemistry, 1073*, 131-138.

[24] **Qi, X., Zhang, H., Shao, A., Zhu, L., Xu, T., Gao, M., . . . Lan, Y.** (2015). Silver Migration Facilitates Isocyanide-Alkyne [3+ 2] Cycloaddition Reactions: Combined Experimental and Theoretical Study. *ACS Catalysis, 5*, (11), 6640-6647.

[25] **Boren, B. C., Narayan, S., Rasmussen, L. K., Zhang, L., Zhao, H., Lin, Z., . . . Fokin, V. V.** (2008). Ruthenium-catalyzed azide− alkyne cycloaddition: Scope and mechanism. *Journal of the American Chemical Society, 130*, (28), 8923-8930.

[26] **Zhang, L., Chen, X., Xue, P., Sun, H. H., Williams, I. D., Sharpless, K. B., . . . Jia, G.** (2005). Ruthenium-catalyzed cycloaddition of alkynes and organic azides. *Journal of the American Chemical Society, 127*, (46), 15998-15999.

[27] **Boz, E., Tüzün, N. Ş.** (2013). Reaction mechanism of ruthenium-catalyzed azide–alkyne cycloaddition reaction: A DFT study. *Journal of Organometallic Chemistry, 724*, 167-176.

[28] **Powers, A. R., Ghiviriga, I., Abboud, K. A., Veige, A. S.** (2015). Au-iClick mirrors the mechanism of copper catalyzed azide–alkyne cycloaddition (CuAAC). *Dalton Transactions, 44*, (33), 14747-14752.

[29] **Del Castillo, T. J., Sarkar, S., Abboud, K. A., Veige, A. S.** (2011). 1, 3-Dipolar cycloaddition between a metal–azide (Ph 3 PAuN 3) and a metal–acetylide (Ph 3 PAuC [triple bond, length as m-dash] CPh): an inorganic version of a click reaction. *Dalton Transactions, 40*, (32), 8140-8144.

[30] **Silvestri, I. P., Andemarian, F., Khairallah, G. N., Yap, S. W., Quach, T., Tsegay, S., . . . Williams, S. J.** (2011). Copper (i)-catalyzed cycloaddition of silver acetylides and azides: incorporation of volatile acetylenes into the triazole core. *Organic & Biomolecular Chemistry, 9*, (17), 6082-6088.

[31] **Connell, T. U., Schieber, C., Silvestri, I. P., White, J. M., Williams, S. J., Donnelly, P. S.** (2014). Copper and Silver Complexes of Tris (triazole) amine and Tris (benzimidazole) amine Ligands: Evidence that Catalysis of an Azide–Alkyne Cycloaddition ("Click") Reaction by a Silver Tris (triazole) amine Complex Arises from Copper Impurities. *Inorganic Chemistry, 53*, (13), 6503-6511.

[32] **McNulty, J., Keskar, K., Vemula, R.** (2011). The First Well-Defined Silver (I)-Complex-Catalyzed Cycloaddition of Azides onto Terminal Alkynes at Room Temperature. *Chemistry-A European Journal, 17*, (52), 14727-14730.

[33] **McNulty, J., Keskar, K.** (2012). Discovery of a robust and efficient homogeneous silver (I) catalyst for the cycloaddition of azides onto terminal alkynes. *European Journal of Organic Chemistry, 2012*, (28), 5462-5470.

[34] **Ortega-Arizmendi, A. I., Aldeco-Pérez, E., Cuevas-Yañez, E.** (2013). Alkyne-Azide Cycloaddition Catalyzed by Silver Chloride and “Abnormal” Silver N-Heterocyclic Carbene Complex. *The Scientific World Journal, 2013*.

[35] **Özen, C., Tüzün, N. Ş.** (2012). The mechanism of copper-catalyzed azide–alkyne cycloaddition reaction: A quantum mechanical investigation. *Journal of Molecular Graphics and Modelling, 34*, 101-107.

[36] **Wells, A. F.** *Structural inorganic chemistry*. Oxford University Press: 1984.

[37] **Zheng, S. L., Zhang, J. P., Wong, W. T., Chen, X. M.** (2003). A novel, highly electrical conducting, single-component molecular material:[Ag2 (ophen) 2](Hophen= 1 H-[1, 10] phenanthrolin-2-one). *Journal of the American Chemical Society, 125*, (23), 6882-6883.

[38] **Su, C. Y., Kang, B. S., Du, C. X., Yang, Q. C., Mak, T. C.** (2000). Formation of mono-, bi-, tri-, and tetranuclear Ag (I) complexes of C 3-symmetric tripodal benzimidazole ligands. *Inorganic Chemistry, 39*, (21), 4843-4849.

[39] **Chai, J. D., Head-Gordon, M.** (2008). Long-range corrected hybrid density functionals with damped atom–atom dispersion corrections. *Physical Chemistry Chemical Physics, 10*, (44), 6615-6620.

[40] **Frisch, M. J., Trucks, G. W., Schlegel, H. B., Scuseria, G. E., Robb, M. A., Cheeseman, J. R., . . . Cioslowski, J.** Gaussian 09, Revision B. 01. Wallingford CT: Gaussian. In Gaussian Inc: 2009.

[41] **Fukui, K.** (1970). Formulation of the reaction coordinate. *The Journal of Physical Chemistry, 74*, (23), 4161-4163.

[42] **Fukui, K.** (1981). The path of chemical reactions-the IRC approach. *Accounts of Chemical Research, 14*, (12), 363-368.

[43] **Tornøe, C. W., Christensen, C., Meldal, M.** (2002). Peptidotriazoles on solid phase:[1, 2, 3]-triazoles by regiospecific copper (I)-catalyzed 1, 3-dipolar cycloadditions of terminal alkynes to azides. *The Journal of Organic Chemistry, 67*, (9), 3057-3064.

[44] **Bock, V. D., Hiemstra, H., Van Maarseveen, J. H.** (2006). CuI-Catalyzed Alkyne–Azide “Click” Cycloadditions from a Mechanistic and Synthetic Perspective. *European Journal of Organic Chemistry, 2006*, (1), 51-68.

[45] **Meldal, M., Tornøe, C. W.** (2008). Cu-catalyzed azide− alkyne cycloaddition. *Chemical Reviews, 108*, (8), 2952-3015.

[46] **Straub, B. F.** (2007). μ-Acetylide and μ-alkenylidene ligands in “click” triazole syntheses. *Chemical Communications*, (37), 3868-3870.

[47] **Cantillo, D., Ávalos, M., Babiano, R., Cintas, P., Jiménez, J. L., Palacios, J. C.** (2011). Assessing the whole range of CuAAC mechanisms by DFT

calculations—on the intermediacy of copper acetylides. *Organic & Biomolecular Chemistry, 9*, (8), 2952-2958.

[48] **Rodionov, V. O., Fokin, V. V., Finn, M.** (2005). Mechanism of the Ligand-Free CuI-Catalyzed Azide–Alkyne Cycloaddition Reaction. *Angewandte Chemie, 117*, (15), 2250-2255.

[49] **Rodionov, V. O., Presolski, S. I., Díaz Díaz, D., Fokin, V. V., Finn, M.** (2007). Ligand-accelerated Cu-catalyzed azide− alkyne cycloaddition: A mechanistic report. *Journal of the American Chemical Society, 129*, (42), 12705-12712.

[50] **Niu, Y. N., Yan, Z. Y., Gao, G. L., Wang, H. L., Shu, X. Z., Ji, K. G., Liang, Y. M.** (2009). Synthesis of isoquinoline derivatives via Ag-catalyzed cyclization of 2-alkynyl benzyl azides. *The Journal of Organic Chemistry, 74*, (7), 2893-2896.

[51] **Létinois-Halbes, U., Pale, P., Berger, S.** (2005). Ag NMR as a tool for mechanistic studies of Ag-catalyzed reactions: Evidence for in situ formation of alkyn-1-yl silver from alkynes and silver salts. *The Journal of Organic Chemistry, 70*, (23), 9185-9190.

[52] **Calvo-Losada, S., Pino-González, M. S., Quirante, J. J.** (2015). Rationalizing the Catalytic Activity of Copper in the Cycloaddition of Azide and Alkynes (CuAAC) with the Topology of∇ 2ρ (r) and∇∇ 2ρ (r). *The Journal of Physical Chemistry B, 119*, (4), 1243-1258.

[53] **Himo, F., Lovell, T., Hilgraf, R., Rostovtsev, V. V., Noodleman, L., Sharpless, K. B., Fokin, V. V.** (2005). Copper (I)-catalyzed synthesis of azoles. DFT study predicts unprecedented reactivity and intermediates. *Journal of the American Chemical Society, 127*, (1), 210-216.

[54] **Schmidbaur, H., Schier, A.** (2015). Argentophilic interactions. *Angewandte Chemie International Edition, 54*, (3), 746-784.

[55] **Pyykkö, P., Li, J., Runeberg, N.** (1994). Predicted ligand dependence of the Au (I)… Au (I) attraction in (XAuPH3) 2. *Chemical Physics Letters, 218*, (1-2), 133-138.

[56] **Pyykkö, P.** (1997). Strong closed-shell interactions in inorganic chemistry. *Chemical Reviews, 97*, (3), 597-636.

[57] **Pyykkö, P., Runeberg, N., Mendizabal, F.** (1997). Theory of the d10–d10 Closed-Shell Attraction: 1. Dimers Near Equilibrium. *Chemistry-A European Journal, 3*, (9), 1451-1457.

[58] **Pyykkö, P.** (2002). Relativity, Gold, Closed-Shell Interactions, and CsAu· NH3. *Angewandte Chemie International Edition, 41*, (19), 3573-3578.

[59] **Muñiz, J., Wang, C., Pyykkö, P.** (2011). Aurophilicity: the effect of the neutral ligand L on [{ClAuL} 2] systems. *Chemistry-A European Journal, 17*, (1), 368-377.

[60] **Sculfort, S., Braunstein, P.** (2011). Intramolecular d10–d10 interactions in heterometallic clusters of the transition metals. *Chemical Society Reviews, 40*, (5), 2741-2760.

[61] **Cui, Y., He, C.** (2003). Efficient aziridination of olefins catalyzed by a unique disilver (I) compound. *Journal of the American Chemical Society, 125*, (52), 16202-16203.

[62] **El-Zaria, M. E., Keskar, K., Genady, A. R., Ioppolo, J. A., McNulty, J., Valliant, J. F.** (2014). High yielding synthesis of carboranes under mild reaction conditions using a homogeneous silver (I) catalyst: direct evidence of a bimetallic intermediate. *Angewandte Chemie, 126*, (20), 5256-5260.

[63] **Houte, H., Valnot, J. Y., Piettre, S. R.** (2002). Tropolonyl ethers of saccharides and cyclitol derivatives. *Tetrahedron Letters, 43*, (50), 9217-9220.

[64] **Pietra, F.** (1973). Seven-membered conjugated carbo-and heterocyclic compounds and their homoconjugated analogs and metal complexes. Synthesis, biosynthesis, structure, and reactivity. *Chemical Reviews, 73*, (4), 293-364.

[65] **Pietra, F.** (1979). Revival of troponoid chemistry. *Accounts of Chemical Research, 12*, (4), 132-138.

[66] **Koufaki, M., Theodorou, E., Alexi, X., Nikoloudaki, F., Alexis, M. N.** (2010). Synthesis of tropolone derivatives and evaluation of their in vitro neuroprotective activity. *European Journal of Medicinal Chemistry, 45*, (3), 1107-1112.

[67] **Baya, M., Soulounganga, P., Gelhaye, E., Gerardin, P.** (2001). Fungicidal activity of β-thujaplicin analogues. *Pest Management Science, 57*, (9), 833-838.

[68] **Pauson, P. L.** (1955). Tropones and tropolones. *Chemical Reviews, 55*, (1), 9-136.

[69] **Lee, J. C., Cho, S. Y., Cha, J. K.** (1999). Stereo-and regiocontrolled hydroxylation of oxyallyl [4+ 3] cycloadducts. A concise synthesis of hinokitiol. *Tetrahedron Letters, 40*, (43), 7675-7678.

[70] **Najda-Bernatowicz, A., Krawczyk, M., Stankiewicz-Drogoń, A., Bretner, M., Boguszewska-Chachulska, A. M.** (2010). Studies on the anti-hepatitis C virus activity of newly synthesized tropolone derivatives: identification of NS3 helicase inhibitors that specifically inhibit subgenomic HCV replication. *Bioorganic & Medicinal Chemistry, 18*, (14), 5129-5136.

[71] **Bass, R., Gordon, D.** (1985). A Convenient Route to Tropolone Ethers. *Synthetic Communications, 15*, (3), 225-228.

[72] **Potenziano, J., Spitale, R., Janik, M. E.** (2005). Improved and Highly Versatile Synthesis of 5-Aryltropones. *Synthetic Communications, 35*, (15), 2005-2016.

[73] **Ponaras, A. A., Zaim, O., Pazo, Y., Ohannesian, L.** (1988). Synthetic elaboration of diosphenols. Part 3. Replacement of enolic oxygen by hydrogen. *The Journal of Organic Chemistry, 53*, (5), 1110-1112.

[74] **Ponaras, A., Zaim, O.** (1986). Synthetic elaboration of diosphenols. Replacement of hydroxyl by halogen. *The Journal of Organic Chemistry, 51*, (24), 4741-4743.

[75] **Boz, M., Zaim, O., Esen, H.** (2009). A Convenient Synthesis of 2-Azido and 2-Thiocyanato-2, 3-Unsaturated Cyclic Ketones. *Turkish Journal of Chemistry, 33*, (1), 59-65.

[76] **Reineke, C. E., Goralski, C. T.** (1977). Thermal rearrangement of O-(2, 4, 6-trihalophenyl) N, N-dimethylthiocarbamates. An abnormal pathway. *The Journal of Organic Chemistry, 42*, (7), 1139-1142.

[77] **Lee, C., Yang, W., Parr, R. G.** (1988). Development of the Colle-Salvetti correlation-energy formula into a functional of the electron density. *Physical Review B, 37*, (2), 785.

[78] **Becke, A. D.** (1993). Density-functional thermochemistry. III. The role of exact exchange. *The Journal of Chemical Physics, 98*, (7), 5648-5652.

[79] **Miehlich, B., Savin, A., Stoll, H., Preuss, H.** (1989). Results obtained with the correlation energy density functionals of Becke and Lee, Yang and Parr. *Chemical Physics Letters, 157*, (3), 200-206.

[80] **Ess, D. H., Houk, K.** (2005). Activation energies of pericyclic reactions: Performance of DFT, MP2, and CBS-QB3 methods for the prediction of activation barriers and reaction energetics of 1, 3-dipolar cycloadditions, and revised activation enthalpies for a standard set of hydrocarbon pericyclic reactions. *The Journal of Physical Chemistry A, 109*, (42), 9542-9553.

[81] **Iafe, R. G., Houk, K.** (2008). Intramolecular Hetero-Diels− Alder Reactions of Imine and Iminium Dienophiles: Quantum Mechanical Exploration of Mechanisms and Stereoselectivities. *The Journal of Organic Chemistry, 73*, (7), 2679-2686.

[82] **Gallardo-Godoy, A., Fierro, A., McLean, T. H., Castillo, M., Cassels, B. K., Reyes-Parada, M., Nichols, D. E.** (2005). Sulfur-substituted α-alkyl phenethylamines as selective and reversible MAO-A inhibitors: Biological activities, CoMFA analysis, and active site modeling. *Journal of Medicinal Chemistry, 48*, (7), 2407-2419.

[83] **Ballmann, J., Fuchs, M. G., Dechert, S., John, M., Meyer, F.** (2008). Synthesis and Coordination Properties of Chelating Dithiophenolate Ligands. *Inorganic Chemistry, 48*, (1), 90-99.

[84] **Giese, B.** *Radicals in organic synthesis: formation of carbon-carbon bonds*. Pergamon Press: 1986; Vol. 5.

[85] **Jasperse, C. P., Curran, D. P., Fevig, T. L.** (1991). Radical reactions in natural product synthesis. *Chemical Reviews, 91*, (6), 1237-1286.

[86] **Jiaang, W. T., Lin, H. C., Tang, K. H., Chang, L. B., Tsai, Y. M.** (1999). The Study of the Kinetics of Intramolecular Radical Cyclizations of Acylsilanes via the Intramolecular Competition Method. *Journal of Organic Chemistry, 64*, (2), 618-628.

[87] **Orito, K., Uchiito, S., Satoh, Y., Tatsuzawa, T., Harada, R., Tokuda, M.** (2000). Aryl Radical Cyclizations of 1-(2 ‘-Bromobenzyl)

isoquinolines with AIBN− Bu3SnH: Formation of Aporphines and Indolo [2, 1-a] isoquinolines. *Organic Letters, 2*, (3), 307-310.

[88] **Togo, H.** *Advanced free radical reactions for organic synthesis*. Elsevier: 2004.

[89] **Beckwith, A. L., Bowry, V. W., Schiesser, C. H.** (1991). Ring closure of the 6-methylenecyclodecyl radical. *Tetrahedron, 47*, (1), 121-130.

[90] **Enholm, E. J., Burroff, J. A.** (1997). Tandem radical cyclizations promoted by O-stannyl ketyls. *Tetrahedron, 53*, (40), 13583-13602.

[91] **Ikeda, M., Hamada, M., Yamashita, T., Matsui, K., Sato, T., Ishibashi, H.** (1999). Stereoselective synthesis of (3 R*, 3a S*, 7a S*)-3-aryloctahydroindol-2-ones using radical cyclisation: a formal synthesis of (±)-pancracine. *Journal of the Chemical Society, Perkin Transactions 1*, (14), 1949-1956.

[92] **Majumdar, K., Islam, R.** (2008). Regioselective Synthesis of 1, 8-Naphthyridinone-Annulated Oxygen and Sulfur Heterocycles by Tri-n-butyl Tinhydride–Mediated Aryl Radical Cyclization. *Synthetic Communications, 38*, (23), 4053-4067.

[93] **Della, E. W., Smith, P. A.** (2001). Regioselectivity of ring closure of the 2-azonia-2, 2, 5-trimethyl-5-hexenyl radical. *Tetrahedron Letters, 42*, (3), 481-483.

[94] **Stork, G., Sher, P. M.** (1986). A catalytic tin system for trapping of radicals from cyclization reactions. Regio-and stereocontrolled formation of two adjacent chiral centers. *Journal of the American Chemical Society, 108*, (2), 303-304.

[95] **Beckwith, A. L.** (1981). Regio-selectivity and stereo-selectivity in radical reactions. *Tetrahedron, 37*, (18), 3073-3100.

[96] **Smith, T. W., Butler, G. B.** (1978). Effect of substituents on ring size in radical cyclizations. 1. Methyl vs. phenyl. *Journal of Organic Chemistry, 43*, (1), 6-13.

[97] **Majumdar, K. C., Basu, P. K., Chattopadhyay, S. K.** (2007). Formation of five-and six-membered heterocyclic rings under radical cyclisation conditions. *Tetrahedron, 63*, (4), 793-826.

[98] **Beckwith, A. L., Gara, W. B.** (1975). Mechanism of cyclization of aryl radicals containing unsaturated ortho-substituents. *Journal of the Chemical Society, Perkin Transactions 2*, (7), 795-802.

[99] **Murphy, J. A., Scott, K. A., Sinclair, R. S., Lewis, N.** (1997). A new synthesis of indoles. *Tetrahedron Letters, 38*, (41), 7295-7298.

[100] **Yang, C. C., Chang, H. T., Fang, J. M.** (1993). Nucleophilic-type radical cyclizations of indoles: conversion of 2-cyano 3-substituted indoles to spiro-annelated indolines and tetrahydrocarbazolones. *Journal of Organic Chemistry, 58*, (11), 3100-3105.

[101] **Ponaras, A. A., Zaim, Ö.** (1993). Radical cyclizations of diosphenol ω-haloalkyl ethers to oxabicycloalkanones. *Tetrahedron Letters, 34*, (18), 2879-2882.

[102] **Beckwith, A., Gream, G., Struble, D.** (1972). Cyclization and cupric-ion oxidation of 4-(cyclohex-1-enyl) butyl radical. *Australian Journal of Chemistry, 25*, (5), 1081-1105.

[103] **Zaim, Ö., Tüzün, N. Ş., Çevik, B., Özcan, H., Boz, E.** (2015). Synthesis, reactions and DFT study of tropolone N, N-dimethylthiocarbamate. *Tetrahedron, 71*, (33), 5391-5398.

[104] **Zhao, Y., Schultz, N. E., Truhlar, D.** Exchange-correlation functional with broad accuracy for metallic and nonmetallic compounds, kinetics, and noncovalent interactions. In AIP: 2005.

[105] **Galano, A., Muñoz-Rugeles, L., Alvarez-Idaboy, J. R., Bao, J. L., Truhlar, D. G.** (2015). Hydrogen abstraction reactions from phenolic compounds by peroxyl radicals: multireference character and density functional theory rate constants. *Journal of Physical Chemistry A, 120*, (27), 4634-4642.

[106] **Gonzalez, C., Schlegel, H. B.** (1989). An improved algorithm for reaction path following. *Journal of Chemical Physics, 90*, (4), 2154-2161.

[107] **Gonzalez, C., Schlegel, H. B.** (1990). Reaction path following in mass-weighted internal coordinates. *Journal of Physical Chemistry, 94*, (14), 5523-5527.

[108] **Tomasi, J., Mennucci, B., Cammi, R.** (2005). Quantum mechanical continuum solvation models. *Chemical Reviews, 105*, (8), 2999-3094.

[109] **Cioslowski, J.** (1989). A new population analysis based on atomic polar tensors. *Journal of the American Chemical Society, 111*, (22), 8333-8336.

[110] **Bergner, A., Dolg, M., Küchle, W., Stoll, H., Preuß, H.** (1993). Ab initio energy-adjusted pseudopotentials for elements of groups 13–17. *Molecular Physics, 80*, (6), 1431-1441.

[111] **Spellmeyer, D., Houk, K.** (1987). Force-field model for intramolecular radical additions. *Journal of Organic Chemistry, 52*, (6), 959-974.

[112] **Beckwith, A. L., Schiesser, C. H.** (1985). Regio-and stereo-selectivity of alkenyl radical ring closure: A theoretical study. *Tetrahedron, 41*, (19), 3925-3941.

[113] **Hayes, K. S.** (2001). Industrial processes for manufacturing amines. *Applied Catalysis A: General, 221*, (1), 187-195.

[114] **Behr, A., Fiene, M., Buß, C., Eilbracht, P.** (2000). Hydroaminomethylation of fatty acids with primary and secondary amines—A new route to interesting surfactant substrates. *European Journal of Lipid Science and Technology, 102*, (7), 467-471.

[115] **Constable, D. J. C., Dunn, P. J., Hayler, J. D., Humphrey, G. R., Leazer, J. L., Linderman, R. J., . . . Zhang, T. Y.** (2007). Key green chemistry research areas - a perspective from pharmaceutical manufacturers. *Green Chemistry, 9*, (5), 411-420.

[116] **Behr, A., Vorholt, A. J., Ostrowski, K. A., Seidensticker, T.** (2014). Towards resource efficient chemistry: tandem reactions with renewables. *Green Chemistry, 16*, (3), 982-1006.

[117] **Rische, T., Eilbracht, P.** (1997). One-Pot Synthesis of Secondary and Tertiary Amines by Carbonylative Hydroaminomethylation of Alkenes Catalyzed by Di(μ-chloro)bis(η4-1,5-cyclooctadiene)dirhodium. *Synthesis, 1997*, (11), 1331-1337.

[118] **Faßbach, T. A., Gaide, T., Terhorst, M., Behr, A., Vorholt, A. J.** (2017). Renewable Surfactants through the Hydroaminomethylation of Terpenes. *ChemCatChem, 9*, 1359-1362.

[119] **Fuchs, S., Lichte, D., Dittmar, M., Meier, G., Strutz, H., Behr, A., Vorholt, A. J.** (2017). Tertiary Amines as Ligands in a Four-Step Tandem Reaction of Hydroformylation and Hydrogenation: An Alternative Route to Industrial Diol Monomers. *ChemCatChem, 9*, 1436-1441.

[120] **AbdelMagid, A. F., Carson, K. G., Harris, B. D., Maryanoff, C. A., Shah, R. D.** (1996). Reductive amination of aldehydes and ketones with sodium triacetoxyborohydride. Studies on direct and indirect reductive amination procedures. *Journal of Organic Chemistry, 61*, (11), 3849-3862.

[121] **Abdelmagid, A. F., Maryanoff, C. A., Carson, K. G.** (1990). Reductive Amination of Aldehydes and Ketones by Using Sodium Triacetoxyborohydride. *Tetrahedron Letters, 31*, (39), 5595-5598.

[122] **Abdel-Magid, A. F., Mehrman, S. J.** (2006). A review on the use of sodium triacetoxyborohydride in the reductive amination of ketones and aldehydes. *Organic Process Research & Development, 10*, (5), 971-1031.

[123] **Mehrman, S. J.** (2006). A Review on the Use of Sodium Triacetoxyborohydride in the Reductive Amination of Ketones and Aldehydes. *Organic Process Research & Development, 10*, 971-1031.

[124] **Varjosaari, S.E., Skrypai, V., Suating, P., Hurley, J. J. M., De Lio, A. M., Gilbert, T. M., Adler, M. J.** (2017). Simple Metal-Free Direct Reductive Amination Using Hydrosilatrane to Form Secondary and Tertiary Amines. *Adv. Synth. Catal, 359*, 1872-1878.

[125] **Tripathi, R. P., Verma, S. S., Pandey, J., Tiwari, V. K.** (2008). Recent development on catalytic reductive amination and applications. *Current Organic Chemistry, 12*, (13), 1093-1115.

[126] **Gomez, S., Peters, J. A., Maschmeyer, T.** (2002). The Reductive Amination of Aldehydes and Ketones and the Hydrogenation of Nitriles: Mechanistic Aspects and Selectivity Control. *Advanced Synthesis & Catalysis, 344*, (10), 1037-1057.

[127] **Qian Lei, Y. W., Dinesh Talwar, Chao Wang, Dong Xue, and Jianliang Xiao** (2013). Fast Reductive Amination by Transfer Hydrogenation “on Water”. *Chem. Eur. J., 19*, 4021-4029.

[128] **Mizuta, T., Sakaguchi, S., Ishii, Y.** (2005). Catalytic reductive alkylation of secondary amine with aldehyde and silane by an iridium compound. *The Journal of Organic Chemistry, 70*, (6), 2195-2199.

[129] **Wang, C., Pettman, A., Bacsa, J., Xiao, J.** (2010). A Versatile Catalyst for Reductive Amination by Transfer Hydrogenation. *Angewandte Chemie International Edition, 49*, (41), 7548-7552.

[130] **Tararov, V. I., Kadyrov, R., Riermeier, T. H., Fischer, C., Börner, A.** (2004). Direct reductive amination versus hydrogenation of intermediates–A comparison. *Advanced Synthesis & Catalysis, 346*, (5), 561-565.

[131] **Sabine Pisiewicz, T. S., Annette-Enrica Surkus, Kathrin Junge, and Matthias Beller** (2015). Synthesis of Amines by Reductive Amination of Aldehydes and Ketones using Co_3O_4/NGr@C Catalyst. *ChemCatChem, 7*, 62-64.

[132] **Nayal, O. S., Bhatt, V., Sharma, S., Kumar, N.** (2015). Chemoselective Reductive Amination of Carbonyl Compounds for the Synthesis of Tertiary Amines Using $SnCl_2{\cdot}2H_2O$/PMHS/MeOH. *The Journal of Organic Chemistry, 80*, 5912-5918.

[133] **Seidel, D.** (2015). The Azomethine Ylide Route to Amine C−H Functionalization: Redox-Versions of Classic Reactions and a Pathway to New Transformations. *Accounts of Chemical Research, 48*, 317-328.

[134] **Dieckmann, A., Richers, M. T., Platonova, A. Y., Zhang, C., Seidel, D., Houk, K. N.** (2013). Metal-Free α-Amination of Secondary Amines: Computational and Experimental Evidence for Azaquinone Methide and Azomethine Ylide Intermediates. *J. Org. Chem., 78*, 4132-4144.

[135] **Richers, M. T., Breugst, M., Platonova, A. Y., Ullrich, A., Dieckmann, A., Houk, K. N., Seidel, D.** (2014). Redox-Neutral α-Oxygenation of Amines: Reaction Development and Elucidation of the Mechanism. *J. Am. Chem. Soc, 136*, 6123-6135.

[136] **Markert, J., Brunsch, Y., Munkelt, T., Kiedorf, G., Behr, A., Hamel, C., Seidel-Morgenstern, A.** (2013). Analysis of the reaction network for the Rh-catalyzed hydroformylation of 1-dodecene in a thermomorphic multicomponent solvent system. *Applied Catalysis A: General, 462-463*, 287-295.

[137] **Lemberg, M., Gerlach, M., Kohls, E., Hamel, C., Seidel-Morgenstern, A., Stein, M., Sadowski, G.** (2017). Predicting Solvent Effects on the 1-dodecene Hydroformylation Reaction Equilibrium. *AIChE Journal*.

[138] **Gerlach, M., Wajid, D. A., Hilfert, L., Edelmann, F., Seidel-Morgenstern, A., Hamel, C.** (2017). Impact of minor amounts of hydroperoxides on rhodium-catalyzed hydroformylation of long-chain olefins. *Catalysis Science & Technology, 7*, (7), 1465-1469.

[139] **Jörke, A., Gaide, T., Behr, A., Vorholt, A., Seidel-Morgenstern, A., Hamel, C.** (2017). Hydroformylation and tandem isomerization–hydroformylation of n-decenes using a rhodium-BiPhePhos catalyst:

Kinetic modeling, reaction network analysis and optimal reaction control. *Chemical Engineering Journal, 313*, 382-397.

[140] **Behr, A., Roll, R.** (2005). Hydroaminomethylation in thermomorphic solvent systems. *Journal of Molecular Catalysis A: Chemical, 239*, (1), 180-184.

[141] **Patil, M. P., Sunoj, R. B.** (2007). Insights on co-catalyst-promoted enamine formation between dimethylamine and propanal through ab initio and density functional theory study. *The Journal of Organic Chemistry, 72*, (22), 8202-8215.

[142] **Møller, C., Plesset, M. S.** (1934). Note on an approximation treatment for many-electron systems. *Physical Review, 46*, (7), 618.

[143] **Marenich, A. V., Cramer, C. J., Truhlar, D. G.** (2009). Universal solvation model based on solute electron density and on a continuum model of the solvent defined by the bulk dielectric constant and atomic surface tensions. *The Journal of Physical Chemistry B, 113*, (18), 6378-6396.

[144] **Reed, A. E., Weinhold, F.** (1983). Natural bond orbital analysis of near-Hartree–Fock water dimer. *The Journal of Chemical Physics, 78*, (6), 4066-4073.

[145] **Reed, A. E., Weinstock, R. B., Weinhold, F.** (1985). Natural population analysis. *The Journal of Chemical Physics, 83*, (2), 735-746.

[146] **Kiedorf, G., Hoang, D. M., Müller, A., Jörke, A., Markert, J., Arellano-Garcia, H., . . . Hamel, C.** (2014). Kinetics of 1-dodecene hydroformylation in a thermomorphic solvent system using a rhodium-biphephos catalyst. *Chemical Engineering Science, 115*, 31-48.

[147] **Hentschel, B., Kiedorf, G., Gerlach, M., Hamel, C., Seidel-Morgenstern, A., Freund, H., Sundmacher, K.** (2015). Model-Based Identification and Experimental Validation of the Optimal Reaction Route for the Hydroformylation of 1-Dodecene. *Industrial & Engineering Chemistry Research, 54*, (6), 1755-1765.

[148] **Schäfer, E., Brunsch, Y., Sadowski, G., Behr, A.** (2012). Hydroformylation of 1-Dodecene in the Thermomorphic Solvent System Dimethylformamide/Decane. Phase Behavior–Reaction Performance–Catalyst Recycling. *Industrial & Engineering Chemistry Research, 51*, (31), 10296-10306.

[149] **Lemberg, M., Sadowski, G., Gerlach, M., Kohls, E., Stein, M., Hamel, C., Seidel-Morgenstern, A.** (2017). Predicting solvent effects on the 1-dodecene hydroformylation reaction equilibrium. *AIChE Journal, 63*, (10), 4576-4585.

[150] **Wei, Y., Xue, D., Lei, Q., Wang, C., Xiao, J.** (2013). Cyclometalated iridium complexes for transfer hydrogenation of carbonyl groups in water. *Green Chemistry, 15*, (3), 629-634.

[151] **Menche, D., Hassfeld, J., Li, J., Menche, G., Ritter, A., Rudolph, S.** (2006). Hydrogen bond catalyzed direct reductive amination of ketones. *Organic Letters, 8*, (4), 741-744.

[152] **Solís-Calero, C., Ortega-Castro, J., Hernández-Laguna, A., Munoz, F.** (2012). A comparative DFT study of the Schiff base formation from acetaldehyde and butylamine, glycine and phosphatidylethanolamine. *Theoretical Chemistry Accounts, 131*, (9), 1263.

[153] **Hoffmann, S., Nicoletti, M., List, B.** (2006). Catalytic asymmetric reductive amination of aldehydes via dynamic kinetic resolution. *Journal of the American Chemical Society, 128*, (40), 13074-13075.

[154] **Marcelli, T., Hammar, P., Himo, F.** (2008). Phosphoric acid catalyzed enantioselective transfer hydrogenation of imines: a density functional theory study of reaction mechanism and the origins of enantioselectivity. *Chemistry-A European Journal, 14*, (28), 8562-8571.

[155] **Simón, L., Goodman, J. M.** (2008). Theoretical study of the mechanism of Hantzsch ester hydrogenation of imines catalyzed by chiral BINOL-phosphoric acids. *Journal of the American Chemical Society, 130*, (27), 8741-8747.

[156] **Renzi, P., Hioe, J., Gschwind, R. M.** (2017). Enamine/Dienamine and Brønsted Acid Catalysis: Elusive Intermediates, Reaction Mechanisms, and Stereoinduction Modes Based on in Situ NMR Spectroscopy and Computational Studies. *Accounts of Chemical Research, 50*, (12), 2936-2948.

CURRICULUM VITAE

Name Surname : Esra Boz

Place and Date of Birth : İstanbul, 26.09.1986

E-Mail : bozesra@gmail.com , boze@itu.edu.tr

EDUCATION :

- **B.Sc.** : 2009, Istanbul Technical University, Faculty of Science and Letters, Department of Chemistry
- **M.Sc.** : 2011, Istanbul Technical University, Faculty of Science and Letters, Department of Chemistry

PROFESSIONAL EXPERIENCE AND REWARDS:

- Max Planck Institut for Dynamics of Complex Technical Systems, Magdeburg, Germany. Molecular Simulation and Design Group, (April 2016-).
- Research Grant for Doctorate Students (2214-A) by the Scientific and Technological Research Council of Turkey (TÜBİTAK).
- Istanbul Technical University, Faculty of Science and Letters, Department of Chemistry, Istanbul, Turkey. Teaching & Research Assistant-General Chemistry and Physical Chemistry Laboratory (2010-2017).

PUBLICATIONS, PRESENTATIONS AND PATENTS ON THE THESIS:

- **Boz, E** and Tüzün, N. Ş. (2016). Ag-catalyzed azide alkyne cycloaddition: a DFT approach. *Dalton Transactions*, 45, 5752-5764. (*article*)

- Zaim, Ö., Tüzün, N. Ş.¸ Çevik, B., Özcan, H., **Boz, E.** (2015), Synthesis, reactions and DFT study of tropolone N,N-dimethylthiocarbamate. *Tetrahedron*, 71, 5391-5398. (*article*)

- **Boz, E.**, Tüzün, N. Ş. and Stein, M. “A Computational Approach to Sustainable Industrial Amines.” Chemistry Via Computation, 2017, Boğaziçi University, Istanbul, Turkey. *(poster presentation)*

- **Boz, E**., Tüzün, N. Ş. and Stein, M. “The Role of Solvents in the Reductive Amination of Aldehydes”, Hands-on Workshop Density-Functional Theory and Beyond: Accuracy, Efficiency and Reproducibility in Computational Materials Science, July 31 - August 11, 2017, Berlin, Germany. *(poster presentation)*

- Tüzün, N. Ş., **Boz, E.** “Ag in Click Reaction: A DFT Study”, ESPA 2016, 10th Congress on Electronic Structure: Principles and Applications, 28 June – 1 July 2016, Spain. *(poster presentation)*

- **Boz, E.**, Tüzün, N. Ş., “A Quantum Mechanical Study on Ag Catalyzed Triazole Synthesis”, 11. Kimyasal Fizik Kongresi, 2014, Piri Reis Universitesi, İstanbul, Turkey. *(poster presentation)*

OTHER PUBLICATIONS, PRESENTATIONS AND PATENTS:

- **Boz, E**., Haslak, Z. P., Tüzün, N. Ş., Konuklar, F.A.S. (2014) A Theoretical Study On Rh(I) Catalyzed Enantioselective Conjugate Addition Reactions of Fluoroalkylated Olefins. *Organometallics*, 33, 19, 5111-5119. (*article*)

- **Boz, E.,** Tüzün, N. Ş. (2013) Reaction mechanism of ruthenium-catalyzed azide-alkyne cycloaddition reaction: A DFT study. *Journal of Organometallic Chemistry*, 724, 167-176. (*article*)

- **Boz, E.** and Stein, M., Investigation of Perfluorinated Compound-Binding to Human Hepatocyte Nuclear Factor (HNF4α), The 11th Triennial Congress of the World Association of Theoretical and Computational Chemists, WATOC 2017, August 27 to September 1, 2017, Munich, Germany. *(poster presentation)*

- **E. Boz**, N. Ş. Tüzün, S. Durdağı, “Molecular Dynamics Simulation of The Free and Inhibitor-Bound Kras-Pdeδ Systems: Insights on The Inhibition Mechanism”, ESPA 2016, 10th Congress on Electronic Structure: Principles and Applications, 28 June – 1 July, 2016, Spain. *(poster presentation)*

- **E. Boz**, N. Ş. Tüzün, S. Durdağı, " In Silico Analysis of the Inhibition of KRAS-PDEδ Interactions", ICQC, International Congress of Quantum Chemistry, 8-13 June, 2015, Beijing, China. *(poster presentation)*

- **Boz, E.,** Tüzün, N. Ş., "Ru Katalizörlü Azit-Alkin Tepkimeleri Üzerine Hesapsal Bir Çalışma”, IV. Fiziksel Kimya Kongresi, 5- 8 June 2014, Denizli, Turkey. *(oral presentation)*

- **Boz, E.,** Tüzün, N. Ş., Durdağı, S., "Inhibition of KRAS-PDEδ Interactions By Small Molecules Using Multi-Scale Molecular Modeling Approaches", 11. Kimyasal Fizik Kongresi, Piri Reis Universitesi, 2014, İstanbul, Turkey. *(poster presentation)*

- **E. Boz**, P. Haşlak, F. A. S. Konuklar, N.S. Tüzün, "A Theoretical Study On Rh(I) Catalyzed Enantioselective Conjugate Addition Reactions of Fluoroalkylated Olefins", 2-7 September, 2012, TACC-2012 Pavia, Spain. *(poster presentation)*

- Tüzün, N. Ş., **Boz, E.**, Özen, C., "Mechanism of Copper and Ruthenium Catalyzed Azide Alkyne Cycloaddition Reactions: A DFT Study", 25-28 June, 2011, Cesky Krumlov, Czech Republic. *(poster presentation)*

- **E. Boz**, N. Tüzün, "A Theoretical Study on Ru Catalyzed Azide Alkyne Cycloaddition", The Ninth Triennal Congress of the World Association of Theoretical and Computational Chemists-WATOC 2011, July 17- 22, 2011, Santiago de Compostela, Spain. *(poster presentation)*

- Tüzün, N. Ş., **Boz, E.**, Özen, C., "A Quantum Mechanical Study on the Mechanism of Ru and Cu Catalyzed Azide-Alkyne Addition Reactions" Gordon Research Conferences, 29 August-3 September 2010, Les Diablerets, Switzerland. *(poster presentation)*

- **E. Boz**, N. Tüzün, "A Theoretical Approach to Ru Catalyzed Azide-Alkyne Cycloaddition Reactions", 7th Congress on Electronic Structure: Principles and Applications, June 29-July 2, 2010 Oviedo, Spain. *(poster presentation)*

- Tüzün, N. Ş., **Boz, E**., Özen, C. “A DFT Study on the Mechanism of Ruthenium Catalyzed Azide-Alkyne Cycloaddition Reaction”, DFT09, 2009, Paris, France. *(poster presentation)*